Comparison of heat transfer models at the pebble, gas and reflector interface in the PBMR

Kamantha Mannar

Dissertation submitted in partial fulfilment of the requirements for the degree

Master of Science

at the Potchefstroom Campus of the North-West University

Supervisors: Prof. C.G. Du Toit

Dr. O. Ubbink

May 2010

ABSTRACT

It is a great challenge in the design of the PBMR to accurately predict gas flow and heat transfer in the reactor. Understanding the heat transfer at the core-reflector interface in particular is a very important aspect as the reactivity of the control rods housed in the reflectors is highly temperature dependent. It is also very important because the core-reflector interface is on the critical path for heat removal during accident conditions. PBMR has developed an OECD/NEA coupled neutronic/thermal-hydraulic benchmark to aid in the understanding of the different modelling approaches currently employed at PBMR. A comparison of THERMIX-KONVEK and DIREKT results showed large temperature differences at the core-reflector interfaces. Further investigation showed that these differences are as a result of the numerical methods used i.e. Cell-Centred (CC) vs. Vertex-Centered (VC). The present study extended this comparison to Star-CD (CC) and Flownex (VC) which are also used to simulate the reactor at PBMR. A 1D MATLAB program that mimics the CC and VC numerical methods was verified against Star-CD and Flownex. This program was then used to model a 1D version of the OECD/NEA benchmark. Results were compared with DIREKT and THERMIX-KONVEK. Although the results compared well, there were significant errors at the core-reflector interfaces. The findings of this study were that different numerical methods will predict different temperatures, heat fluxes and (temperature-dependent) sink terms. It was also shown that in addition to the differences resulting from numerical methods, differences were seen between Star-CD and DIREKT and Flownex and THERMIX-KONVEK in the region of the core-reflector boundary. In general, for complicated simulations like that of the pebble bed, the numerical basis of software used to simulate the problem needs to be understood for the problem to be correctly modelled.

Keywords: Numerical Modelling, Heat Transfer, PBMR, Core/Reflector Interface, Star-CD, DIREKT, THERMIX-KONVEK, Flownex

DEDICATION

Pravesh, you were always my inspiration.
Tara, I hope someday to be yours…

ACKNOWLEDGEMENTS

Firstly, I would like to thank both my supervisors for their invaluable guidance.

I would also like to acknowledge the people that have made the greatest contribution to the completion of this dissertation.

My husband, Reshendren Naidoo, who has always been my motivation.

My late brother, Pravesh Mannar, who, despite his recent efforts to make things difficult, has always been by role model.

And my dogs, Boog and Lucy, who waited so patiently for me to finish so I would throw the ball…

TABLE OF CONTENTS

LIST OF FIGURES

LIST OF TABLES

NOMENCLATURE

Roman Lettering (Lowercase)

c_p	Specific Heat	J/kg.K
d	Sphere Diameter	m
e	Specific Internal Energy	J
h	Heat Transfer Coefficient	$W/m^2.K$
k	Thermal Conductivity	W/m.K
k_e^g	Equivalent Thermal Conductivity for Fluid	W/m.K
k_e^r	Equivalent Thermal Conductivity for Radiation	W/m.K
k_{eff}	Effective Thermal Conductivity	W/m.K
k_e^c	Equivalent Thermal Conductivity for Contact	W/m.K
k_g	Fluid Thermal Conductivity	W/m.K
k_{mol}	Molecular Thermal Conductivity	W/m.K
p	Pressure	Pa
r	Radius	m
q_{fs}	Convective Source	W/m^3
$q_{nuclear}$	Nuclear Related Heat Source	W/m^3

Roman Lettering (Uppercase)

A	Face Area	m^2
D	Hydraulic Diameter	m
D_{ch}	Reactor Hydraulic Diameter	m
E	Modulus of Elasticity	GPa
H	Reactor Height	m
N_A	No. of Spheres per Unit Area	-
N_L	No. of Spheres per Unit Length	-
T	Temperature	°C or K
T_{gas}	Gas Temperature	°C or K
V	Volume	m^3
V_0	Superficial Velocity	m/s

Dimensionless Numbers

Λ	Planck Number
Nu	Nusselt Number
Pe	Péclet Number
Pr	Prandtl Number
Re	Reynolds Number

Greek Letters

δx	Distance	m
ε	Porosity	-
ε_r	Emissivity	-
λ_{cw}	Convective Wall Heat Transfer Correlation	-
λ_{fp}	Fluid to Particle Thermal Conductivity	-
μ	Viscosity	kg/m.s
ρ	Density	kg/m^3
σ	Stefan-Boltzmann constant	$W/m^2.K^4$

Abbreviations

AVR	Arbeitsgemeinschaft Versuchs Reaktor
BCC	Body-Centred Cubical
CB	Core Barrel
CC	Cell-Centred
CFD	Computational Fluid Dynamics
DID	Defence-In-Depth
DNS	Direct Numerical Simulation
FCC	Face-Centred Cubical
GIF	Generation IV International Forum
HP	High Pressure
HPTU	High Pressure Test Unit
HTR	High Temperature Reactor
HTGR	High Temperature Gas Reactor
HTTF	Heat Transfer Test Facility
HTTU	High Temperature Test Unit

INET	Institute of Nuclear Energy Technology
KTA	Kern Technisches Ausschuss
LES	Large Eddy Simulation
LP	Low Pressure
MPS	Main Power System
NEA	Nuclear Energy Agency
NECSA	Nuclear Energy Corporation of South Africa
OECD	Organisation for Economic Cooperation and Development
PBMR	Pebble Bed Modular Reactor
PWR	Pressurised Water Reactor
RANS	Reynolds-Averaged Navier-Stokes
RCCS	Reactor Cavity Cooling System
RPV	Reactor Pressure Vessel
SANA	Selbsttätige Abfuhr von Nachwärme
SAPP	South African Power Pool
TDMA	Tri-Diagonal Matrix Algorithm
TINTE	TIme-dependent Neutronics and Temperatures
VC	Vertex-Centred
VSOP	Very Superior Old Programs

1 INTRODUCTION

1.1 BACKGROUND

On the necessity of nuclear power, John Ritch, the Director General of the World Nuclear Association wrote, "*Today, one by one and in ever increasing numbers, governments around the world are embracing nuclear power as fundamental to their strategies of national energy security and global environmental responsibility. In doing so, they are responding to an imperative that is gaining ever greater cogency on every continent. After assessing the human and environmental realities around them, national leaders are recognizing that nuclear energy today represents nothing less than an indispensable asset if our world is to meet what must be recognised as the greatest challenge in human history.*" (Ritch, 2008)

The challenge that Ritch refers to is the ever increasing world population. By 2050 this is expected to swell from the current 6.6 billion to an upward of 9 billion. This increase in population is anticipated to consume more energy than the total consumed in history as an entirety. It is also predicted that there will be an increase in greenhouse gas emissions because of this increase in energy consumption. Authoritative estimates show that by 2050 the world must reduce global greenhouse emissions by 60% even though the world energy consumption is estimated to triple in this time. (Ritch, 2008) Because of this dire situation the case for nuclear energy has become very strong with leading environmentalists like James Lovelock and Patrick Moore now expressing their support. More and more major countries without nuclear power are now embracing and even, in some instances, leading in reactor technology innovation.

Nuclear energy currently supplies more than 16% of the world's electricity. Today this is more than the world utilized from all its combined sources in 1960. Fifty six countries now operate civil research reactors and thirty operate 435 commercial reactors. Furthermore, thirty power reactors are currently under construction while over seventy are firmly planned. (Ritch, 2008)

John Ritch also wrote, "*The nuclear industry is clearly on the rise. But for serious environmentalists, such projections can provide little comfort – not because nuclear energy is*

growing but because it is not yet growing fast enough to play its needed role in the clean energy revolution our world so desperately needs." (Ritch, 2008) From this statement stems the fundamental question of "what is being done to accelerate the nuclear renaissance?'

The Generation IV International Forum (GIF) is an international collective committed to joint development of the next generation of nuclear technology. In 2002 they announced their selection of six reactor technologies which they believe will shape the future of nuclear energy. One of these technologies is the High Temperature Gas Reactor (HTGR). This technology offers the advantages of inherent safety, improved economics, quicker construction, distributed generation and high temperature availability. The latter advantage makes the HTGR suitable for process heat applications. According to the World Nuclear Association, electricity generation from fossil fuels only accounts for one-third of global CO_2 emissions. Half of all emissions is apparently generated from the industrial and transport sectors. (World Nuclear Association, 2008) An opportunity exists to introduce nuclear energy into these sectors by supplying process heat to produce cleaner gases, chemical products and liquid petroleum fuels.

An example of a Generation IV reactor in operation is the 10 MW Chinese HTR-10. This reactor was commissioned in 2000 as a demonstration and research facility for pebble bed HTR technology. In an experiment in September 2004 the reactor was shut down with no cooling; fuel temperatures reached less than 1600°C and there was no failure thus demonstrating the intrinsic safety of an HTR. (World Nuclear Association, 2009) The proposed South African Pebble Bed Modular Reactor (PBMR) is similar to the HTR-10 and will be used for electricity generation.

Eskom, in collaboration with international shareholders, has been involved in developing the PBMR since 1993. Electricity consumption in South Africa has drastically increased since 1980 and the country, which is part of the South African Power Pool (SAPP), supplies more than 60% of Africa's electricity. The total generating capacity in South Africa is 41.3 GWe and this is mostly coal-fired. In early 2008 regional electricity demand exceeded supply capacity and as a result South African power exports had to be curtailed. Major industrial energy cutbacks are now being used to manage domestic demand and this is foreseen to lead to a significant decline in the country's economic growth. By 2025, Eskom expects to double its generating capacity to 80 GWe and half of that is expected to be as a result of nuclear power (World Nuclear Association, 2008). The Nuclear Energy Corporation of South Africa (NECSA) expects the South African nuclear capacity to increase to approximately 27 GWe, supplying 30% of electricity, by 2030.

This is expected to include 12 new large pressurised water reactors (PWR) and an initial set of 24 PBMR's. (World Nuclear Association, 2008)

The PBMR is a graphite-moderated, helium-cooled High Temperature Reactor in which the helium is heated by nuclear fission. The heat is converted into electrical energy in a direct cycle power conversion unit by means of a turbine-driven generator. The physical layout is shown in Figure 1-1.

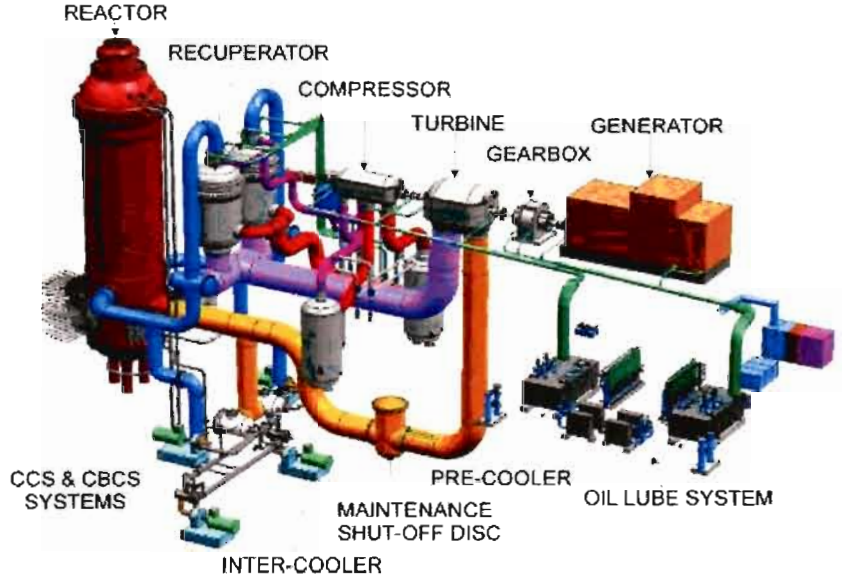

Figure 1-1: Detail of the PBMR Main Power System (www.pbmr.co.za, 2008)

The PBMR is based on reactor technology originally developed in Julich, Germany. Between 1965 and 1988 a demonstration and research pebble bed reactor, the Arbeitsgemeinschaft Versuchs Reaktor (AVR) was built and successfully operated. It had a steel pressure vessel that housed a helium circulator and steam generator above the pebble bed core. The steam generator drove a traditional Rankine power generation cycle. The AVR demonstrated the inherent safety of HTR's as well as the reliability of pebble fuel.

The PBMR has a vertical steel reactor pressure vessel (RPV) which is 27 m high and has a 6.2 m inner diameter. The RPV contains and supports a metallic core barrel which in turn supports the annular pebble fuel core. The reactor core is 8.5 m high and has an inner diameter of 1.75 m and an outer diameter of 3.7 m. The annular pebble fuel core is located in between a central and an

outer graphite reflector. The PBMR reactor core uses spherical fuel elements referred to as pebbles. When fully loaded the core houses approximately 450 000 pebbles. (www.pbmr.co.za, 2008)

The PBMR fuel sphere, which is shown in Figure 1-2, is cold pressed from a matrix of natural graphite, electrographite and a phenolic resin that acts as a binder. It has an inner region that contains fuel in the form of spherical coated particles. These particles are embedded in the graphite mixture. This is surrounded by a shell of the matrix graphite that does not contain any fuel particles. Each coated particle consists of a uranium dioxide kernel surrounded by four concentric coating layers. The first coating layer is a porous pyrocarbon layer (buffer layer). This is surrounded by an inner high density pyrocarbon layer, a silicon carbide layer and an outer high density pyrocarbon layer. The buffer layer contains any mechanical deformation that the kernels undergo as well as any fission products diffusing out of the kernel. The remaining layers act as an impenetrable barrier for fuel and fission products. (Slabber, 2006)

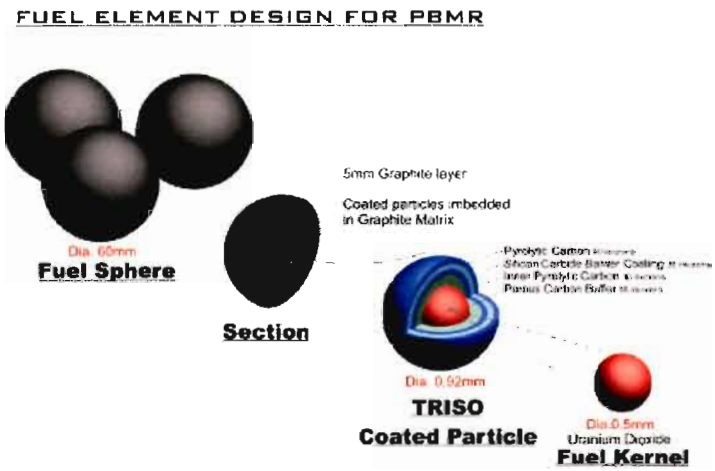

Figure 1-2: PBMR Fuel Design (Slabber, 2006: 98)

One of the key features of the PBMR is online refuelling. While the reactor is at power it is continuously being reloaded with fuel at the top of the reactor. After each pass through the core the pebbles are measured for burn-up and if still usable are returned to the reactor for a further cycle. Each pebble is expected to pass through the reactor six times and last about three years before it is spent. It is intended to operate the PBMR uninterrupted for six years before the reactor needs to be shut down for scheduled maintenance. (www.pbmr.co.za, 2008)

During normal operation the heat generated in the core is removed by the helium coolant which enters the reactor at 500°C. The coolant then passes through the hot fuel spheres, exiting at the bottom of the vessel at 900°C. The hot gas passes though the turbine, which is mechanically connected to the generator and gas compressors, exiting at 500°C. The helium is then cooled in a high efficiency recuperator. It is passed through the precooler, LP compressor, intercooler and HP compressor, before returning through the recuperator to the reactor core. (www.pbmr.co.za, 2008) A schematic of the main power system (MPS) is shown in Figure 1-3.

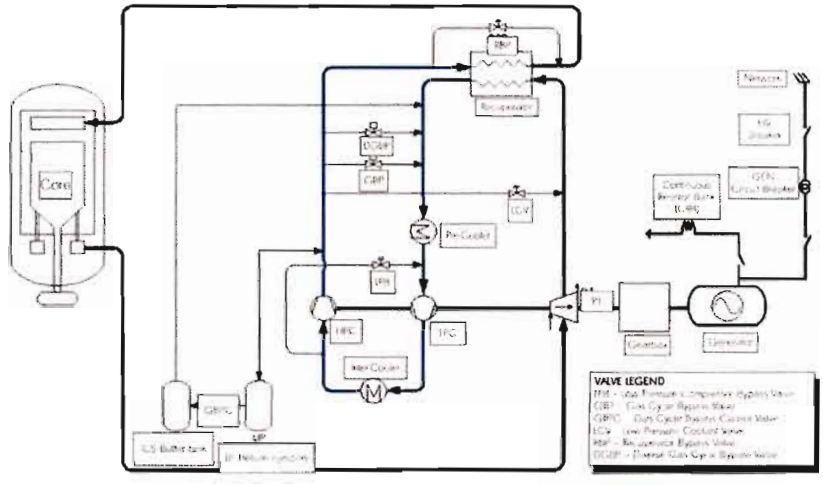

Figure 1-3: Main Power System Schematic (www.pbmr.co.za, 2008)

From the birth of nuclear power there has been a strong awareness of the potential hazard of nuclear criticality and the release of radioactive materials. To achieve optimum safety, nuclear plants operate using a defence-in depth (DID) approach with multiple safety provisions supplementing the natural features of the reactor core. The safety provisions include a number of physical barriers as well as the provision of multiple safety systems, each with backup and designed to accommodate human error. Where existing commercial reactors use active safety systems, the PBMR achieves its safety through passive systems. The main safety features of the PBMR lies in the inherently safe characteristics resulting from the design approach, materials used and form of fuel. (Ion *et al*, 2003:2) The inherent safe design of the PBMR renders the need for safety backup systems obsolete.

In the event of a worst case scenario, the passive safety features of the PBMR require no short term human intervention. A large negative temperature coefficient of reactivity and a passive heat

removal capability, which is discussed further in 2.1.1, are some of the key safety features of the PBMR. Even if there is a failure of the active systems that are designed to shutdown the nuclear reaction and remove decay heat, the reactor will shut itself down and cool down naturally by means of heat transport to the environment. This is because of the strong negative temperature coefficient of reactivity which results in the reactivity, and consequently the neutronic power, adjusting to counteract any temperature changes in the core. (www.pbmr.co.za, 2008) This was demonstrated in the AVR in Germany and more recently in the HTR-10 in China. Furthermore, as explained in (www.pbmr.co.za, 2008), the very low power density of a PBMR core and the resistance to high temperature of the fuel spheres are excellent temperature control measures.

It is a great challenge in the design of the PBMR to accurately predict gas flow and heat transfer in the reactor. It is an extremely expensive exercise to design a nuclear reactor experimentally due to the high radiation and temperatures in and around the reactor. As a result the capability to accurately predict these phenomena is vital.

Understanding the pebble/reflector/gas heat transfer is a very important aspect in the design of the PBMR as the reactivity of the control rods housed in the reflectors is highly temperature dependent. It is also very important because the pebble/reflector/gas interface is on the critical path for heat removal during accident conditions. There are a number of correlations that are used to calculate the pebble/reflector/gas heat transfer coefficient. These correlations are the basis for all relevant numerical simulations carried out at PBMR. Due to the pebble/reflector/gas heat transfer not yet being completely resolved however, the approaches to modelling the heat transfer vary widely across codes.

A reactor benchmark definition (Strauss, 2006) was drawn up at PBMR in 2003. The purpose of these benchmarks was to validate the thermo-hydraulic components of the reactor models used at PBMR as well as to identify any possible discrepancies between the different codes used to simulate the reactor. The codes compared included TINTE, Flownex and STAR-CD. All three of these codes and VSOP, discussed further in 2.2.1, are used at PBMR to simulate the reactor. Strauss, (2006) contains a number of simplified reactor unit flow cases selected specifically for benchmarks purposes. This included heat transfer through the pebble bed only, with and without the central and side reflectors. An investigation into the reports of Strauss, (2007) and Viljoen and Mtyobile, (2007), shows that for the cases involving heat transfer through the pebble bed, discrepancies exist.

1.2 OBJECTIVE OF STUDY

It is the aim of this research to investigate the various ways that software used at PBMR deals with the heat transfer at the pebble/reflector/gas interface. An important aspect of this study is to understand the different methods used and interpret the differences in results. It is important to determine the most effective approach or, at least, the pros and cons of each method.

It is necessary during the duration of this research to investigate the following issues:

- What are the methods currently used by STAR-CD, Flownex, VSOP and TINTE to model the heat transfer at the pebble/gas/reflector interface?
- What are the common assumptions between the various methods?
- What are the limitations, if any, of each of the codes in implementing a heat transfer model?

The approach of this study is to thoroughly investigate the implementation of the most current heat transfer models in VSOP, TINTE, STAR-CD and Flownex which will then be coded in a common platform, MATLAB. A number of benchmark test cases will be developed and used to verify the MATLAB implementation. This understanding will later aid with the development of a "best approach".

1.3 OUTLINE OF STUDY

Chapter 2 presents a review of published literature with relevance to the modelling of heat transfer in the PBMR. The heat transfer phenomena that exist in the pebble bed are discussed, as well as the accepted modelling approaches. The HTTF, a High Temperature Test Facility used to validate the heat transfer correlations used at PBMR and the different simulation methodologies employed for the integrated reactor models, is also discussed. Some background is provided into each of the codes used to simulate the reactor at PBMR, viz. Star-CD, VSOP, TINTE and Flownex. Finally, a review of work done on the simulation of a pebble bed is presented.

Chapter 3 presents the OECD/NEA PBMR benchmark and work that has been done at PBMR on this benchmark. A 1D program was written by Du Toit, (2008) to investigate large temperature

differences seen at material interfaces. The results of the study carried out by Du Toit, (2008) are presented. The 1D OECD/NEA benchmark modified by Du Toit, (2008) is also presented.

Chapter 4 presents the discretisations of the 1D steady state equation for the conservation of solid energy using the Cell-Centred (CC) and Vertex-Centred (VC) numerical methods as applicable to the 1D MATLAB implementations.

Chapter 5 presents the verification of the MATLAB implementations. A number of tests were carried out to verify the 1D MATLAB implementations with Star-CD and Flownex.

Chapter 6 presents the results of the 1D MATLAB implementations for the 1D OECD/NEA PBMR benchmark.

2 LITERATURE REVIEW

2.1 HEAT TRANSFER

2.1.1 PBMR Heat Transfer Phenomena

As discussed by Van der Merwe *et al*, (2006) and Van Antwerpen, (2007), the flow and heat transfer mechanisms in the PBMR are extremely complex. One of the major contributors to this complexity is the distribution of the fuel in the core. The spherical coated particles of fuel are randomly embedded in the graphite mixture that makes up the inner region of the pebble. In addition the pebbles of different batches are randomly distributed in the reactor core. The first mode of heat transfer is the conduction from the centre of the pebble to the surface of the pebble. The heat generated in each fuel sphere is determined by its position in the reactor and hence the corresponding neutron flux. This heat is conducted through the layers of the fuel sphere resulting in a radial temperature gradient within the pebble.

The heat that is conducted to the surface of the pebble is then removed by convection to the interstitial fluid (helium). As the temperature of the helium increases axial temperature gradients are developed within the pebble bed. "Dispersion" or "braiding", which is essentially the increase of flow mixing, occurs as a result of the difficult flow path between the randomly packed pebbles. This provides increased heat transfer perpendicular to the main direction of flow.

As explained in Van der Merwe *et al*, (2006), point contact conduction occurs between the pebble surfaces that are in contact with one another. Point contact conduction also occurs between the pebble surface and the reflector as well as through the assumed thin layer of fluid near the contact point between the sphere and the reflector. There is also radiation heat transfer between the reflector and the surface of the pebble. Heat is transferred from the reflector to the fluid by means of convection. The fluid in contact with the reflector is constantly being replaced due to the convective transport of the fluid and the associated dispersion.

The different phenomena are shown in Figure 2-1.

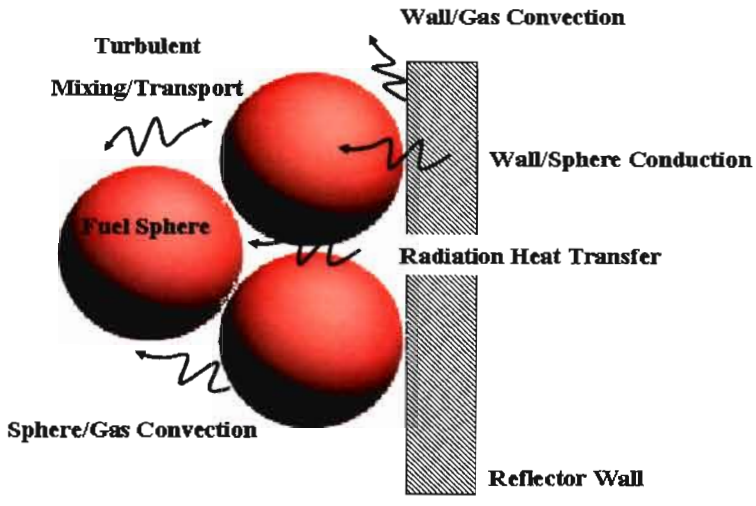

Figure 2-1: Pebble Bed Heat Transfer Phenomena (adapted from Van der Merwe *et al*, 2006:2)

In the event of no coolant flow, the pebbles exchange heat by means of conduction, at points of contact between the spheres, and radiation. Under normal flow conditions the heat that is not removed by the coolant is lost by conduction and radiation to the components surrounding the reactor. This is one of the passive cooling systems that render active cooling systems obsolete in the PBMR. Unlike normal operating conditions where most of the heat is removed from the pebble bed by the coolant flow, in "accident" conditions the core heat is removed by conduction and radiation to the side reflector as well as natural convection. From there it is conducted to the pressure vessel surface which is cooled by radiating to the Reactor Cavity Cooling System (RCCS).

Secondary heating effects occur in the central and side reflectors, which comprise of interlocking graphite blocks. The gaps between the blocks create small flow channels which allow coolant flow to leak into the core. This causes a certain amount of cooling which counters the gamma ray heating in the side reflector. This has serious consequences for the neutron balance in the reactor as the control rods, which are located in the side reflector, are highly temperature dependent.

2.1.2 *Modelling Approaches*

As outlined by Van der Merwe *et al*, (2006), there are three widely accepted approaches to modelling heat transfer in a pebble bed.

- The *homogeneous* or *pseudo-homogeneous* approach solves the solid and gas temperatures using a single energy equation. Consequently this approach is only applicable for small temperature differences between the solid and gas. The pressure drop is calculated using the Ergun equation. (Van der Merwe *et al*, 2006)

- The *pseudo-heterogeneous* approach solves the solid and gas temperatures using separate effective thermal conductivities for conduction and radiation. Control volumes contain both gas and solids indicated by a gas/solid function. The pressure drop is also calculated using the Ergun equation. (Van der Merwe *et al*, 2006)

- The *heterogeneous* approach treats the gas and solid explicitly with separate energy equations. The pressure drop is calculated from the flow resistance through the interstitial gaps. Examples of this include Lattice-Boltzmann and DNS simulations. (Van der Merwe *et al*, 2006)

Because of the temperature difference limits of the homogeneous approach and the computational effort required by the heterogeneous approach the pseudo-heterogeneous approach is generally used to model a pebble bed nuclear reactor. This approach accounts for the high temperature gradients that exist between the solid and gas in the bed.

Substantial work was done by Wijngaarden and Westerterp, (1992) in developing a pseudo-heterogeneous model for heat transfer in packed beds. Prior to this development various studies had been conducted on the radial effective heat transfer conductivity and the heat transfer coefficient at the wall. This included work by Zehner, (1973), Hennecke and Schlünder, (1973), Zehner and Schlünder, (1973), Lerou and Froment, (1978), Bauer, (1977) and Dixon and Cresswell, (1979). A review of this work can be found in Westerterp *et al*, (1987). All of these studies however were based on homogeneous models. In the model developed by Wijngaarden and Westerterp, (1992), it was assumed that the heat transport in the solid and gas phase occurs in series by three mechanisms; heat transfer from the solid to the gas, heat transfer through the gas

to the outer wall and heat transfer at the wall through the gas. They concluded that if the heterogeneity of a packed bed is significant their series model could be used successfully to describe the temperature profiles in the bed. Unfortunately all of their experiments were limited to Péclet[1] numbers below 1000. The Péclet numbers of a PBMR are typically in the order of 10000 and hence the results of Wijngaarden and Westerterp, (1992) are not directly applicable to the PBMR.

2.1.3 Existing Heat Transfer Correlations

2.1.3.1 Convection Heat Transfer

The Kugeler-Schulten correlation for calculating convection heat transfer between the interstitial fluid (helium) and 60 mm fuel spheres is recommended by KTA (1983). The correlation is given as:

$$h_{KS} = \frac{k_g}{d}\left[\frac{1.27}{\varepsilon^{1.18}}\mathrm{Re}^{0.36}\,\mathrm{Pr}^{0.33} + \frac{0.033}{\varepsilon^{1.07}}\mathrm{Re}^{0.86}\,\mathrm{Pr}^{0.5}\right] \qquad (2\text{-}1)$$

Where:

k_g	Fluid Thermal Conductivity
d	Sphere Diameter, m
ε	Porosity

The Reynolds number is defined by:

[1] The Peclet number, named after Jean Claude Eugéne Péclet, is the product of the Reynolds and Prandtl number, defined in 2.1.3.1.

$$\mathrm{Re} = \frac{\rho V_0 d}{\mu} \tag{2-2}$$

The Prandtl number of the fluid is defined by:

$$\mathrm{Pr} = \frac{c_p \mu}{k_g} \tag{2-3}$$

This correlation is valid under the following conditions:

- $100 \leq \mathrm{Re} \leq 10^5$
- $0.36 \leq \varepsilon \leq 0.42$
- $H / d \geq 4$
- $D_{ch} / d \geq 20$

For lower Reynolds numbers a correlation by Vortmeyer and Le Mong, (1976) is available:

$$h = \frac{k_g}{d} 1.04\,\mathrm{Re}^{0.6} \tag{2-4}$$

This correlation is valid under the following conditions:

- $10 < \mathrm{Re} < 200$
- $k_{eff}/k_g = 25$

2.1.3.2 Pebble Bed Thermal Conduction

The effective thermal conductivity between the pebbles consists of radiation, solid thermal conduction and contact area conduction. The proper evaluation of this effective thermal conductivity in a packed bed has been the subject of research for many years. A number of mathematical models were proposed for the prediction of the effective thermal conductivity in a packed bed and most of these models used a representative geometric unit. The heat conduction in the cell was generally assumed to be through two parallel paths viz. conduction through the fluid filled voids and conduction through the solid and fluid phases. Also the thermal resistances

of the fluid and solid phases were assumed to be in series. Based on this, Zehner and Schlünder, (1970), Bauer and Schlünder, (1978) and Tsotsas and Schlünder, (1991), derived a predictive equation by considering the heat transfer in a cylindrical cell with two contacting, deformable particles.

The Zehner-Schlünder correlation (Tsotsas, 1991) has become the generally accepted correlation for modelling this phenomenon. As described in Van Antwerpen, (2007), this correlation accounts for all the complex heat transfer phenomena in the pebble bed, as described in 2.1.1. The assumptions of this correlation are (Hoffmann and van Rensburg, 2006):

- Heat flux through the cell is axi-symmetric.
- All the radiation leaving the bottom surface is intercepted by the top surface and vice versa.
- The thermal conductivity of the pebbles is uniform.
- Spheres flatten at contact points and solid-solid conduction is included.

In the study of Van Antwerpen, (2007) a modified version of the Zehner-Schlünder correlation is used. This correlation modified by Breitbach and Bartels, as quoted by Niessen and Stöcker, (1997), was used to model the SANA experiment. The difference in the correlations is that the Breitbach and Bartles version uses the particle thermal conductivity as reference for related correlated ratios while the original correlation uses the fluid thermal conductivity as reference.

The correlation for the effective thermal conductivity due to radiation is given by Niessen and Stöcker, (1997). Here the subscript "p" refers to the sphere.

$$k_e^r = \left\{ \left[1-(1-\varepsilon)^{1/2} \right] \varepsilon + \frac{(1-\varepsilon)^{1/2}}{(2/\varepsilon_r)-1} \times \frac{B+1}{B} \times \frac{1}{1+\frac{1}{\left[(2/\varepsilon_r)-1\right]\Lambda}} \right\} 4\sigma T^3 d_p \qquad (2\text{-}5)$$

Where:

$$B = 1.25\left(\frac{1-\varepsilon}{\varepsilon}\right)^{10/9} \qquad (2\text{-}6)$$

$$\Lambda = \frac{k_p}{4\sigma T^3 d_p} \qquad (2\text{-}7)$$

The correlation for the stagnant thermal conductivity (taking into account the gas and solid conduction), proposed by Zehner and Schlünder, (1973) was tested by Prasad *et al*, (1989). This correlation is based on a one-dimensional heat flow model for conduction through a packed bed of spherical particles. The superscript "g" refers to the fluid while the subscripts "mol" and "fp" refer to molecular and fluid to particle respectively.

$$\frac{k_e^g}{k_{mol}} = 1-\sqrt{1-\varepsilon}+\frac{2\sqrt{1-\varepsilon}}{1-\lambda_{fp}B}\times\left[\frac{\left(1-\lambda_{fp}\right)B}{\left(1-\lambda_{fp}B\right)^2}\ln\left(\frac{1}{\lambda_{fp}B}\right)-\frac{B+1}{2}-\frac{B-1}{1-\lambda_{fp}B}\right] \tag{2-8}$$

The contact area conduction is given by:

$$\frac{k_e^c}{k_p} = \left[\frac{3\left(1-\mu_p^2\right)}{4E_p}fd_p\right]^{1/3}\frac{1}{0.531S}\left(\frac{N_A}{N_L}\right) \tag{2-9}$$

Where:

$$f = p\frac{S_F}{N_A} \tag{2-10}$$

According to Niessen and Stöcker, (1997), Hertzian elastic deformation is used to determine the radius of the contact area between the pebbles. Furthermore, the conductive heat flux was analysed by Chen and Tien, (1973) for three close-packed cubic arrangements to determine the contact resistance.

It should be noted that for first approximations implementation of the thermal conductivity may be simplified as follows:

$$k_{eff}\left(T\right) = aT^b \tag{2-11}$$

The coefficients a and b are generated from curve fits to the Zehner-Schlünder model.

Another model that is used to predict the effective thermal conductivity in a packed bed is that of Robold, (1982). The Robold model allows for a separate formulation for the pebbles adjacent to the wall and hence, accounts for near wall effects on the heat transfer. Robold's model consists of layers of pebbles. Radiation can pass through the voids between the pebbles or it can be

conducted through the pebbles and radiated on the opposite surface. Point contacts between pebbles are assumed and conduction between the pebbles can only happen through the interstitial fluid. Robold simplified this geometry by replacing the pebble layers with porous plates. The assumptions of this correlation are (Hoffmann and van Rensburg, 2006):

- The pebble bed comprises of layers of spheres.
- The temperature gradient is small compared to the temperature itself.
- Only point contacts exist between spheres.
- The spheres have a uniform thermal conductivity.

The various conduction models discussed above are investigated as the different codes used to simulate the PBMR reactor employ different methods.

2.1.3.3 Pebble Bed/Wall Heat Transfer

The main topic of interest in this study is the heat transfer that occurs at the pebble bed wall interface. This includes the effective thermal conductivity in the bed described above, the thermal conduction in the reflector as well as the heat transfer between the pebble bed and the reflector. The majority of correlations for the pebble bed/wall heat transfer coefficient were generated assuming a homogeneous bed. As pointed out by Van der Merwe *et al*, (2006) they are also limited to Péclet numbers in the order of 1000. The heat transfer correlation most widely referenced in literature seems to be the one developed by Martin and Nilles, (1993). This is possibly because of its comprehensive experimental basis.

$$\lambda_{cw} = \frac{k_{mol}}{d}\left[\left(1.3+5\frac{d}{D}\right)\frac{k_{bed}}{k_{mol}} + 0.19\,\mathrm{Re}_0^{0.75}\,\mathrm{Pr}^{0.33}\right] \qquad (2\text{-}12)$$

This correlation is valid under the following conditions:

- $1 \leq \mathrm{Pe} \leq 10^4$
- $1.2 \leq D/d \leq 51$

Van der Merwe *et al*, (2006) note that the research of Martin and Nilles, (1993) was carried out at temperatures ranging from 20°C to 300°C and as a result radiation was considered negligible.

A more complicated model, the so-called Λ_r model, for packed beds was developed by Winterberg *et al*, (2000). The Λ_r model calculates the effective thermal conductivity as a function of position. Where Martin and Nilles, (1993) use an explicit wall heat transfer coefficient, the effective thermal conductivity in the Λ_r model reduces towards the wall as a result of two empirical parameters. Winterberg *et al*, (2000) goes on to compare the Λ_r model with the α_w model which also uses an explicit wall heat transfer coefficient. Their findings are that the Λ_r model is only advantageous when there are large temperature differences between the solid and the gas. However, the Λ_r model follows a pseudo-homogeneous approach and therefore is not applicable to the PBMR.

The SANA test facility in Julich, Germany exists to investigate the heat transport mechanisms in the core of a HTR. In Van der Merwe *et al*, (2006), FLOWNEX simulations were compared with the SANA experimental results to give an indication of the correlation for different temperatures and fluid properties. It was found that the Zehner-Schlünder model over predicts the effective thermal conductivity at the reflector interface. At higher temperatures the radiation heat transfer component dominates all other heat transfer components. This same trend was found in the comparison of the SANA-1 experiment with TINTE by Lee *et al*, (1995) and IAEA, (2000). To compensate for this effect and due to a lack of understanding at the time, IAEA, (2000) introduced a correction coefficient of 0.6 at the heating element and 0.5 at the outer reflector interface. Both corrections were introduced at a half pebble diameter from the reflector. However results from Van der Merwe *et al*, (2006) show that the effective thermal conductivity in the boundary region is not close to 0.5 of the effective thermal conductivity in the reflector as IAEA, (2000) implies.

The HTR-10 is a 10MW pebble bed HTR. It was designed, constructed and is operated by the Institute of Nuclear Energy Technology (INET), Tsinghua University in China. It was used to verify and demonstrate the inherent safety and technical features of HTR's as well as to create an experimental base for process heat applications. Results from the HTR10 research programme have been widely publicised and provides valuable experimental data for computer code validation. Comparison of the HTR-10 experimental results with FLOWNEX simulations done by Van der Merwe *et al*, (2006) showed the influence of the pebble bed/reflector interface heat transfer correlations on the reactor temperature distribution.

The study concluded that at low flow the heat transfer at the pebble bed reflector is dominated by the effective conductivity whilst at high flow the heat transfer is dominated by convection. It is suggested by Van der Merwe *et al*, (2006) that the well accepted correlations are revisited and the correction factors suggested by IAEA, (2000) be investigated more fundamentally. It was also concluded by Van Antwerpen, (2007) that the heat transfer between the pebble bed and the reflector wall requires considerable research. It is suggested in this study that the experimental datasets from the High Temperature Test Unit (HTTU) and the High Pressure Test Unit (HPTU) can assist in this regard. These two experimental test units make up the PBMR Heat Transfer Test Facility (HTTF).

2.1.4 Heat Transfer Test Facility

The correlations used by PBMR are generally accepted within the industry but unfortunately were not all derived from experiments performed under suitable quality assurance certification. Also, as in the case of the SANA experiment, the limited applicability reduces the worth of the results as a reference for PBMR simulations. The range covered by these correlations does not provide for the low Re typically encountered during depressurised loss of forced cooling accidents. To compensate for this the HTTF was designed to validate the correlations that are currently used at PBMR and to validate the different simulation methodologies that are currently applied in the integrated reactor models. (Rousseau and van Staden, 2006)

Specific phenomena to be tested include (Rousseau and van Staden, 2006):

- Pebble to pebble effective thermal conductivity within the pebble bed
- Pebble to reflector effective thermal conductivity in the near-wall region
- Pebble surface to fluid heat transfer coefficient within the pebble bed
- Reflector surface to fluid heat transfer coefficient in the near-wall region
- Total pressure drop in fluid flow through the pebble bed
- Effective fluid heat conduction due to turbulent mixing (braiding)

The HTTF was designed to capture/measure typical PBMR mass and heat transfer phenomena. It consists of two test units, the HPTU and the HTTU. Both of these units mimic specific conditions found in the PBMR. The HPTU uses high pressure and low heat to examine conduction,

convection and thermal radiation in isolation. This is done at various positions in the core. It is the smaller of the two test units and is a controlled closed-flow loop with twelve interchangeable test sections. (www.pbmr.co.za, 2008)

The HTTU uses high temperature to accurately represent the conditions in a PBMR. The three heat transfer mechanisms are examined together at different conditions. The HTTU is a 1.2 m high section of the PBMR core with a graphite central column, graphite bricks and 28 000 graphite pebbles. Heat is provided by nine graphite tube heaters. A water jacket surrounds the side reflectors and the top and bottom of the bed are insulated. (www.pbmr.co.za, 2008)

The layout and test section of the HPTU are shown in Figure 2-2. The layout and test section of the HTTU are shown in Figure 2-3.

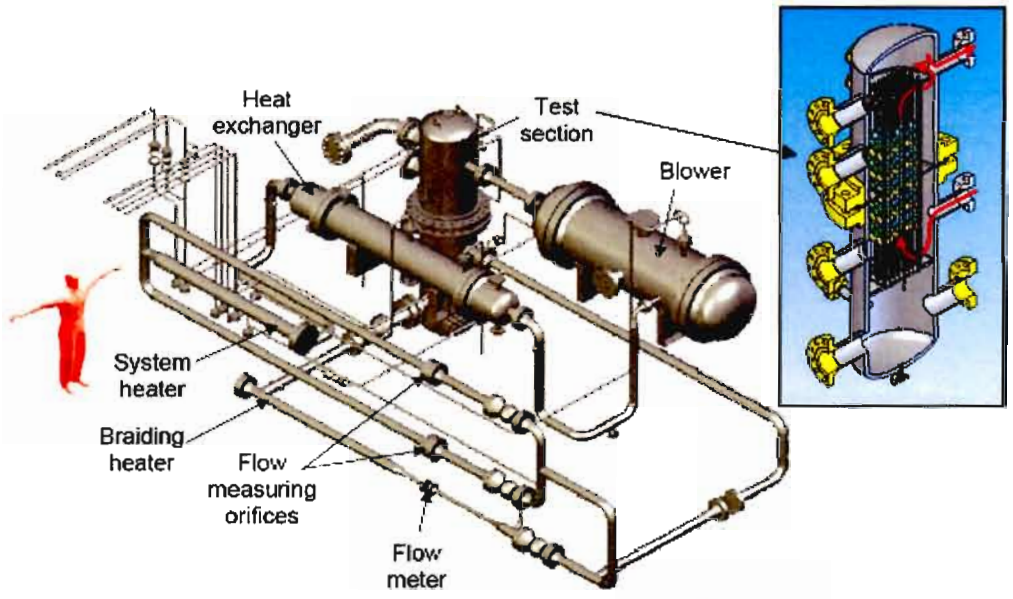

Figure 2-2: HPTU Layout and Test Section (www.pbmr.co.za, 2008)

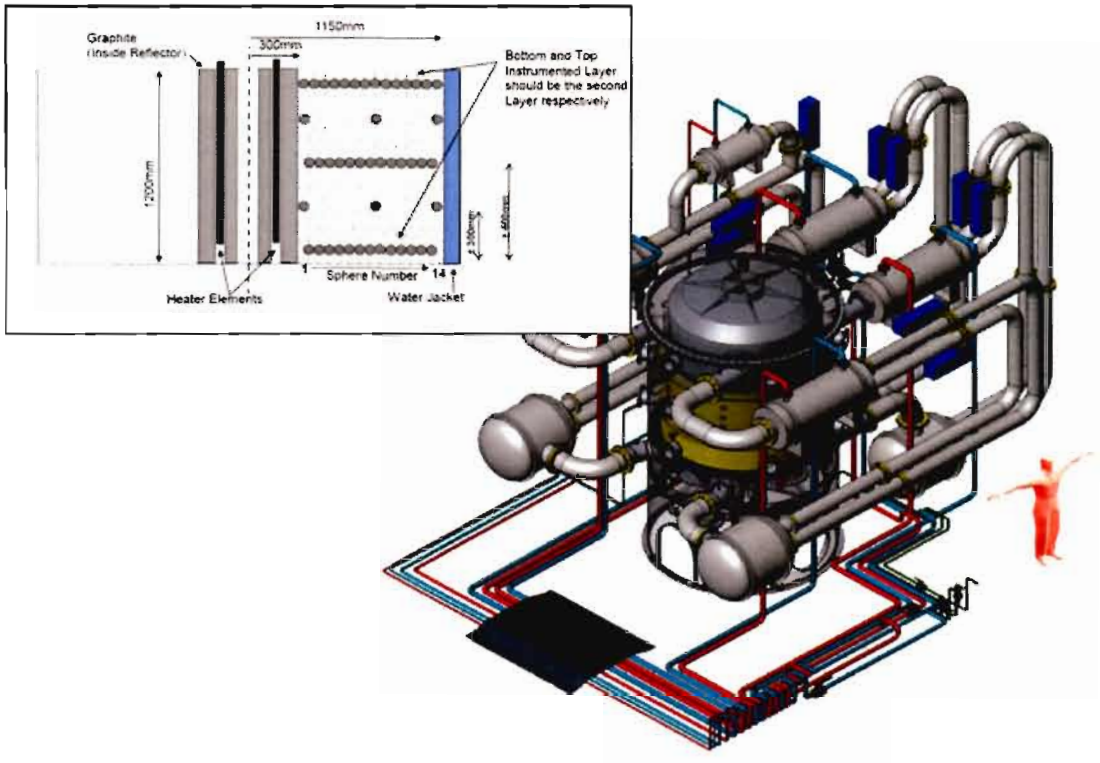

Figure 2-3: HTTU Layout and Test Section (www.pbmr.co.za, 2008)

2.2 REACTOR SIMULATION

2.2.1 PBMR Reactor Simulation

As mentioned in 1.2, it is the purpose of this study to evaluate the codes used at PBMR to simulate the reactor core. The codes of interest are Star-CD, VSOP, TINTE and Flownex. Some background will now be provided into each of these codes.

Because of the complexity of the heat transfer paths in a nuclear reactor, dedicated codes have been developed to analyse the pebble bed cores. Such codes, like the VSOP suite, are necessary to deal with the link between the neutronic properties and the temperature field in the reactor. In addition these codes consider important phenomena like fuel burnup, interaction of old and new fuel as well as the effect of the fast fluence on the conductivity of the reflectors. (Van Antwerpen, 2007)

Similarly, Computational Fluid Dynamics (CFD) codes, like STAR-CD, attempt to include as many phenomena as possible in modelling detailed flow and temperature profiles in components. (Versteeg and Malalasekera, 1995). The focus on detail, however, comes at an expense in terms of computational time and resources. For these reasons both reactor design codes and CFD codes are limited to detail component design.

In order to bridge this gap, systems simulation codes such as Flownex are used. This allows all plant components to be simulated simultaneously and hence perform such tasks as sensitivity analyses, optimisation and transient analyses. The focus of such analyses is to gain an understanding of the behaviour of the system as a whole and the interactions between the various elements. (Greyvenstein and Luarie, 1994)

CFD is used extensively to calculate pressure drops, flow distributions, temperature fields and temperature gradients in the PBMR reactor. The neutronic heat that is generated in the pebble bed and top, bottom, side and central reflectors is calculated using VSOP. These heat sources are then mapped onto the CFD model using a two-dimensional interpolation method (Hoffmann and van Rensburg, 2006). The temperature field that is calculated from the CFD model is then mapped onto the VSOP mesh where the new power profile is calculated. This process is iterated until convergence is achieved. (Van Staden *et al*, 2002) The CFD models also serve as alternative calculations for the systems analyses done using Flownex. Flownex is used extensively in evaluating system performance under postulated accident conditions. (Hoffmann and van Rensburg, 2006)

All of these numerical codes are based on the fundamental equations of conservation of mass, momentum and energy.

2.2.1.1 Reactor Codes

The VSOP (Very Superior Old Programs) suite was developed in the German HTR research programme for the design of pebble bed HTR's. It is an assembly of many specialised reactor codes with each code calculating a specific aspect of the reactor. Included in the VSOP suite is a code that solves the 4-group neutron diffusion equations.

THERMIX-KONVEK is used for steady state and quasi-steady state thermal fluid calculations of pebble bed reactor cores. It uses the finite difference approach on an axi-symmetric two-dimensional geometry. Sphere internal conduction and heat generation are calculated as well as the effective heat transfer between the fuel spheres. If the nuclear power source is provided as an input, THERMIX-KONVEK calculates the temperature of the solids in the pebble bed. The KONVEK sub module calculates the flow conditions and fluid temperatures. The inlet mass flow rate and associated fluid temperature is required as an input. The THERMIX sub module calculates the solids temperature. It accounts for heat transfer through convection, conduction and radiation as well as the heat sink/source. The distribution of the nuclear source is a required input. KONVEK solves the two-dimensional axi-symmetric equations for the conservation of mass, momentum and energy of the fluid. THERMIX solves the equation for conservation of energy of the solids. Empirical correlations are used for the pressure drop per unit length in the core and for the heat transfer coefficient between the pebbles and the fluid. THERMIX-KONVEK does allow for the use of a heat transfer correlation at the pebble bed reflector interface. (Du Toit, 2007)

The TIme-dependent Neutronics and TEmperatures (TINTE) code was also developed in the German HTR research programme, for the simulation of pebble bed HTR's. It solves the 2-group neutron diffusion equations in order to determine the time-dependent nuclear and thermal behaviour of HTR's in a two-dimensional axi-symmetric geometry. Conduction, forced and natural convection as well as radiative heat transfer in cavities are calculated. The radiative heat transfer calculations are very important due to the high temperatures that HTR's operate at. TINTE solves the 2-group neutron diffusion equations, accounting for the effects of delayed neutrons, fission product poisoning and temperature changes. (Van Antwerpen, 2007)

TINTE solves four separate models iteratively (Van Antwerpen, 2007):

- Gas flow model
- Gas, solid and fuel surface temperature model
- Fuel element internal model
- Chemical model

The pebble bed pressure drop and convection heat transfer are based on correlations.

2.2.1.2 Computational Fluid Dynamics (CFD)

CFD is the science of predicting fluid flow, heat and mass transfer, chemical reactions, and related phenomena by solving numerically the set of governing mathematical equations. The fundamentals of CFD lie in the conservation of mass, momentum and energy, using a continuum approach. Using the finite volume method, a domain is discretised into a finite set of control volumes. The partial differential equations are discretised into a system of algebraic equations and all the equations are then solved numerically to render the solution field. STAR-CD is an example of a commercial CFD code. It provides a robust multi-grid solver for the three-dimensional heat and mass transport equations, using fully unstructured meshes. (Versteeg and Malalasekera, 1995)

One of the greatest advantages of CFD is that the accurate representation of geometry is possible. Also there is the ability to interface with other codes for accurate and realistic representations of boundary conditions as well as to perform transient and steady state simulations. One of the greatest disadvantages is that all this flexibility comes at an expense in terms of computational resources and time required.

The complex nature of the heat transfer through the pebble bed requires a significant amount of user coding added to Star-CD to attain a realistic, credible solution. The heat transfer by conduction and radiation between the pebbles is modelled using the Zehner-Schlünder correlation discussed in 2.1.3.2. This correlation is used to describe the thermal transport between the pebbles at medium to low temperatures (100°C - 1400°C). For temperatures in excess of 1400°C the thermal transport is described by Robold, (1982), also discussed in 2.1.3.2.

A verification and validation study of the PBMR CFD reactor model was carried out by Hoffmann and Van Rensburg, (2006). A CFD model containing five layers of densely, regularly packed pebbles was constructed to determine the effective thermal conductivity of the pebble bed. It should be noted that this regular packing structure yields a porosity of 0.395. Because of the symmetry a 120° slice of the bed was modelled. The model consisted of an interstitial fluid region, the graphite skin and a fuel zone. The domain walls were fixed with the temperature of the hotter wall 50°C higher than that of the colder wall. When compared with Robold's model, the CFD model was found to consistently over-predict the effective thermal conductivity, across the entire temperature range. This was attributed by Hoffmann and Van Rensburg, (2006) to the

spaces in the regular packing structure that allow radiation to pass unhindered between the pebbles. In general, however, the gradients agreed fairly well. At lower temperatures the CFD model predicted lower effective thermal conductivities than the Zehner-Schlünder model. This was attributed by Hoffmann and Van Rensburg, (2006) to the pebble-pebble conduction. The Zehner-Schlünder model assumes a deformation of the pebbles at contact points whereas the CFD model assumes point contact. This trend is not seen at higher temperatures (>1000°C) as at higher temperatures radiation dominates and surface flattening becomes insignificant.

2.2.1.3 Systems Simulation

Systems simulations codes link together component models, with different levels of complexity, in a network to represent a complex system. The advantage of such codes, like Flownex, is its ability to solve flow, pressure and temperature distributions in large unstructured thermal-fluid networks providing essential information on the effect of network components on the behaviour of the complex system. Moreover, as a result of the systems approach, Flownex has a distinguishing feature of speed of execution. (Van Antwerpen, 2007)

For the simulation of the thermal-flow behaviour of the reactor core and core structures, Flownex uses a model that is based on the fundamental equations of conservation of mass, momentum and energy for the helium flowing through the fixed bed as well as the equations for the conservation of energy for the pebbles and core structures. The equations are reformulated resulting in a collection of one-dimensional elements accounting for pressure drop through the reactor, convective heat transport by the gas, convective heat transfer between pebble and gas, radiative contact and conductive heat transfer between pebbles and heat conduction in the pebbles.

The basic building block of the network approach is the control volume, or node, which represents a certain volume of fluid or solid. The single scalar values are assumed to be representative of average conditions in the control volume as a whole. Mass and energy conservation is applied to determine the change in thermal properties of the fluid within the control volume. By dividing a thermal-fluid system into control volumes and linking the control volumes with flow elements, a network can be set up that represents a whole thermal-fluid system (Van Antwerpen, 2007)

The discretised network gives rise to a set of simultaneous non-linear equations. Flownex solves compressible and incompressible momentum and mass conservation with an adaptation of the SIMPLE algorithm. The Implicit Pressure Correction Method (IPCM) was developed by Greyvenstein and Laurie, (1994). The energy conservation is solved separately from the flow equation in one single matrix. (Van Antwerpen, 2007)

Du Toit *et al*, (2003), introduced a pseudo-heterogeneous approach to model the pebble bed. This meant that the fluid and solid temperatures at all positions in the pebble bed are calculated separately. The temperature distribution in the pebbles, the effective pebble bed conduction, the convection heat transfer as well as the fluid energy conservation are all solved as a single system. There is fully implicit coupling between all components in the simulation resulting in the shortest possible solution time. The use of a pseudo-heterogeneous pebble bed model, however, also causes great uncertainty, as the old, pseudo-homogeneous pebble bed/wall heat transfer correlations do not apply and there is not yet consensus on the ideal network topology at the pebble bed wall.

2.2.2 Reactor Simulation Review

As discussed in 2.1.3.2 the evaluation of the effective thermal conductivity has been the topic of many studies throughout the years. Most of these models, including the widely accepted Zehner-Schlünder correlation, are based on a unit cell with the heat flux through parallel paths. However, because of the simplicity of the packing structure in these models a large degree of empiricism is required in their use. Cheng *et al*, (1999) suggested incorporating the packing structure in the determination of the effective thermal conductivity to overcome this problem.

Taylor *et al*, (2002) introduced an artificial spacing between adjacent pebbles to overcome the problem of mesh quality at contact points. The effect of the pebble spacing in a unit cell of the pebble bed structure was investigated. It was shown that such differences in geometrical modelling affect the prediction results significantly. Lee *et al*, (2007) concluded that the locations of flow-induced local hotspots varied according to modelling of the inter-pebble region. The approximated gaps may provide inaccurate information about the local flow field despite the advantages of simpler calculations and elimination of mesh problems.

Early studies were done by Dalman *et al*, quoted in Logtenberg *et al*, (1998), using CFD to simulate a two-dimensional packed bed reactor. The study investigated the flow around rectangular compacts near the wall. In later studies the axi-symmetric fluid flow and heat transfer past two spheres in a cylindrical tube was studied. The study showed the existence of eddies in between the spheres indicating poor heat transfer. In the study heat transfer parameters were not specified but the influence of *Re*, *Pr*, sphere size and sphere separation on the eddy was investigated. Logtenberg *et al*, (1998) also reported that the first attempt to use CFD in a packed bed to obtain values for *Nu* at the wall was made by Derkx and Dixon in 1996. This study involved using the finite element method. Logtenberg *et al*, (1998) concluded that future studies including particle-wall and particle-particle contacts would have to be made in order to obtain a more realistic geometric model. This improvement was carried out by Logtenberg *et al*, (1999). However this study was also done using the finite element method.

More recent CFD analyses, using the finite difference method, focussing on the flow induced heat transfer in a pebble bed have been carried out. Hassan and Yesilyurt, (2002) investigated the flow distribution in an aligned pebble geometry consisting of 27 pebble spheres. Yesilyurt and Hassan, (2003) analysed the local heat transfer due to the complexity of flow distribution in a body-centred cubical (BCC) structure of pebble beds. They achieved a point contact between neighbouring pebbles. Similarly, Lee *et al*, (2005) simulated the flow induced heat transfer in a face-centred cubical (FCC) bed structure. The point contacts between the pebbles were modelled and the turbulent fluid motion was simulated using a Reynolds-Averaged Navier-Stokes (RANS) approach.

There has been great interest in investigating the turbulence model performance in bluff body flows. Tomboulides *et al*, (1993) compared Direct Numerical Simulation (DNS) and Large Eddy Simulation (LES) results for flow past a sphere with a low *Re* number. Rodi, (1997) and Lübcke *et al*, (2001) compared LES with RANS for flow over a cubical cylinder with a moderate *Re* number. In their studies LES compared well with RANS. Lee *et al*, (2007) investigated the turbulence-induced heat transfer in a pebble bed core with randomly distributed spherical fuel pebbles. LES results were compared with RANS results. The structure of the bed was modelled with BCC and FCC close-packed geometries. They concluded that the LES is a more powerful approach within the feasible computer technology. They also concluded that the turbulent nature of the coolant flow affects the fuel surface temperature distributions and causes random local hotspots on the surface of the fuel.

2.3 SUMMARY

In this chapter a review of published literature with relevance to the modelling of heat transfer in the PBMR is presented. The heat transfer phenomena that exist in the pebble bed are discussed, as well as the accepted modelling approaches. The existing heat transfer correlations which include the widely used Kugeler-Schulten convective heat transfer correlation and the Zehner-Schlünder pebble bed thermal conduction correlation are discussed. Also of interest is the Robold pebble bed thermal conduction model which is used by Star-CD for temperatures in excess of 1400°C.

Work done by Van der Merwe *et al*, (2006) and Hoffmann and Van Rensburg, (2006) showed that the Zehner-Schlünder model over predicts the effective thermal conductivity at the reflector interface. It was suggested by both Van der Merwe *et al*, (2006) and Van Antwerpen, (2007) that the heat transfer between the pebble bed and the reflector wall still requires considerable research. The HTTF, a High Temperature Test Facility used to validate the heat transfer correlations used at PBMR and the different simulation methodologies employed for the integrated reactor models, is also discussed.

Some background is provided into the each of the codes used to simulate the reactor at PBMR, viz. Star-CD, VSOP, TINTE and Flownex. Finally, a review of work done on the simulation of a pebble bed is presented.

In order to investigate the uncertainty surrounding the heat transfer in the pebble bed, PBMR was involved in setting up a benchmark of the 400 MW PBMR design. The following chapter looks at the work done at PBMR on this benchmark.

3 OECD/NEA PBMR THERMAL-HYDRAULIC BENCHMARK

3.1 BACKGROUND

The Nuclear Energy Agency (NEA) of the Organisation for Economic Cooperation and Development (OECD) have, since 2005, included in its programme a PBMR coupled neutronic/thermal-hydraulic benchmark. The benchmark which is based on the 400 MW PBMR design was established with the following objectives (OECD/NEA, 2009):

- The establishment of a standard benchmark for coupled neutronic/thermal-hydraulic codes used in the PBMR design
- A comparison of codes using a common cross-section library
- To aid in the understanding of PBMR events and processes
- Understanding the benefits of different approaches, including limitations and approximations

The steady state benchmark case consists of the following exercises (OECD/NEA, 2009):

- Exercise 1: Neutronic Solution with Fixed Cross-Sections
- Exercise 2: Thermal-Hydraulic Solution with Given Power/Heat Sources
- Exercise 3: Combined Neutronic/Thermal-Hydraulic Calculation

3.2 PBMR COMPARISON OF THERMIX-KONVEK AND DIREKT RESULTS

Exercise 2 of the steady state benchmark case, the thermal-hydraulic solution with given power/heat sources, was modelled at PBMR using the THERMIX-KONVEK module of VSOP 99-03 and DIREKT. As explained in Du Toit, (2008), these results showed large temperature differences at some of the material interfaces.

However, before discussing the THERMIX-KONVEK and DIREKT results, the simplified reactor geometry that was modelled will be explained. As described in Du Toit, (2008), the different regions of the benchmark's simplified reactor geometry are labelled in Figure 3-1.

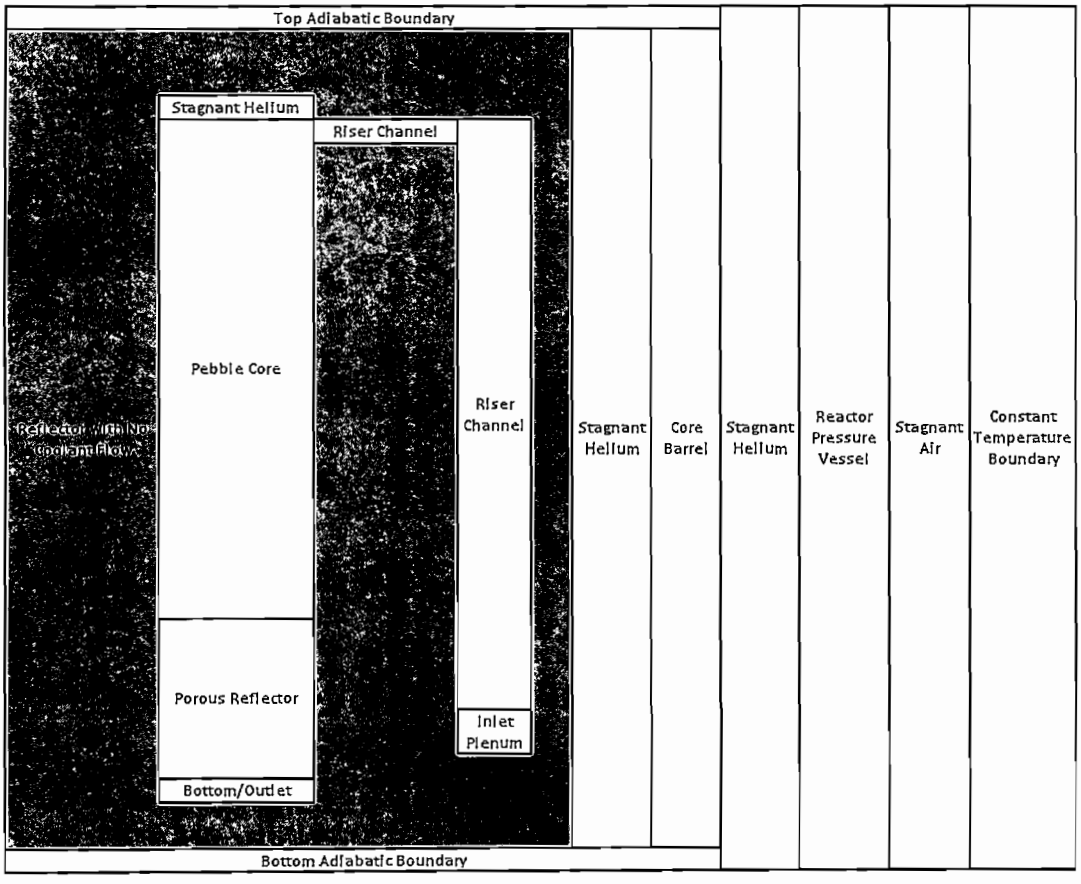

Figure 3-1: Simplified Reactor Geometry Regions

From the inlet plenum, shown in Figure 3-1, the helium flows up the riser channels, which has a graphite volume fraction of 80%, through the upper plenum towards the pebble core. The helium enters the pebble core at the top and flows downwards through the core, through the porous reflector below the core and is then collected in the bottom or outlet plenum. The pebbles in the pebble core have a volumetric fraction of 61%. (Du Toit, 2008)

Now, presenting the results of Du Toit (2008), the temperatures (in °C) predicted by THERMIX-KONVEK are shown in Figure 3-2. The temperatures (also in °C) predicted by DIREKT are shown in Figure 3-3.

Figure 3-2: THERMIX-KONVEK 2D Benchmark Results (Du Toit, 2008:10)

Each value in Figure 3-2 and Figure 3-3 represents a temperature in a single cell. The colours represent the geometric regions as described in Figure 3-1. The colour representations are as follows:

- Yellow - Inlet Plenum
- Green - Riser Channel
- Cyan - Stagnant Helium
- Red - Pebble Core
- White - Porous Reflector
- Magenta - Outlet Plenum
- Grey - Adiabatic Boundary/Core Barrel
- Dark Blue - Reactor Pressure Vessel
- Light Blue - Stagnant Air

Figure 3-3: DIREKT 2D Benchmark Results (Du Toit, 2008:11)

As Du Toit, (2008) goes on to explain, although the results of THERMIX-KONVEK and DIREKT agree reasonably well, especially at the bottom of the core, there are large temperature differences originating at the material interfaces. This is seen clearly at the reflector interface with the core and riser channel. Du Toit, (2008) believes that this difference can be attributed to the difference in the way that THERMIX-KONVEK and DIREKT deals with the solid-gas heat transfer in a cavity. THERMIX-KONVEK assumes a zero solid-gas heat transfer coefficient for the cavity while DIREKT calculates the solid-gas heat transfer. Du Toit, (2008) also believes however, that although this difference in methodology can explain the difference in temperatures at these interfaces, it can not explain the differences in temperature further away from these cavities.

3.3 1D PROGRAM TO INVESTIGATE THE DIFFERENCES BETWEEN THERMIX-KONVEK AND DIREKT

In order to investigate and understand the reason for the disparities mentioned in 3.2, Du Toit, (2008) wrote a 1D program that mimics the numerical methods of THERMIX-KONVEK and DIREKT. THERMIX-KONVEK defines temperatures at vertices and is an example of a Vertex-Centred (VC) method while DIREKT defines temperature at cell centres and is an example of a Cell-Centred (CC) method. It was the intention of Du Toit, (2008) to use these 1D programs to understand the properties of each of these methods that could give rise to the different behaviours. Furthermore, Du Toit, (2008) set out to investigate the effect of grid refinement on these different behaviours.

3.3.1 Input Data

It was decided by Du Toit, (2008) that the horizontal cut, shown by the dotted line in Figure 3-3, is a good representation of the problem being investigated. A significant amount of the input data for this 1D problem was obtained from the benchmark definition while the remaining data was determined from the 2D results. The radii of the different regions are shown in Table 1.

Table 1: Simplified Reactor Geometry Radii (Du Toit, 2008:14)

Region	Outside Radius (m)
Inner Reflector	0.1
	0.41
	0.736
	0.8055
	0.9205
	1.0
Pebble Core	1.17
	1.34
	1.51
	1.68
	1.85
Outer Reflector	1.9295
	2.0445
	2.114
	2.25
	2.436
Riser Channel	2.606
Outer Reflector	2.75
Stagnant Helium	2.875
CB	2.925
Stagnant Helium	3.1
RPV	3.28
Stagnant Air	4.62
Constant Temperature Boundary	4.63

The mesh size in the axial direction as specified in the benchmark definition is 0.5m. In the pebble core and riser channel there is heat transfer due to convection. The surface area of the solid is calculated as a function of the porosity and pebble diameter (in the pebble core) or hydraulic diameter (in the riser channel). These values were obtained directly from the benchmark. The pebble diameter is 0.06 m and the hydraulic diameter of the riser channel is

0.17 m. The porosity in the core region is 0.39 while the porosity in the riser channel is 0.2. (Du Toit, 2008)

In both of these regions it is necessary to specify a heat transfer coefficient, *h*. In the core region, both THERMIX-KONVEK and DIREKT use the KTA (1983) correlation discussed in 2.1.3.1. A slight radial variation in the 2D results for different mesh sizes resulted in Du Toit, (2008) using an average value of 4400 W/m^2K. In the riser channel, THERMIX-KONVEK and DIREKT use different correlations. Again, differences in the 2D results were compensated for by using an average value of 3060 W/m^2K.

The benchmark definition prescribes the nuclear power source density per cell. Du Toit, (2008) shows that the radial variation for the selected cell row is small. As a result a volume-weighted average of the cell values was used. This corresponds to 1.056 W/cm^3. The solid temperature of the outside boundary was specified as 20°C. As the 1D model only simulates heat transfer in the solid, the gas temperatures must be specified. A gas temperature of 500°C was specified in the riser channel.

The remainder of the inputs were determined from the results of the 2D models. Du Toit, (2008) found that gas temperature in the pebble core varies significantly between the inner and outer radii. A linear variation, $T = -61.765*r + 1258.4$ was applied. The effective thermal conductivities for the different regions which were calculated by Du Toit, (2008) from the 2D results are shown in Table 2. Stagnant Helium 1 represents the region of stagnant helium closer to the pebble core.

Table 2: Effective Thermal Conductivities

Region	Effective Thermal Conductivity (k) – W/mK
Inner and Outer Reflectors	26.0
Pebble Core	15.3
Riser Channel	20.8
CB	17.0
RPV	38.0
Stagnant Helium 1	7.0
Stagnant Helium 2	6.35
Stagnant Air	14.5

The Zehner-Schlünder model, as discussed in 2.1.3.2, is used by THERMIX-KONVEK and DIREKT to calculate the effective thermal conductivity in the pebble core region. However, the codes implement the correlation in different ways and hence yield different conductivities. Du Toit, (2008) ascertained that while the temperature across the core reflector boundary is relatively insensitive to the conductivities in THERMIX-KONVEK, this is not true for DIREKT. As a result the effective thermal conductivity for the 1D geometry was specified the same as the thermal conductivity calculated by DIREKT.

3.3.2 Comparison of 1D and 2D Results

A comparison of the 2D THERMIX-KONVEK and 1D VC Method results from Du Toit, (2008) are shown in Table 3. The results compare well with a maximum difference in temperature of approximately 3°C at the outer reflector-core interface. (Du Toit, 2008)

Table 3: 2D THERMIX-KONVEK and 1D VC Method Results (Du Toit, 2008:21)

2D THERMIX-KONVEK (°C)	1D VC Method (°C)	Difference (°C)
926.3	927.35	-1.05
926.4	927.35	-0.95
926.7	927.35	-0.65
927.0	927.35	-0.35
927.2	927.35	-0.15
927.3	927.35	-0.05
924.7	922.2	2.5
913.3	911.7	1.6
898.7	901.2	-2.5
887.5	890.7	-3.2
880.5	879.8	0.7
848.8	845.6	3.2
782.3	779.55	2.75
721.5	719.2	2.3
657.1	655.6	1.5
563.4	562.3	1.1
504.1	503.8	0.3
486.2	486.2	0.0
440.1	439.6	0.5
399.9	398.9	1.0
344.7	342.7	2.0
286.8	283.8	3.0
149.5	148.0	1.5
20.1	20.1	0.0

A comparison of the 2D DIREKT and 1D CC Method results from Du Toit, (2008) are shown in Table 4. The results compare well with a maximum difference in temperature of approximately 2.5°C at the outer reflector-core interface. (Du Toit, 2008)

Table 4: 2D DIREKT and 1D CC Method Results (Du Toit, 2008:24)

2D DIREKT (°C)	1D CC Method (°C)	Difference (°C)
924.3	924.8	-0.5
924.4	924.8	-0.4
924.6	924.8	-0.2
925.1	924.8	0.3
925.2	924.8	0.4
925.5	924.8	0.7
924.0	922.2	1.8
913.1	911.7	1.4
899.0	901.2	-2.2
888.3	890.7	-2.4
882.0	879.9	2.1
815.5	813.0	2.5
762.7	760.7	2.0
714.9	712.8	2.1
664.0	662.4	1.6
589.2	588.4	0.8
503.1	502.7	0.4
475.3	474.1	1.2
430.3	428.7	1.6
390.7	389.1	1.6
336.3	334.3	2.0
279.4	277.0	2.4
146.3	144.7	1.6
20.6	20.15	0.45

3.3.3 Effect of Grid Refinement at the Outer Reflector-Core Interface

Du Toit, (2008) then conducted a grid refinement study for both the 1D models. The intention of this study was to determine if the results of both models converge for a very fine grid. As the outer reflector-core interface was identified to have the largest temperature differences, this

region was chosen as the first area of interest. The results for both the CC and VC method are shown in Table 5.

Table 5: Temperature Difference across Outer Reflector-Core Interface as a Function of Mesh Refinement (Du Toit, 2008:25)

Number of Coarse Mesh Cell Subdivisions	1	2	4	8	16	32	32*	'∞'
1D VC method results (°C)	33.5 (-6.0)	33.8 (-5.7)	34.7 (-4.8)	36.4 (-3.1)	38.1 (-1.4)	39.1 (-0.4)	39.4 (-0.1)	39.5 (0.0)
1D CC method results (°C)	97.3 (57.8)	70.0 (30.5)	53.4 (13.9)	44.7 (5.2)	41.1 (1.6)	39.9 (0.4)	39.6 (0.1)	39.5 (0.0)

In each refinement, each cell was halved until each cell in the initial mesh was divided into 32. For the subdivision of 32*, the cells neighbouring the outer core-reflector interface were subdivided into 64. The subdivision of '∞', is an estimate of the temperature difference expected in the limit of mesh refinement. (Du Toit, 2008)

The findings of Du Toit, (2008) with regard to the mesh refinement were as follows:

- The VC method or the 1D model based on THERMIX-KONVEK initially under predicts the temperature difference. As the grid is refined, this under prediction decreases.
- The CC method or the 1D model based on DIREKT initially over estimates the temperature difference. As the grid is refined, this over prediction decreases.
- On the initial mesh, the deviation of the CC method from the converged solution is almost 10 times larger than the VC method.
- Based on the above, the accuracy of the VC method at the outer reflector-core interface is better than that of the CC method.

3.3.4 Effect of Grid Refinement at the Outer Reflector-Riser Channel Interface

The next area of interest for Du Toit, (2008) in the grid refinement study was the outer reflector-riser channel interface. First, the effect of grid refinement was investigated across the inside outer

reflector-riser channel interface. The results for both the CC and VC method are shown in Table 6.

Table 6: Temperature Difference across the Inside Outer Reflector-Riser Channel Interface as a Function of Mesh Refinement (Du Toit, 2008:27)

Number of Coarse Mesh Cell Subdivisions	1	2	4	8	16	32	32*	'∞'
1D VC method results (°C)	58.7 (-10.4)	63.6 (-5.5)	67.5 (-1.6)	69.0 (-0.1)	69.2 (0.1)	69.2 (0.1)	69.1 (0.0)	69.1 (0.0)
1D CC method results (°C)	77.4 (8.3)	71.2 (2.1)	69.0 (-0.1)	68.8 (-0.3)	69.0 (-0.1)	69.1 (0.0)	69.15 (0.05)	69.1 (0.0)

Similarly, the results for the CC and VC method across the outside outer reflector-riser channel interface are shown in Table 7.

Table 7: Temperature Difference across the Outside Outer Reflector-Riser Channel Interface as a Function of Mesh Refinement (Du Toit, 2008:27)

Number of Coarse Mesh Cell Subdivisions	1	2	4	8	16	32	32*	'∞'
1D VC method results (°C)	17.6 (-4.4)	19.6 (-2.4)	21.2 (-0.8)	21.8 (-0.2)	22.0 (0.0)	22.0 (0.0)	22.0 (0.0)	22.0 (0.0)
1D CC method results (°C)	28.6 (6.6)	24.4 (2.4)	22.7 (0.7)	22.1 (0.1)	22.0 (0.0)	22.0 (0.0)	22.0 (0.0)	22.0 (0.0)

The findings of Du Toit, (2008) with regard to this mesh refinement study at the inside and outside outer reflector-riser channel interface were as follows:

- In both cases the 1D VC method under predicts the temperature differences while the CC method over predicts the temperature differences.
- At the inside outer reflector-riser channel interface, the result of CC method is slightly better than the VC method for the coarse mesh.
- At the outside outer reflector-riser channel interface, the result of the VC method is slightly better than the CC method for the coarse mesh.

Du Toit, (2008) goes on to discuss the possible reasons for the difference in the THERMIX-KONVEK and DIREKT results at the material interfaces. This will be returned to in the discussion of the results.

3.4 SUMMARY

In this chapter the OECD/NEA PBMR benchmark was discussed. The thermal-hydraulic exercise with given power/heat sources, was modelled at PBMR using THERMIX-KONVEK and DIREKT by Du Toit, (2008). Large temperature differences were seen at the material interfaces and while some of those differences could be attributed to the different methodologies used by THERMIX-KONVEK and DIREKT to deal with the solid-gas heat transfer in a cavity, Du Toit 2008) felt that this could not explain the temperature differences further away from the cavities. Du Toit, (2008) then wrote a 1D program to mimic the numerical methods of THERMIX-KONVEK and DIREKT i.e. a cell-centred method and a vertex-centred method respectively. Du Toit, (2008) compared the results of both the 1D methods with the 2D results as a verification of the 1D program. The verified 1D program was then used to investigate the effect of grid refinement at the outer reflector-core and outer reflector-riser channel interfaces. Some conclusions were made by Du Toit, (2008) regarding the accuracy of the CC and VC methods at the interfaces of interest.

As discussed in 2.2.1, the purpose of this study is to evaluate the codes used at PBMR to simulate the reactor core. The codes of interest were listed as Star-CD, VSOP, TINTE and Flownex where VSOP and TINTE are reactor codes and Star-CD and Flownex are CFD codes. In Du Toit, (2008), the differences between the THERMIX-KONVEK module of VSOP (cell-centred) and DIREKT, a steady state program that essentially mimics TINTE (both use the vertex-centred numerical method), were investigated. For the purposes of this study, a similar investigation was carried out for Star-CD and Flownex which also use cell-centred and vertex-centred numerical methods respectively. A 1D program was written and verified using Star-CD and Flownex. This 1D program was then used to evaluate the 1D OECD/NEA PBMR benchmark presented by Du Toit, (2008).

The CC and VC methodologies of the 1D program used in this study are presented in the following chapter.

4 DISCRETISATION OF 1D NUMERICAL METHODS

4.1 CELL-CENTRED NUMERICAL METHOD

The energy conservation equation, written in partial differential form, for a porous solid is (Peyret and Taylor, 1983):

$$\frac{\partial}{\partial t}\left[(1-\varepsilon)\rho c_p T\right]+\nabla\left[(1-\varepsilon)\mathbf{q}\right]=q_{fs}+q_{nuclear} \tag{4-1}$$

Where **q**, the heat flux vector, is given by:

$$\mathbf{q}=-k\nabla T \tag{4-2}$$

One-dimensional numerical methods only solve the energy equation in the solid region. The source term due to convection is taken into account but the gas temperatures and heat transfer coefficient as well as the effective conductivity, which accounts for the heat transfer via radiation, must be specified. (Du Toit, 2007)

In equation 4-1, ρ is the density of the solid, c_p is the specific heat of the solid and ε is the porosity of the solid. The term q_{fs} represents the source of energy per unit total volume and time due to convection where "*fs*" refers to the heat flowing from the fluid to the solid. The term $q_{nuclear}$ represents any nuclear related heat source rate in the core or reflector. This nuclear heat source is also per unit total volume. In equation 4-2, k is the thermal conductivity and T represents the solid temperature.

From equation 4-2, the steady state equation for the conservation of solid energy in a 1D Cartesian coordinate system can be written as:

$$\frac{d}{dx}\left[(1-\varepsilon)k\frac{dT}{dx}\right]+q_{fs}+q_{nuclear}=0 \tag{4-3}$$

Where the source of energy per unit total volume due to convection, q_{fs}, is given by:

$$q_{fs} = h\left(\frac{F}{V}\right)\left(T_{gas} - T\right) \tag{4-4}$$

In equation 4-4, h is the solid-gas heat transfer coefficient, F/V is the ratio of the surface area of the solid exposed to the gas, to the volume and T_{gas} represents the gas temperature.

Following the finite volume method for diffusion problems outlined in Versteeg and Malalasekera, (1995), the first step in the finite volume method involves dividing the domain into discrete control volumes. In Figure 4-1, a 1D Cartesian domain with constant temperature boundary conditions has been divided into three uniform control volumes. Each control volume has boundaries and a nodal point. In the case of the control volumes at the edge of the domain, the physical boundaries coincide with the control volume boundaries.

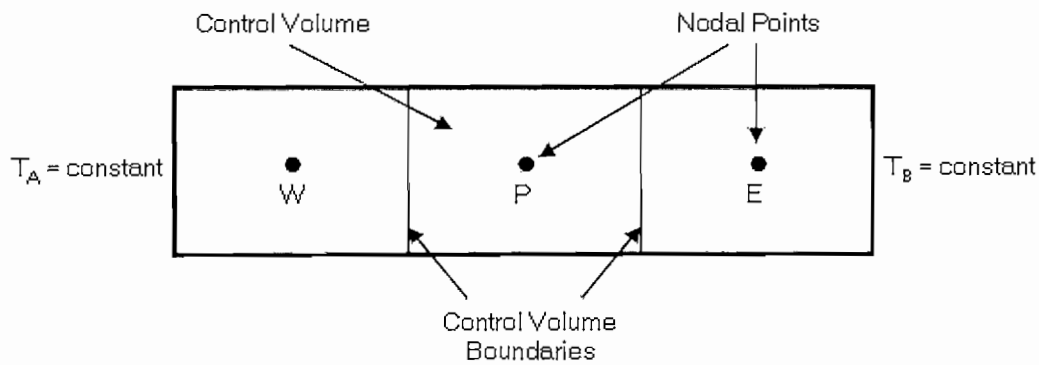

Figure 4-1: Grid Generation – Control Volumes

The conventional system of notation for discrete control volumes is shown in Figure 4-2. A general nodal point is defined as P with its east and west neighbours identified as W and E respectively. The west and east control volume boundaries for P are identified as w and e respectively. The relevant distances are identified accordingly. The control volume width is defined as $\Delta x = \delta x_{we}$. (Versteeg and Malalasekera, 1995)

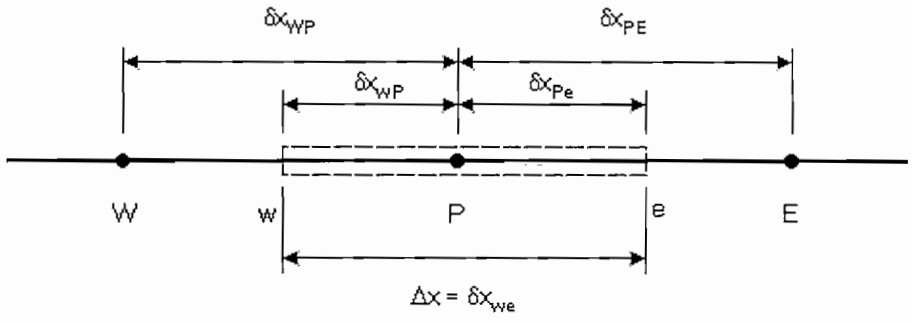

Figure 4-2: Discrete Control Volume Notation

The next step involves integrating the governing equation, equation 4-3, over the control volume to obtain a discretised equation at nodal point P. (Versteeg and Malalasekera, 1995)

$$\int_V \frac{d}{dx}\left[(1-\varepsilon)k\frac{dT}{dx}dV\right] + \int_V (q_{fs} + q_{nuclear})dV = 0 \tag{4-5}$$

This yields the following equations,

$$\int_V \frac{d}{dx}\left[(1-\varepsilon)k\frac{dT}{dx}dV\right] = \left[(1-\varepsilon)kA\frac{dT}{dx}\right]_e - \left[(1-\varepsilon)kA\frac{dT}{dx}\right]_w \tag{4-6}$$

$$\int_V (q_{fs} + q_{nuclear})dV = q_{nuclear}V + hFT_{gas} - hFT \tag{4-7}$$

In equation 4-6, A is the face area and V is the volume. In equation 4-7, F, the area of the gas exposed to the solid. The surface area of all the fuel spheres in a cell is given by (Du Toit, 2007):

$$F = V(1-\varepsilon)\frac{6}{d} \tag{4-8}$$

Where, d is the diameter of the fuel sphere. In a vertical flow channel, the surface area is given by (Du Toit, 2007):

$$F = \frac{4}{D}\varepsilon V \tag{4-9}$$

Where, D is the hydraulic diameter of the channel.

Equations 4-6 and 4-7 can be written as,

$$\left[k_{eff}A\frac{dT}{dx}\right]_e - \left[k_{eff}A\frac{dT}{dx}\right]_w + q_{nuclear}V + hFT_{gas} - hFT = 0 \qquad (4\text{-}10)$$

Where, $k_{eff} = (1-\varepsilon)k$.

While the values of T and k_{eff} are defined and evaluated at the nodal points, the gradients and interface values at the control volume faces are mostly simply determined by linear approximations of the properties between the nodal points, otherwise known as central differencing. It is shown in Versteeg and Malalasekera, (1995) that this central differencing scheme is second order accurate. Furthermore, it is shown that for a non-uniform grid, linearly interpolated values of k_{eff} at the east and west faces can be calculated as follows:

$$k_{eff\ e} = (1-f_P)k_{eff\ P} + f_P k_{eff\ E} \qquad (4\text{-}11)$$

$$k_{eff\ w} = (1-f_W)k_{eff\ W} + f_W k_{eff\ P} \qquad (4\text{-}12)$$

Where,

$$f_P = \frac{\delta x_{Pe}}{\delta x_{Pe} + \delta x_{eE}} \qquad (4\text{-}13)$$

$$f_W = \frac{\delta x_{Ww}}{\delta x_{Ww} + \delta x_{wP}} \qquad (4\text{-}14)$$

For a uniform grid, $f_W = f_P = 0.5$. Hence, equations 4-11 and 4-12 simplify to,

$$k_{eff\ e} = \frac{k_{eff\ P} + k_{eff\ E}}{2} \qquad (4\text{-}15)$$

$$k_{eff\ w} = \frac{k_{eff\ W} + k_{eff\ P}}{2} \qquad (4\text{-}16)$$

In the case of non-uniform thermal conductivity, as explained in Patankar, (1980), the method of linear interpolation can lead to erroneous results as this method is not capable of correctly handling a discontinuity in the diffusion coefficient. Patankar, (1980) goes on to outline a more accurate method where the interface thermal conductivity is calculated as the harmonic mean of k_P and k_E rather than the arithmetic mean as described above.

From a steady state one-dimensional analysis of a composite slab, the heat flux at the interface e is (Patankar, 1980),

$$q_e = \frac{T_P - T_E}{\delta x_{Pe} / k_{eff\,P} + \delta x_{eE} / k_{eff\,E}} \tag{4-17}$$

Combining equations 4-15 and 4-17,

$$k_{eff\,e} = \left(\frac{1 - f_e}{k_{eff\,P}} + \frac{f_e}{k_{eff\,E}} \right)^{-1} \tag{4-18}$$

This is similarly calculated for the thermal conductivity at interface w, $k_{eff\,w}$.

The interface gradients are calculated as,

$$\left[k_{eff} A \frac{dT}{dx} \right]_e = k_{eff\,e} A_e \left(\frac{T_E - T_P}{\delta x_{PE}} \right) \tag{4-19}$$

$$\left[k_{eff} A \frac{dT}{dx} \right]_w = k_{eff\,w} A_w \left(\frac{T_P - T_W}{\delta x_{WP}} \right) \tag{4-20}$$

Substituting equations 4-19 and 4-20 into equation 4-10 and rearranging,

$$\left(\frac{k_{eff\,e} A_e}{\delta x_{PE}} + \frac{k_{eff\,w} A_w}{\delta x_{WP}} + hF \right) T_P = \left(\frac{k_{eff\,w} A_w}{\delta x_{WP}} \right) T_W + \left(\frac{k_{eff\,e} A_e}{\delta x_{PE}} \right) T_E + q_{nuclear} V + hF T_{gas} \tag{4-21}$$

Equation 4-21 can be rewritten as,

$$a_P T_P = a_W T_W + a_E T_E + S_u \tag{4-22}$$

Where,

$$
\begin{aligned}
a_P &= \left(a_W + a_E - S_P\right) \\
a_W &= \left(\frac{k_{eff\ w} A_w}{\delta x_{WP}}\right) \\
a_E &= \left(\frac{k_{eff\ e} A_e}{\delta x_{PE}}\right) \\
S_P &= -hF \\
S_u &= q_{nuclear} V + hFT_{gas}
\end{aligned}
\tag{4-23}
$$

For the interior nodes, equation 4-23 is well specified. However, the boundary nodes require special attention (Versteeg and Malalasekera, 1995).

Let us consider the 1D steady state conduction problem shown in Figure 4-3. The left boundary is maintained at a constant, fixed temperature. The right boundary is an adiabatic wall. The domain has been divided into four control volumes.

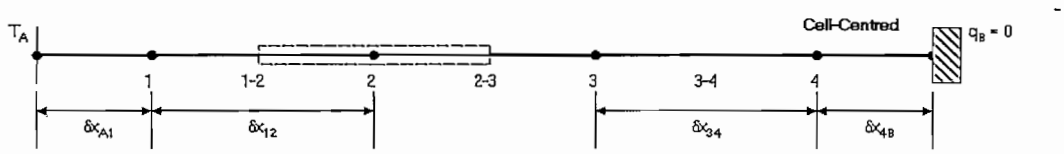

Figure 4-3: 1D Steady State Conduction Problem

For the interior nodes 2 and 3, equation 4-23 applies directly. For boundary node 1, equation 4-23 becomes:

$$
\begin{aligned}
a_1 &= \left(a_W + a_2 - S_1\right) \\
a_W &= 0 \\
a_2 &= \left(\frac{k_{eff\ 1-2} A_{1-2}}{\delta x_{12}}\right) \\
S_1 &= -hF - \left(\frac{k_{eff\ 1} A_1}{\delta_{xA1}}\right) \\
S_u &= q_{nuclear} V + hFT_{gas} + \left(\frac{k_{eff\ 1} A_1}{\delta_{xA1}}\right) T_A
\end{aligned}
\tag{4-24}
$$

And for boundary node 4, equation 4-23 becomes:

$$
\begin{aligned}
a_4 &= (a_3 + a_E - S_4) \\
a_3 &= \left(\frac{k_{eff\,3-4} A_{3-4}}{\delta x_{34}} \right) \\
a_E &= 0 \\
S_4 &= -hF \\
S_u &= q_{nuclear} V + hFT_{gas}
\end{aligned}
\tag{4-25}
$$

In the case of boundary node 1, the fixed boundary condition enters the calculation as a source term and the link to the left boundary is suppressed by setting a_W equal to zero. (Versteeg and Malalasekera, 1995)

In the case of boundary node 4, there are no additional source terms associated with the zero flux boundary condition. As for boundary node 1, the link to the right boundary is suppressed by setting a_E equal to zero. (Versteeg and Malalasekera, 1995)

This discretisation will produce one equation for each of the nodal points resulting in a set of algebraic equations in the form of equation 4-26, which can be solved using a direct method in MATLAB.

$$[B][T] = [S_u] \tag{4-26}$$

Iterative methods like the Jacobi and Gauss-Seidel point-iterative methods or the Tri-Diagonal Matrix Algorithm (TDMA) are generally more economical than direct methods. The main advantage of these iterative methods is that only the non-zero coefficients of the equations need to be stored in memory. (Versteeg and Malalasekera, 1995) An iterative method for the solution of this set of algebraic equations was not considered, as the scope of this work is limited to 1D and hence storage will not be a problem.

4.2 VERTEX-CENTRED NUMERICAL METHOD

The difference between the CC method and the VC method is that the CC method calculates the temperatures at the centre of the cell while the VC method calculates the temperatures at the faces. In the VC method a co-located grid is placed on the original grid as shown in Figure 4-4.

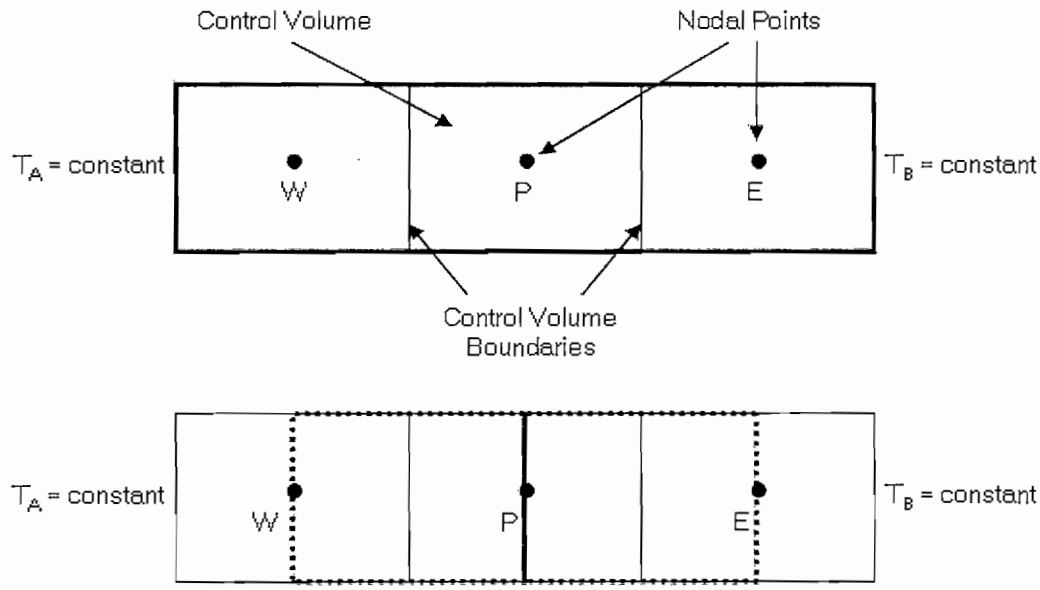

Figure 4-4: Difference in Grid Definition between CC and VC Methods

The cell centres of the co-located grid now coincide with the faces of the original grid and in a uniform grid, the faces of the co-located grid coincide with the cell centres of the original grid. The location of the co-located grid faces relative to the original grid cell centres will be addressed later in this chapter.

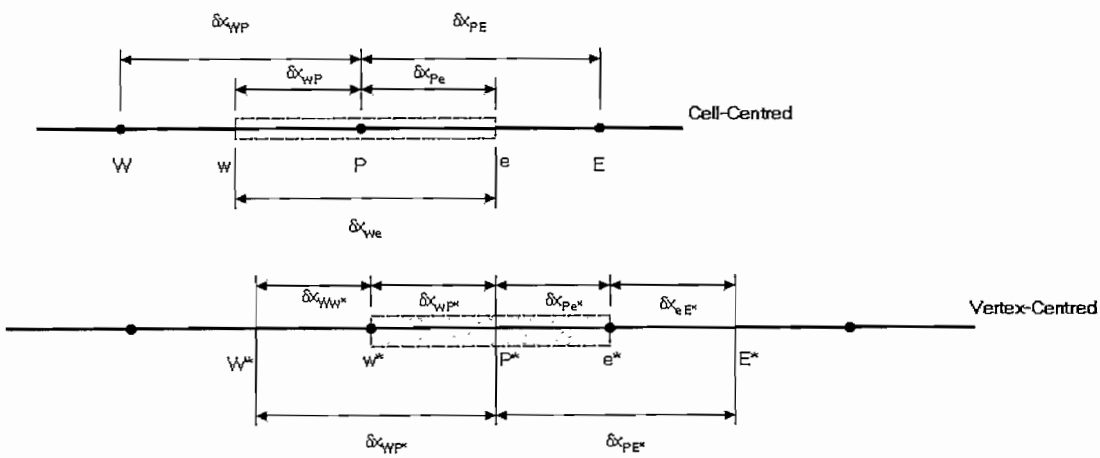

Figure 4-5: CC and VC Discrete Control Volume Notation

Following the notation of Figure 4-5, the nodal points of the co-located grid are identified as P* with a west neighbour, W* and an east neighbour, E*. The east and west faces are identified as e* and w* respectively.

Since the faces of the co-located grid are aligned with the nodal points of the original grid, it is no longer necessary to calculate the harmonic mean of the properties between the nodal points.

Following the same method described for the Cell-Centred numerical discretisation, Equations 4-19 and 4-20 become,

$$\left[k_{eff} A \frac{dT}{dx}\right]_{e*} = k_{eff\ e*} A_{e*} \left(\frac{T_{E*} - T_{P*}}{\delta x_{PE*}}\right) \tag{4-27}$$

$$\left[k_{eff} A \frac{dT}{dx}\right]_{w*} = k_{eff\ w*} A_{w*} \left(\frac{T_{P*} - T_{W*}}{\delta x_{WP*}}\right) \tag{4-28}$$

Substituting equations 4-27 and 4-28 into equation 4-10 and rearranging,

$$\left(\frac{k_{eff\ e*} A_{e*}}{\delta x_{PE*}} + \frac{k_{eff\ w*} A_{w*}}{\delta x_{WP*}} + hF\right) T_{P*} = \left(\frac{k_{eff\ w*} A_{w*}}{\delta x_{WP*}}\right) T_{W*} + \left(\frac{k_{eff\ e*} A_{e*}}{\delta x_{PE*}}\right) T_{E*} + q_{nuclear} V + hFT_{gas} \tag{4-29}$$

Equation 4-29 can be rewritten as,

$$a_{P*} T_{P*} = a_{W*} T_{W*} + a_{E*} T_{E*} + S_u \tag{4-30}$$

Where,

$$\begin{aligned} a_{P*} &= \left(a_{W*} + a_{E*} - S_P\right) \\ a_{W*} &= \left(\frac{k_{eff\ w*} A_{w*}}{\delta x_{WP*}}\right) \\ a_{E*} &= \left(\frac{k_{eff\ e*} A_{e*}}{\delta x_{PE*}}\right) \\ S_{P*} &= -hF \\ S_u &= q_{nuclear} V + hFT_{gas} \end{aligned} \tag{4-31}$$

As mentioned earlier in this chapter, for a uniform grid, δx_{WP*} is equal to δx_{we}. This is because, for a uniform grid, the nodal points for the co-located grid are aligned with the faces of the original grid. This however, is not the case on a non-uniform grid.

In a non-uniform grid,

$$\delta x_{WP*} = \frac{\delta x_{WP}}{2} + \frac{\delta x_{PE}}{2} \tag{4-32}$$

δx_{PE} can be calculated similarly.

As with the CC method, equation 4-31 is well specified for the interior nodes. The boundary nodes still require special attention.

Let us again consider the 1D steady state conduction problem discussed earlier. Figure 4-6 shows the CC and VC discretisation. The domain has now been divided into 5 co-located control volumes represented by the subscript *.

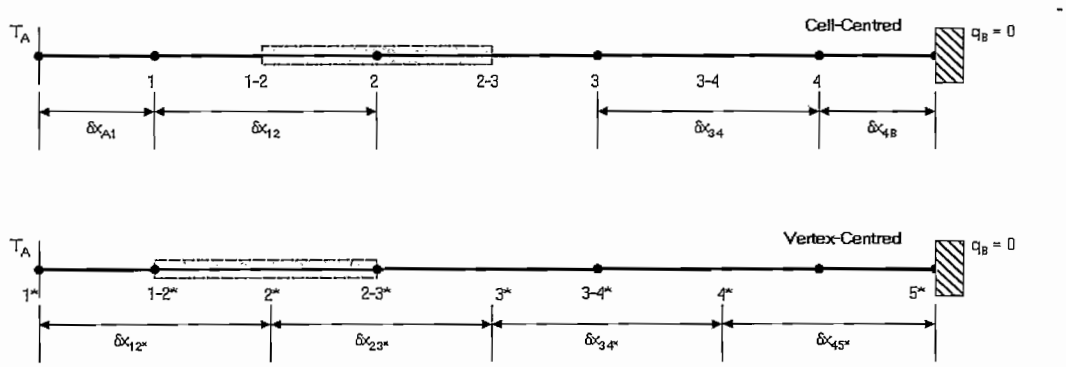

Figure 4-6: 1D Steady State Conduction Problem – CC and VC Method

For boundary node 2*, equation 4-31 becomes:

$$\begin{aligned} a_{2*} &= (a_{W*} + a_{3*} - S_{2*}) \\ a_{W*} &= 0 \\ a_{3*} &= \left(\frac{k_{eff\,2-3*} A_{2-3*}}{\delta x_{23*}} \right) \\ S_{2*} &= -hF - \left(\frac{k_{eff\,1-2*} A_{1-2*}}{\delta x_{12*}} \right) \\ S_u &= q_{nuclear} V + hFT_{gas} + \left(\frac{k_{eff\,1-2*} A_{1-2*}}{\delta x_{12*}} \right) T_A \end{aligned} \tag{4-33}$$

And for boundary node 4*, equation 4-31 becomes:

$$\begin{aligned} a_{4*} &= (a_{3*} + a_E - S_{4*}) \\ a_{3*} &= \left(\frac{k_{eff\,3-4*} A_{3-4*}}{\delta x_{34*}} \right) \\ a_E &= 0 \\ S_4 &= -hF \\ S_u &= q_{nuclear} V + hFT_{gas} \end{aligned} \tag{4-34}$$

As with the CC method, the discretisation yields a set of algebraic equations in the form of equation 4-26, which can be solved using a direct method in MATLAB.

4.3 FROM CARTESIAN TO CYLINDRICAL COORDINATE SYSTEM

In 4.1 and 4.2, the 1D steady state equation for the conservation of solid energy was discretised using both the CC and VC methods for a Cartesian coordinate system. Equations 4-21 and 4-29 are valid in a cylindrical coordinate system when the face area and cell volume are defined as:

$$A = 2\pi rz \tag{4-35}$$

$$V = 2\pi(r_2^2 - r_1^2)z \tag{4-36}$$

Where, r is the radius of the face, z is the height of the cell, r_2 is the outer radius of the cell and r_1 is the inner radius of the cell.

In the CC method the fluxes are calculated at the faces while in the VC method the fluxes are calculated at the nodal points. This means that the face area must be determined at the faces for the CC method and at the centre of the cell for the VC method.

4.4 SUMMARY

In this chapter the steady state equation for the conservation of solid energy in a 1D Cartesian coordinate system was discretised using the Cell-Centred numerical method. It was shown that while the scalar properties and diffusion coefficient is defined and evaluated at the nodal points, the gradients and interface values require some form of approximation. Although, Versteeg and Malalasekera, (1995) suggest a simple linear approximation i.e. central differencing, Patankar, (1980) suggests that this method is not capable of correctly handling a discontinuity in the diffusion coefficient. The more accurate method of calculating the harmonic mean of the diffusion coefficient rather than the harmonic average, suggested by Patankar, (1980), is then discussed. The treatment of the boundary conditions is also discussed with focus on a fixed temperature boundary condition and an adiabatic wall.

The steady state equation for the conservation of solid energy in a 1D Cartesian coordinate system was discretised using the Vertex-Centred numerical method. The treatment of a non-uniform grid was discussed. The treatment of a fixed temperature boundary and an adiabatic wall was also discussed.

Finally, although both discretisations were carried out in a Cartesian coordinate system, they are shown to be valid for a cylindrical coordinate system when the face area and cell volume are correctly defined.

The CC implementation in MATLB was verified in a Cartesian and cylindrical coordinate system against Star-CD which employs a cell-centred based approach. The VC implementation in MATLAB was also verified in both reference frames against Flownex which employs a vertex-centred based approach. The results are presented in the following chapter.

5 VERIFICATION OF MATLAB IMPLEMENTATION

5.1 CARTESIAN TEST CASES

The basic test case selected is a 1m long block of uniform material with fixed temperature conditions at both ends, as shown in Figure 5-1.

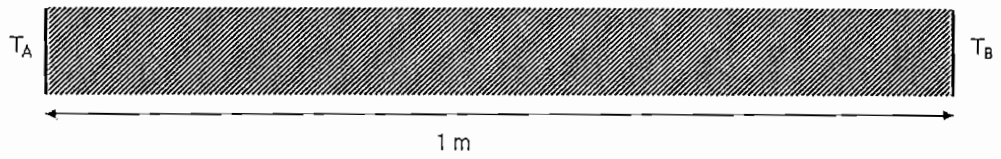

Figure 5-1: Basic Test Case

In each verification test an additional property was added. The verification tests used for both the CC and VC implementations are described in Table 8

Table 8: Cartesian Test Description

Test Number	Test Description
Test 1	Uniform Grid, Constant Conductivity, No Source
Test 2	Non-Uniform Grid, Constant Conductivity, No Source
Test 3	Uniform Grid, Step Change in Conductivity, No Source
Test 4	Non-Uniform Grid, Step Change in Conductivity, No Source
Test 5	Uniform Grid, Step Change in Conductivity, Uniform Heat Source
Test 6	Uniform Grid, Step Change in Conductivity, Step Change in Heat Source
Test 7	Uniform Grid, Uniform Conductivity, No Heat Source, Uniform Convective Sink

5.1.1 *Test 1 – Uniform Grid, Uniform Conductivity, No Source*

The purpose of Test 1 was to verify the grid discretisation for a uniform grid. The length of the block was divided into 10 equal control volumes as shown in Figure 5-2. No sources were added and the effective thermal conductivity across the block was uniform (k_{eff} = 0.02637 W/m.K). The west boundary was fixed at 800 K and the east boundary was fixed at 300 K.

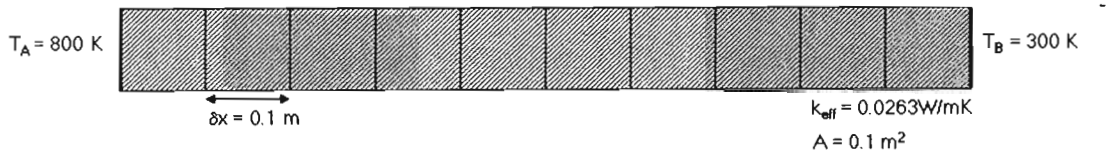

Figure 5-2: Test 1 Geometry

The results of the MATLAB CC implementation are compared with the results from Star-CD in Figure 5-3. The results of the MATLAB VC implementation are compared with the results from Flownex in Figure 5-4.

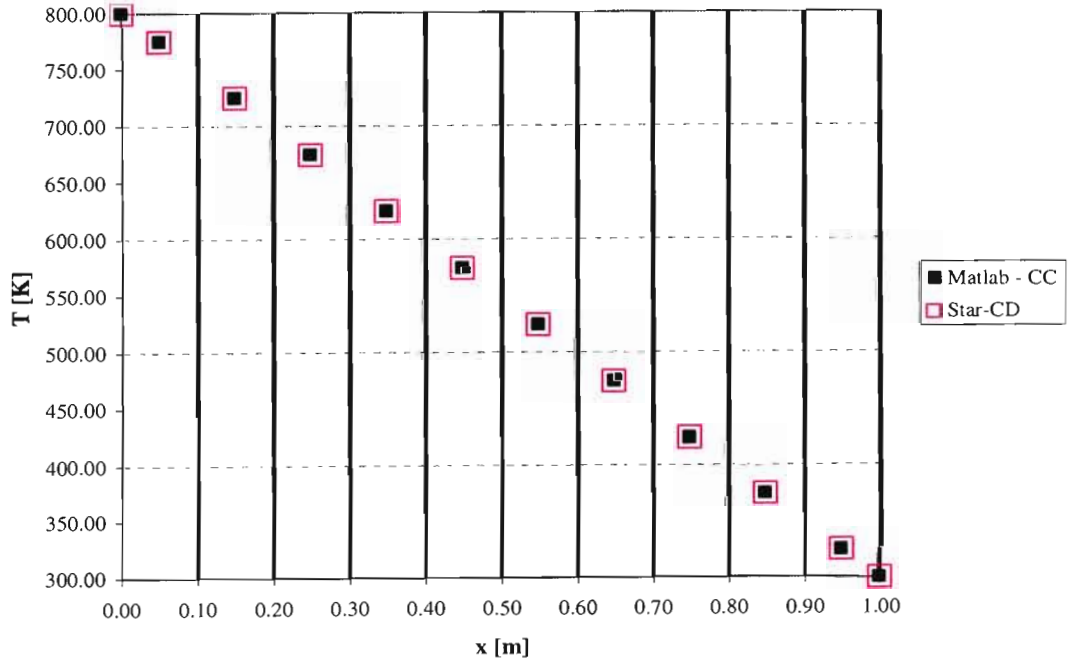

Figure 5-3: Test 1 Result – MATLAB CC vs. Star-CD

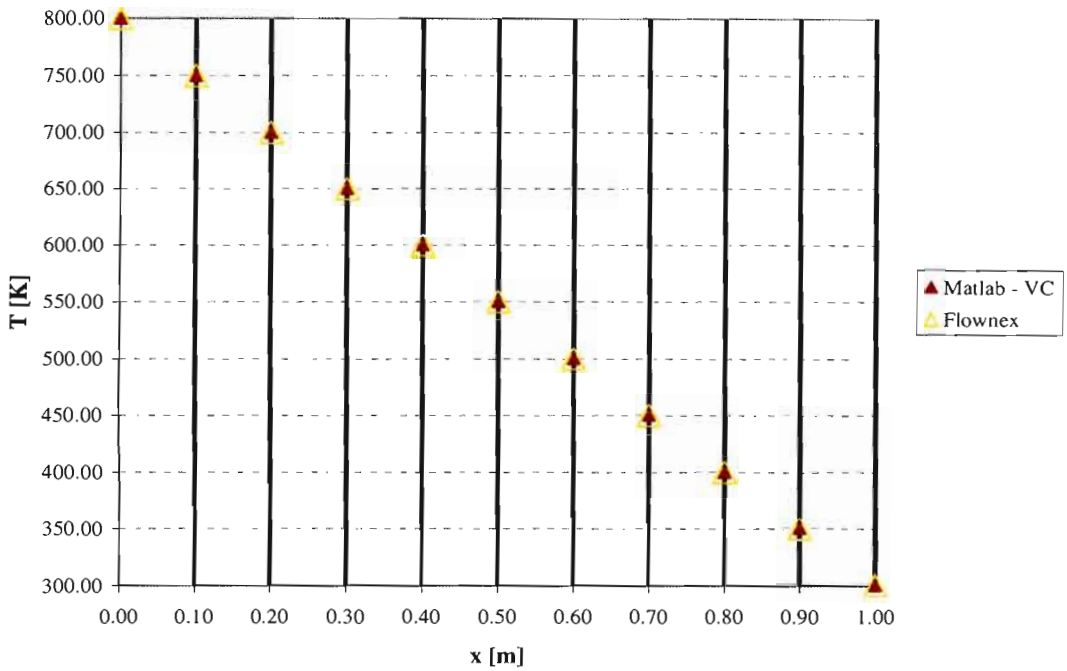

Figure 5-4: Test 1 Result – MATLAB VC vs. Flownex

As expected the results match exactly. This is sufficient verification that the grid discretisation for a uniform grid has been implemented correctly.

5.1.2 Test 2 - Non-Uniform Grid, Uniform Conductivity, No Source

The purpose of Test 2 was to verify the grid discretisation for a non-uniform grid. The length of the block was divided into 10 non-equal control volumes as shown in Figure 5-5. For simplicity, each control volume was chosen as 1.04 times the length of its west neighbour. No sources were added and the effective conductivity across the block was uniform (k_{eff} = 0.02637 W/m.K). The west boundary was fixed at 800 K and the east boundary was fixed at 300 K.

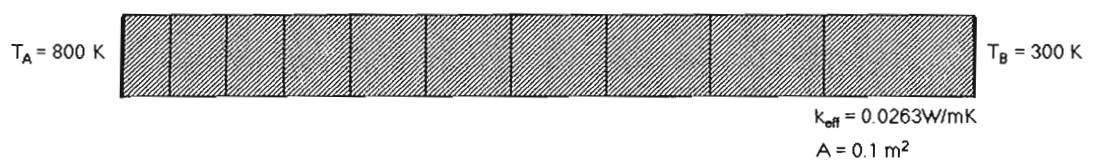

Figure 5-5: Test 2 Geometry

The results of the MATLAB CC implementation are compared with the results from Star-CD in Figure 5-6. The results of the MATLAB VC implementation are compared with the results from Flownex in Figure 5-7.

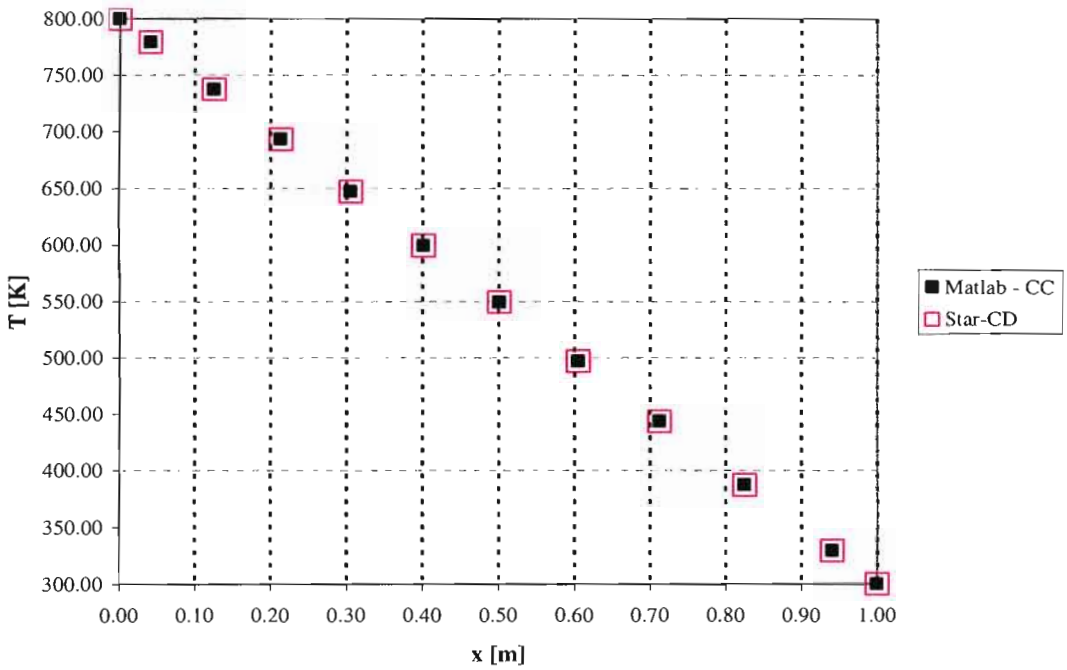

Figure 5-6: Test 2 Result – MATLAB CC vs. Star-CD

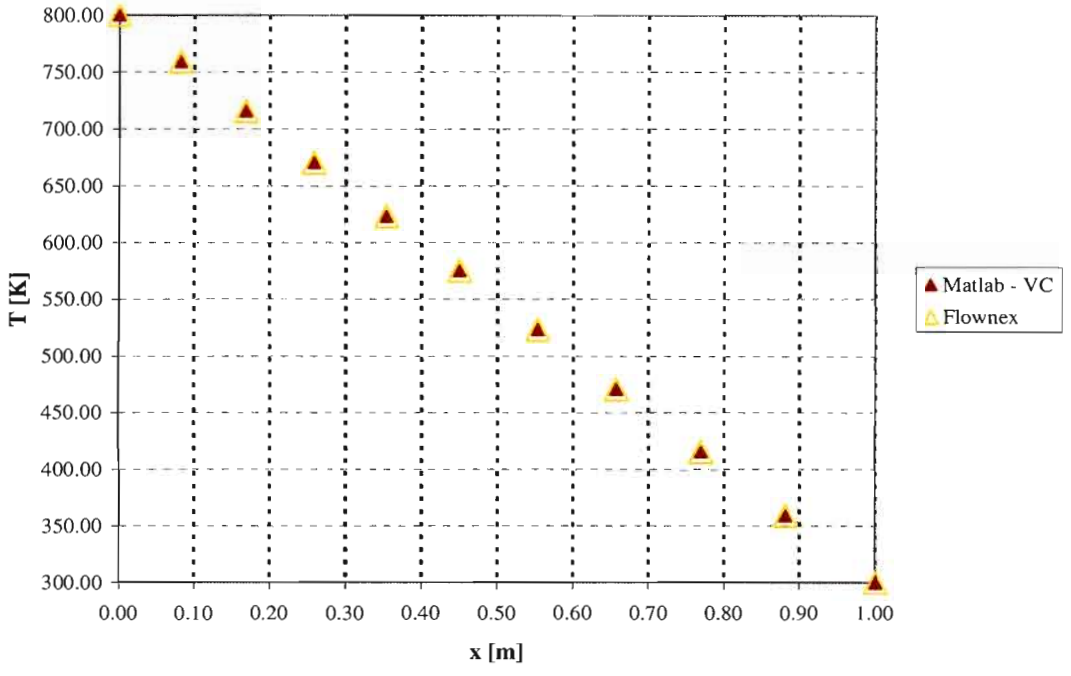

Figure 5-7: Test 2 Result – MATLAB VC vs. Flownex

As expected the results match exactly. This is sufficient verification that the grid discretisation for a non-uniform grid has been implemented correctly.

5.1.3 Test 3 - Uniform Grid, Step Change in Conductivity, No Source

The purpose of Test 3 was to verify the calculation of the effective conductivity at the interfaces for a uniform grid. The length of the block was divided into 10 equal control volumes as shown in Figure 5-8. The west boundary was fixed at 800 K and the east boundary was fixed at 300 K. No sources were added but the effective conductivity across the block was non-uniform. The first 5 cells had an effective conductivity of 0.02637 W/m.K while the next 5 cells had an effective conductivity of 0.018459 W/m.K.

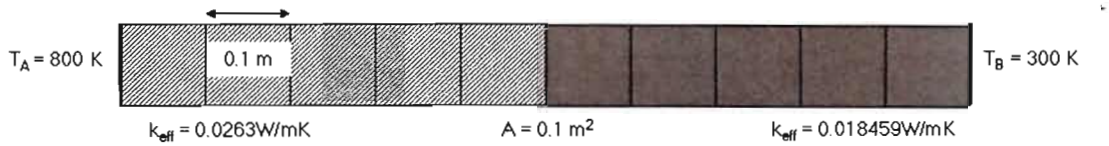

Figure 5-8: Test 3 Geometry

The results of the MATLAB CC implementation are compared with the results from Star-CD in Figure 5-9. Although the VC method does not calculate the effective conductivities at the interfaces, a comparison of the VC results is shown in Figure 5-10 for completeness.

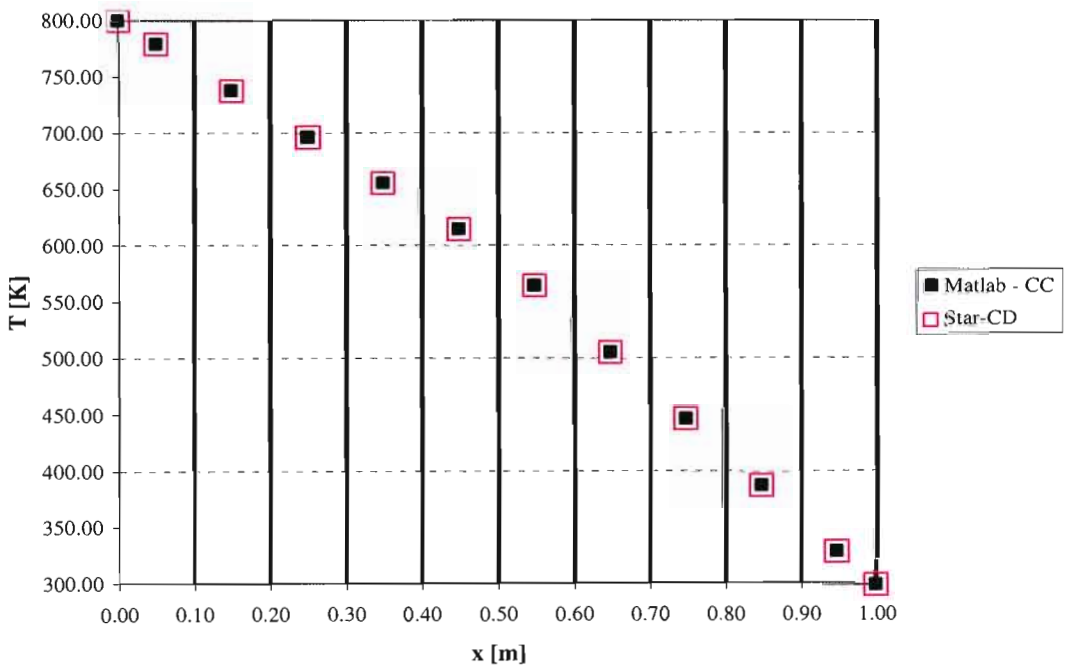

Figure 5-9: Test 3 Result – MATLAB CC vs. Star-CD

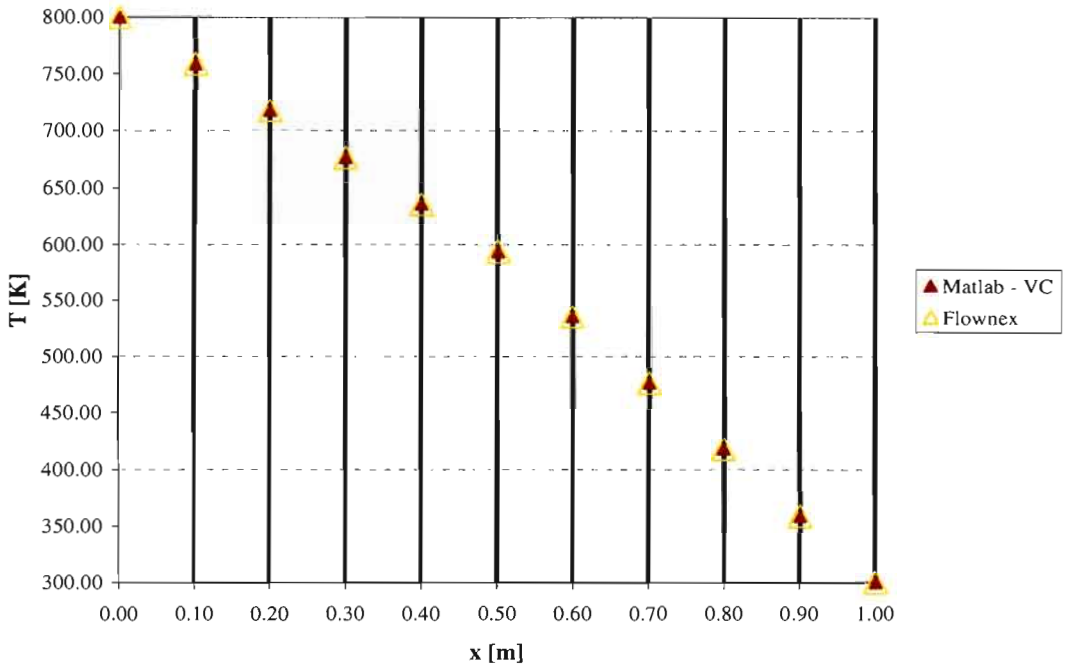

Figure 5-10: Test 3 Result – MATLAB VC vs. Flownex

As expected the results match exactly. This is sufficient verification that the effective conductivities at the interfaces are being calculated correctly for a uniform grid.

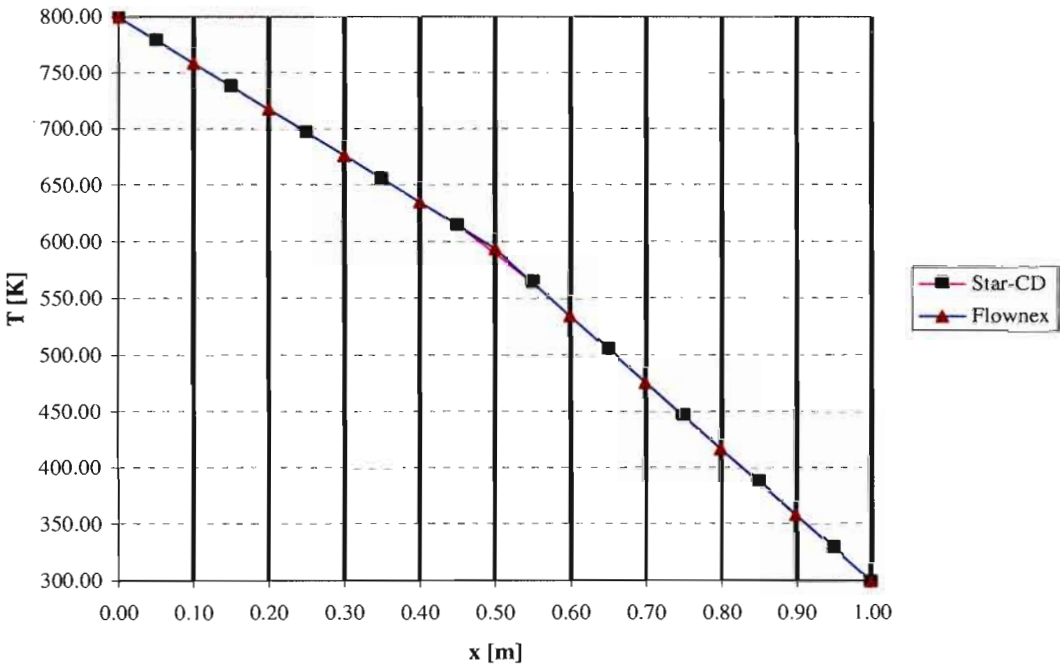

Figure 5-11: Test 3 Result – Star-CD vs. Flownex

Figure 5-11 shows a comparison of the results from Star-CD and Flownex. It is interesting to note that at the interface which sees the discontinuity in the effective conductivity there is a difference between the CC and the VC result. This is because the VC method does not approximate the effective conductivity at the interface like the CC method does. The VC method reports a more accurate value of temperature at the interface that sees the discontinuity. The CC method, on the contrary reports an interpolated value at this interface.

5.1.4 Test 4 - Non-Uniform Grid, Step Change in Conductivity, No Source

The purpose of Test 4 was to verify the calculation of the effective conductivity at the interfaces for a non-uniform grid. The length of the block was divided into 10 non-equal control volumes as shown in Figure 5-12. The cell sizes were the same as for Test 2. The west boundary was fixed at 800 K and the east boundary was fixed at 300 K. No sources were added but the effective conductivity across the block was non-uniform. The first 5 cells had an effective conductivity of 0.02637 W/m.K while the next 5 cells had an effective conductivity of 0.018459 W/m.K.

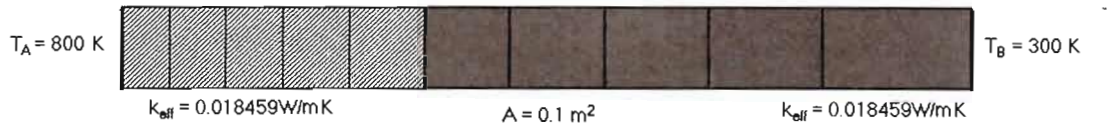

Figure 5-12: Test 4 Geometry

The results of the MATLAB CC implementation are compared with the results from Star-CD in Figure 5-13. Although the VC method does not calculate the effective conductivities at the interfaces, a comparison of the VC results is shown in Figure 5-14 for completeness.

As expected the results match exactly. This is sufficient verification that the effective conductivities at the interfaces are being calculated correctly for a non-uniform grid.

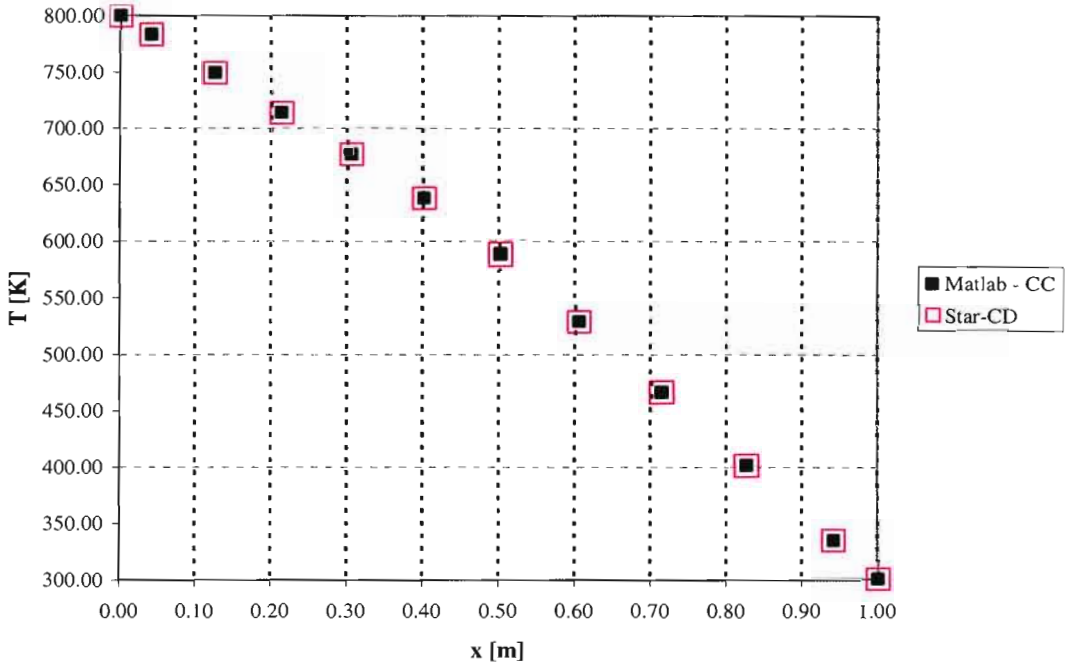

Figure 5-13: Test 4 Result – MATLAB CC vs. Star-CD

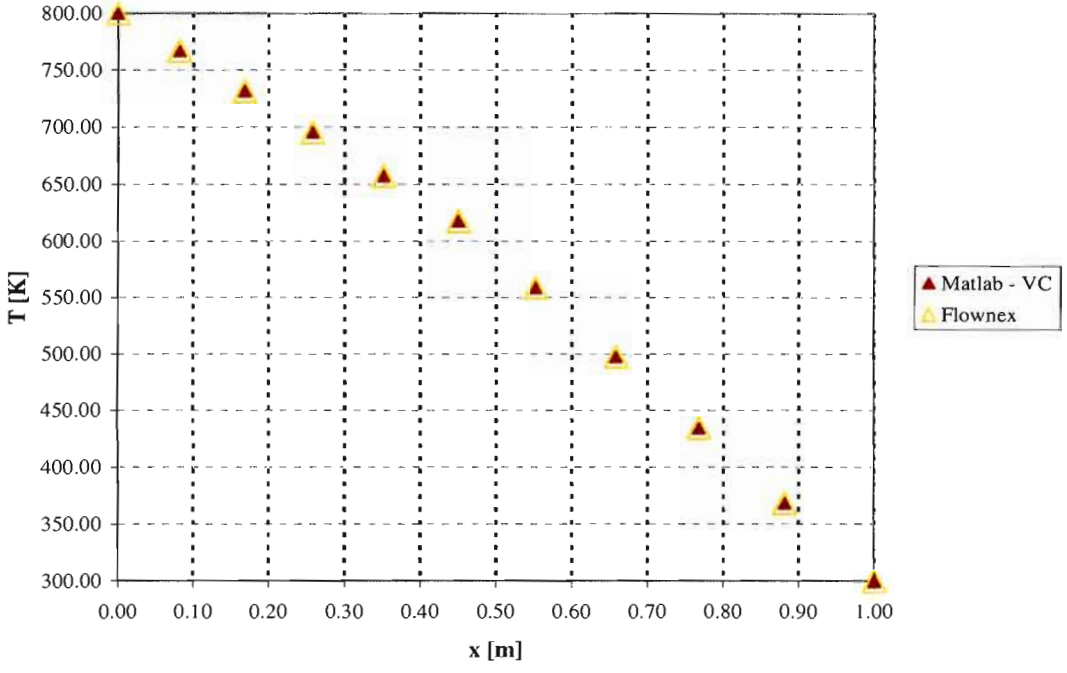

Figure 5-14: Test 4 Result – MATLAB VC vs. Flownex

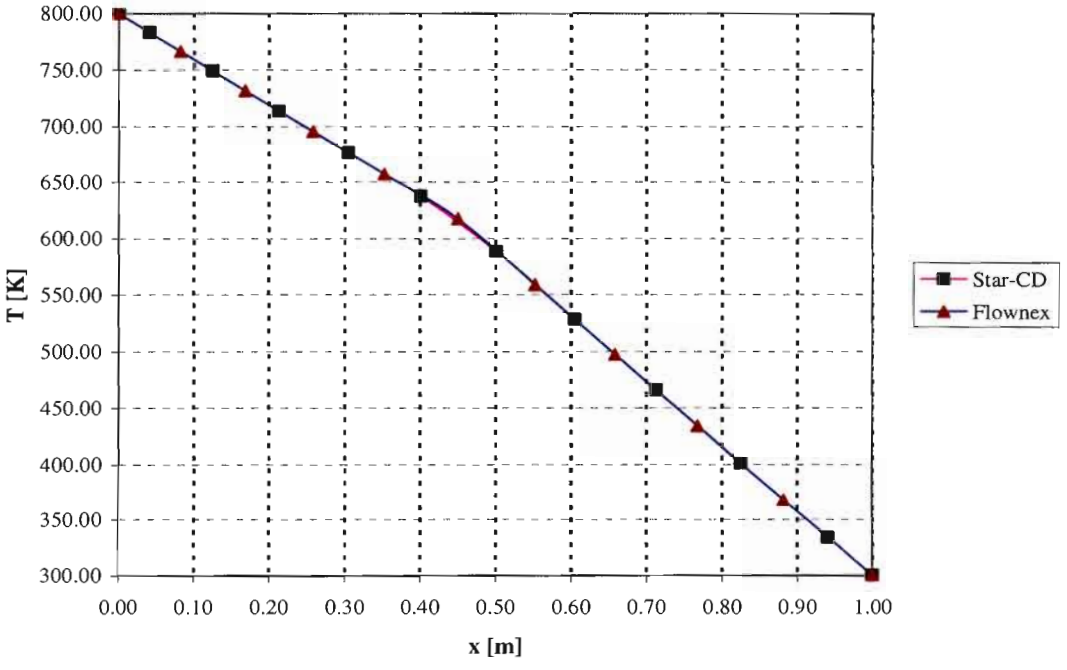

Figure 5-15: Test 4 Result – Star-CD vs. Flownex

Figure 5-15 shows a comparison of the results from Star-CD and Flownex. The difference in the CC and VC result at the interface that sees the discontinuity in the effective conductivity is again visible, as expected.

5.1.5 Test 5 - Uniform Grid, Step Change in Conductivity, Uniform Nuclear Heat Source

The purpose of Test 5 was to verify the source discretisation. As the discretisation of a non-uniform grid has already been adequately verified, this test was only carried out on a uniform grid. (The application of a non-uniform nuclear heat source is tested at a later stage on a non-uniform grid in the cylindrical coordinate system). The length of the block was divided into 10 equal control volumes as shown in Figure 5-16. The west boundary was fixed at 800 K and the east boundary was fixed at 300 K. The effective conductivity across the block was non-uniform. The first 5 cells had an effective conductivity of 0.02637 W/m.K while the next 5 cells had an effective conductivity of 0.018459 W/m.K. A uniform nuclear heat source of 10 W/m^3 was applied across all 10 cells.

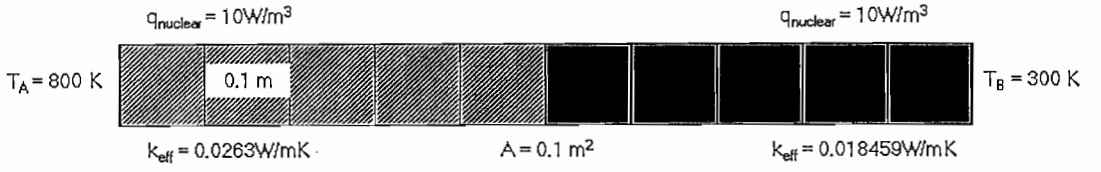

Figure 5-16: Test 5 Geometry

The results of the MATLAB CC implementation are compared with the results from Star-CD in Figure 5-17. The results of the MATLAB VC implementation are compared with the results from Flownex in Figure 5-18.

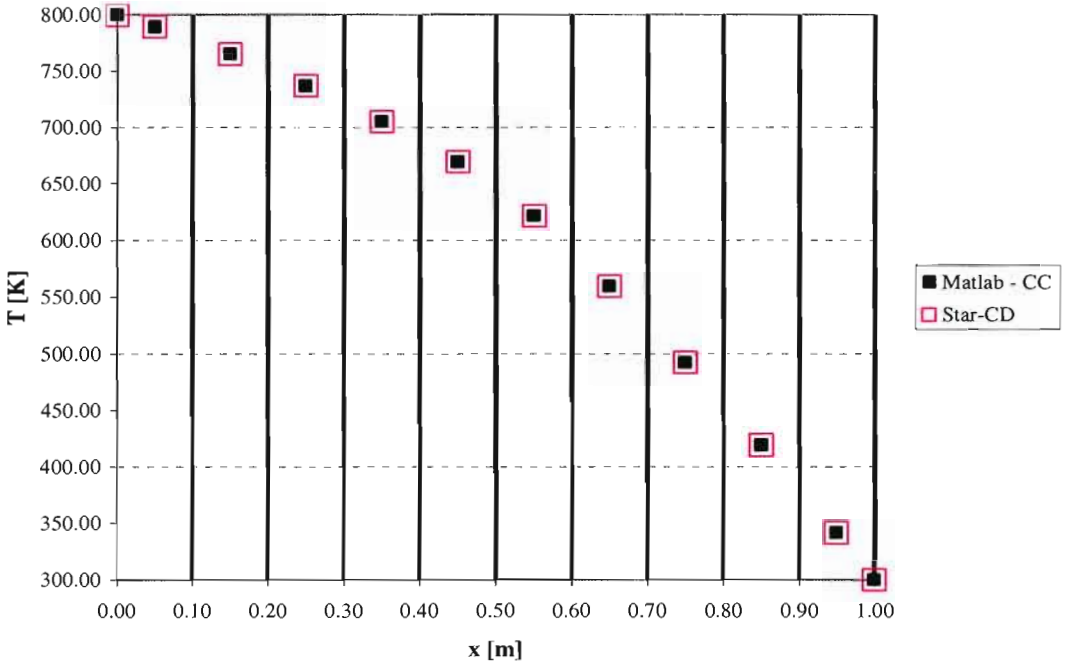

Figure 5-17: Test 5 Result – MATLAB CC vs. Star-CD

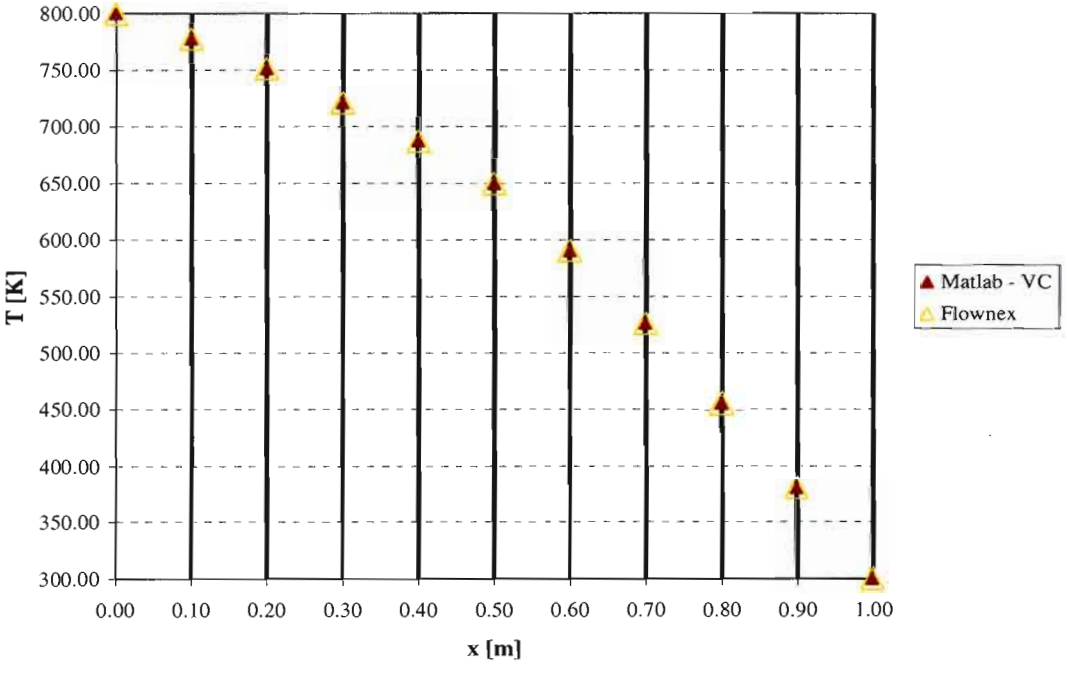

Figure 5-18: Test 5 Result – MATLAB VC vs. Flownex

As expected the results match exactly. This is sufficient verification that the source term is being discretised correctly.

5.1.6 *Test 6 - Uniform Grid, Step Change in Conductivity, Step Change in Nuclear Heat Source*

The purpose of Test 6 was to verify that the source term was being applied over the correct volume. Although this does not directly apply to the CC method, both implementations were tested for completeness. The length of the block was divided into 10 equal control volumes as shown in Figure 5-19. The west boundary was fixed at 800 K and the east boundary was fixed at 300 K. The effective thermal conductivity across the block was non-uniform. The first 5 cells had an effective thermal conductivity of 0.02637 W/m.K while the next 5 cells had an effective thermal conductivity of 0.018459 W/m.K. A uniform nuclear heat source of 10 W/m^3 was applied across the first 5 cells only.

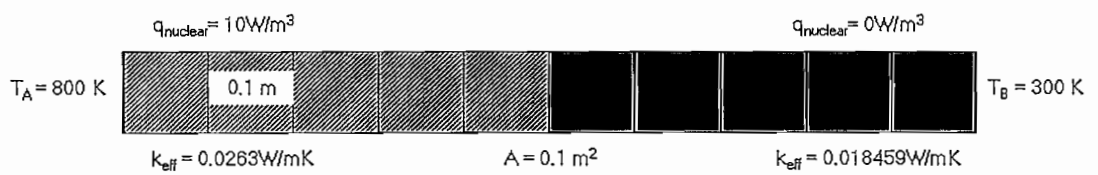

Figure 5-19: Test 6 Geometry

The results of the MATLAB CC implementation are compared with the results from Star-CD in Figure 5-20. The results of the MATLAB VC implementation are compared with the results from Flownex in Figure 5-21.

As expected the results match exactly. This is sufficient verification that the source term is being applied over the correct volume.

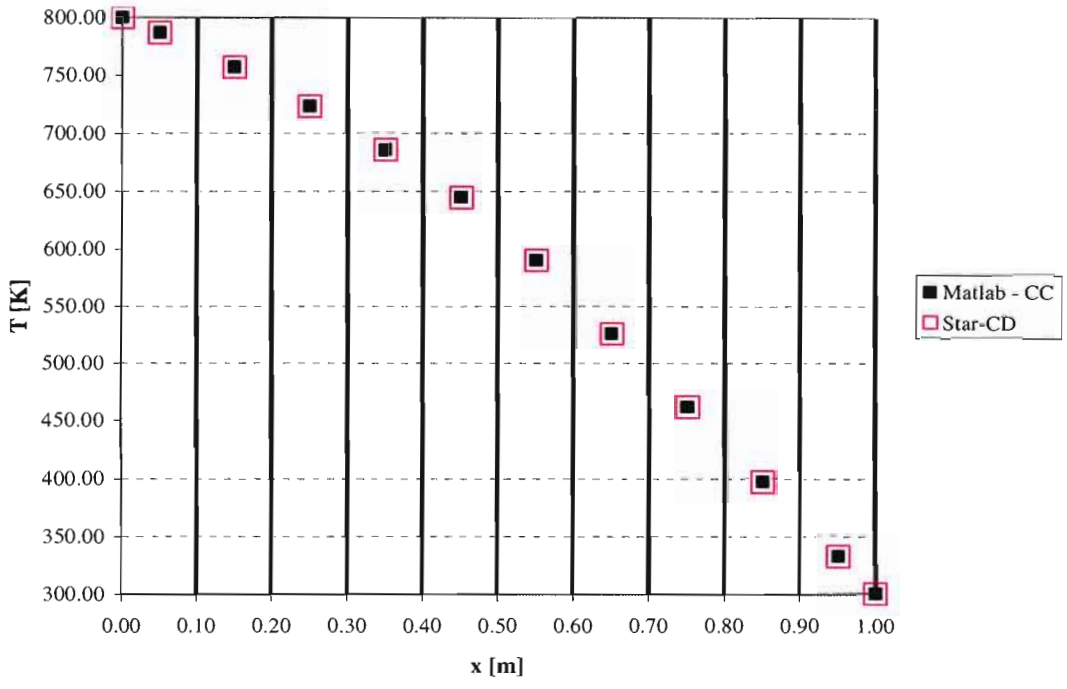

Figure 5-20: Test 6 Result – MATLAB CC vs. Star-CD

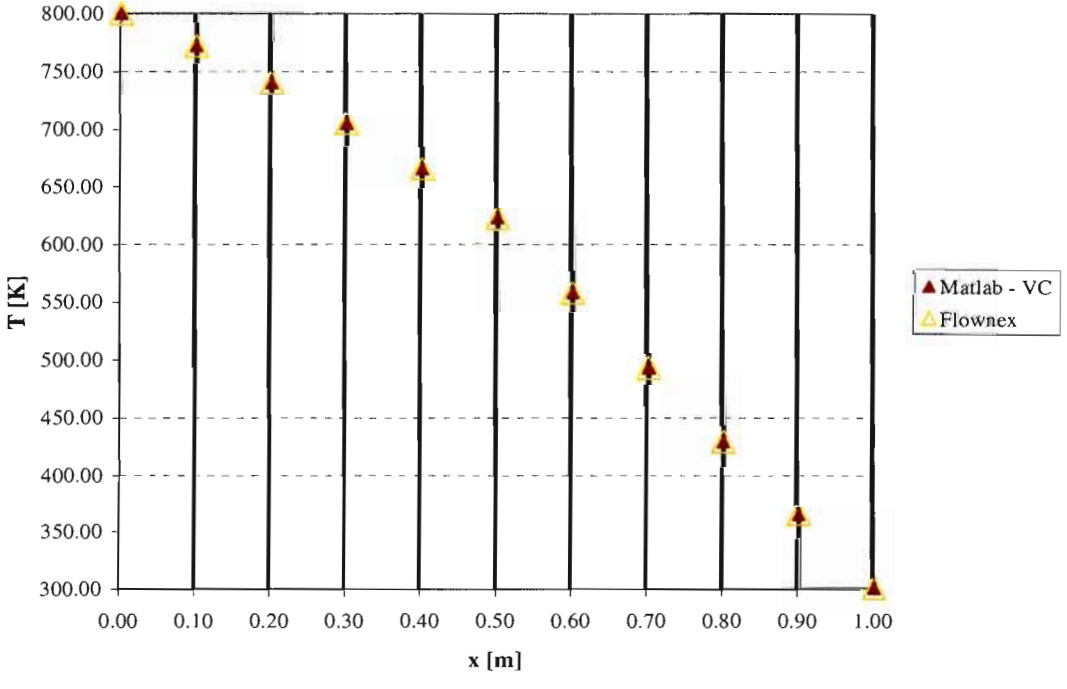

Figure 5-21: Test 6 Result – MATLAB VC vs. Flownex

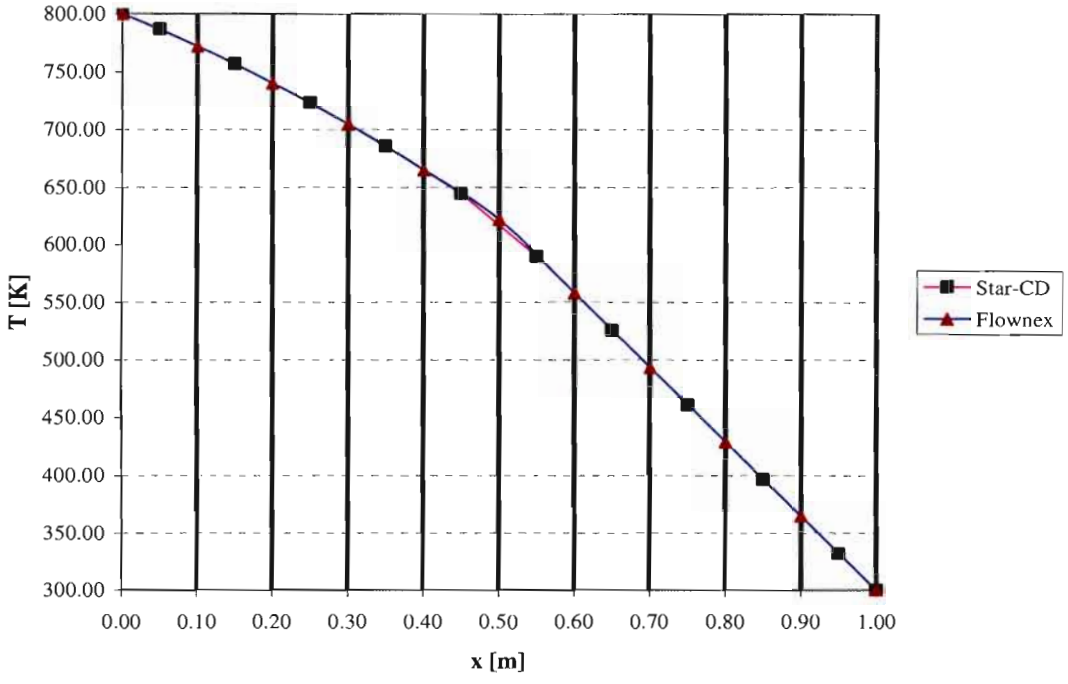

Figure 5-22: Test 6 Result – Star-CD vs. Flownex

Figure 5-22 shows a comparison of the results from Star-CD and Flownex. It has been shown that a difference in the temperatures reported at the interface that sees the discontinuity in the effective thermal conductivity is expected. However in this test case the discontinuity in the effective thermal conductivity coincides with a discontinuity in the source. No definitive conclusion can be made based on this result but it must be noted that the problem with a discontinuity in the source term can only really be seen on a non-uniform grid. In the VC method, on a uniform grid, the source at the interface is acting over half of the cell volume on either side of the interface. This coincides with the interpolated face values of the CC method. However, on a non-uniform grid, this is not the case.

5.1.7 Test 7 - Uniform Grid, Uniform Conductivity, No Nuclear Source, Uniform Convective Sink

The purpose of Test 7 was to verify the implementation of the convective sink. It is necessary to verify that the sink is being applied over the correct volume. Because of the findings from Test 6,

a uniform effective thermal conductivity was applied over the block. This eliminated the effect of a discontinuity in the effective thermal conductivity. The length of the block was divided into 10 equal control volumes as shown in Figure 5-23. The west boundary was fixed at 800 K and the east boundary was fixed at 300 K. The block has a uniform effective thermal conductivity of 0.02637 W/m.K. A uniform heat transfer coefficient of 5 W/m^2K, as well as a gas temperature of 300K, was applied across the last 5 cells.

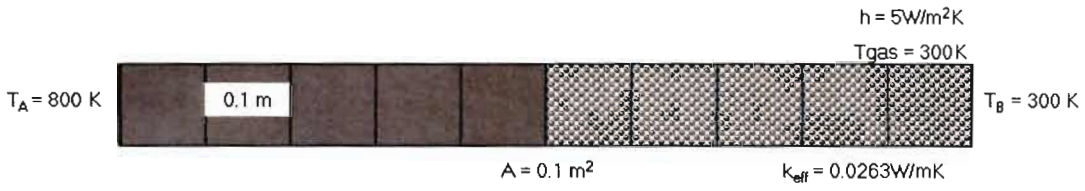

Figure 5-23: Test 7 Geometry

The results of the MATLAB CC implementation are compared with the results from Star-CD in Figure 5-24. The results of the MATLAB VC implementation are compared with the results from Flownex in Figure 5-25.

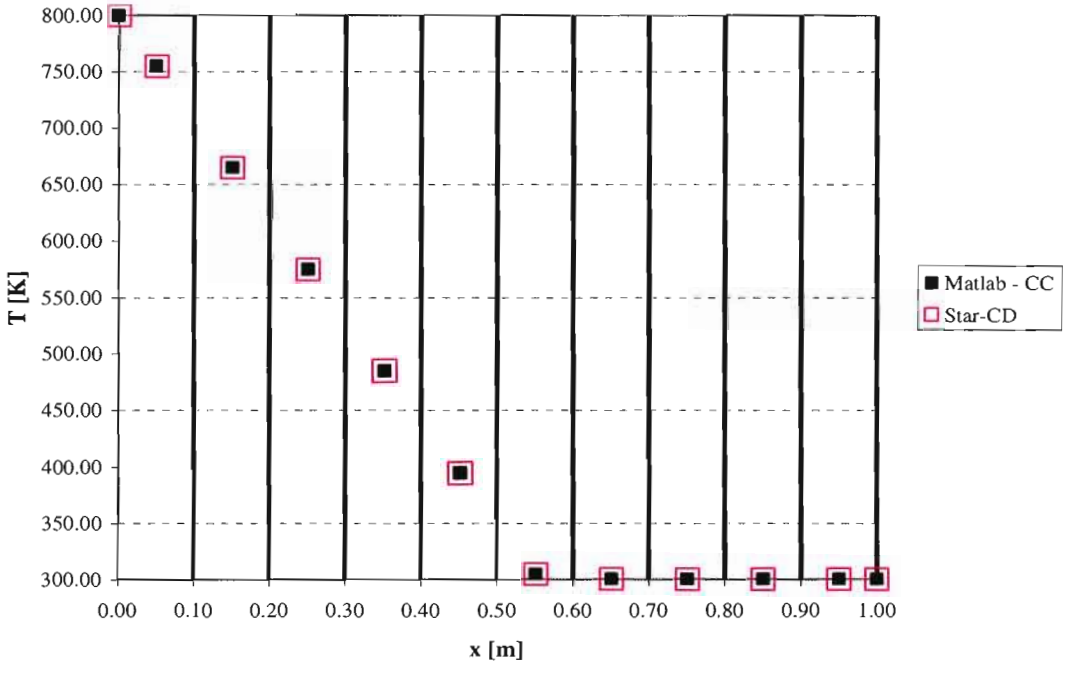

Figure 5-24: Test 7 Result – MATLAB CC vs. Star-CD

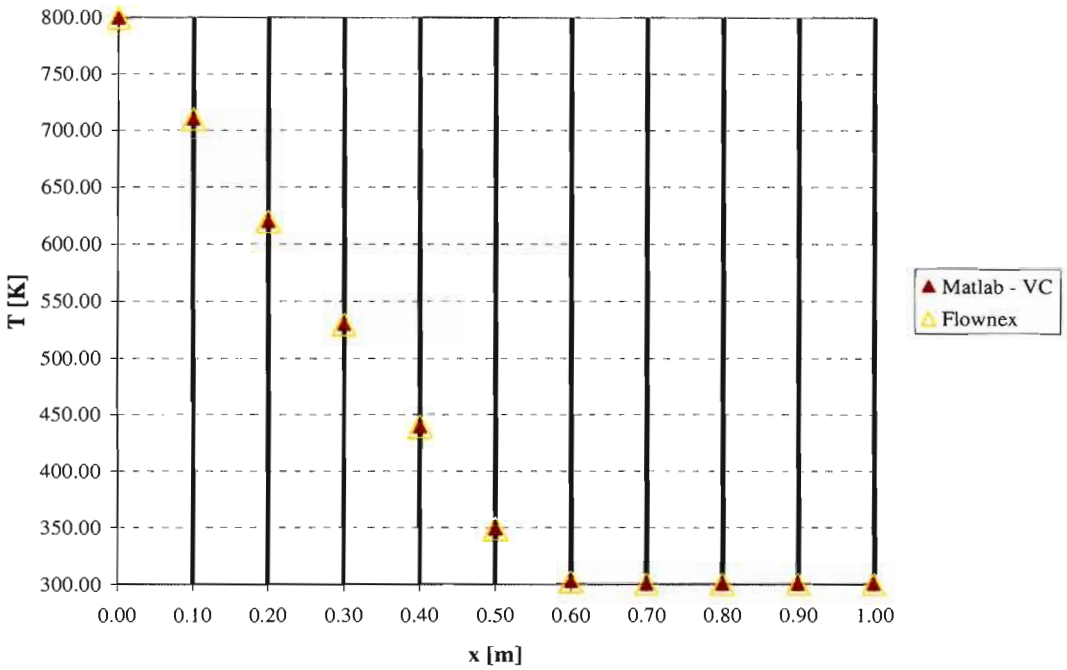

Figure 5-25: Test 7 Result – MATLAB VC vs. Flownex

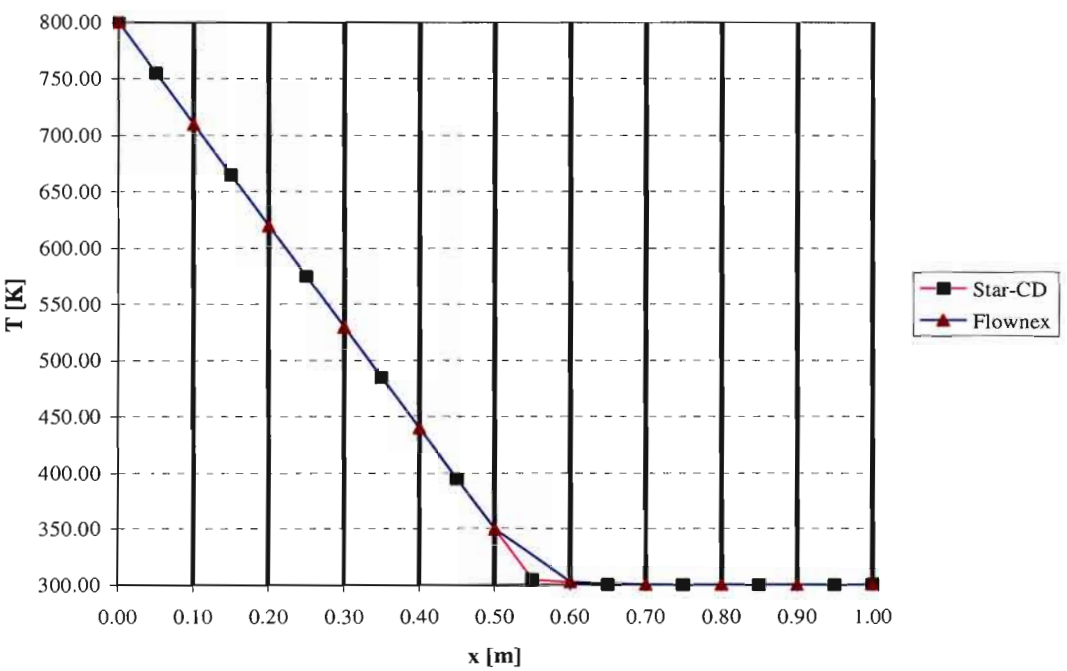

Figure 5-26: Test 7 Result – Star-CD vs. Flownex

As expected the results match exactly. This is sufficient verification that the convective sink is being applied over the correct volume.

Figure 5-26 shows a comparison of the results from Star-CD and Flownex. As explained in Test 6, the interpolated face value of the CC method is a good enough approximation of the VC reported value. However, there is a difference in the reported values of the cell neighbouring the interface.

5.2 CYLINDRICAL TEST CASE

For the cylindrical test case, the simplified reactor geometry described in 3.2 was modelled. The effective thermal conductivities were modelled as for the OECD/NEA benchmark. The convective sink was not modelled. A uniform nuclear heat source of 10 W/m^3 was applied to pebble core region. No other sources were added.

The purpose of this test was to verify that the face areas and cell volumes were being correctly calculated. The results of the MATLAB CC implementation are compared with the results from Star-CD in Figure 5-27. The results of the MATLAB VC implementation are compared with the results from Flownex in Figure 5-28.

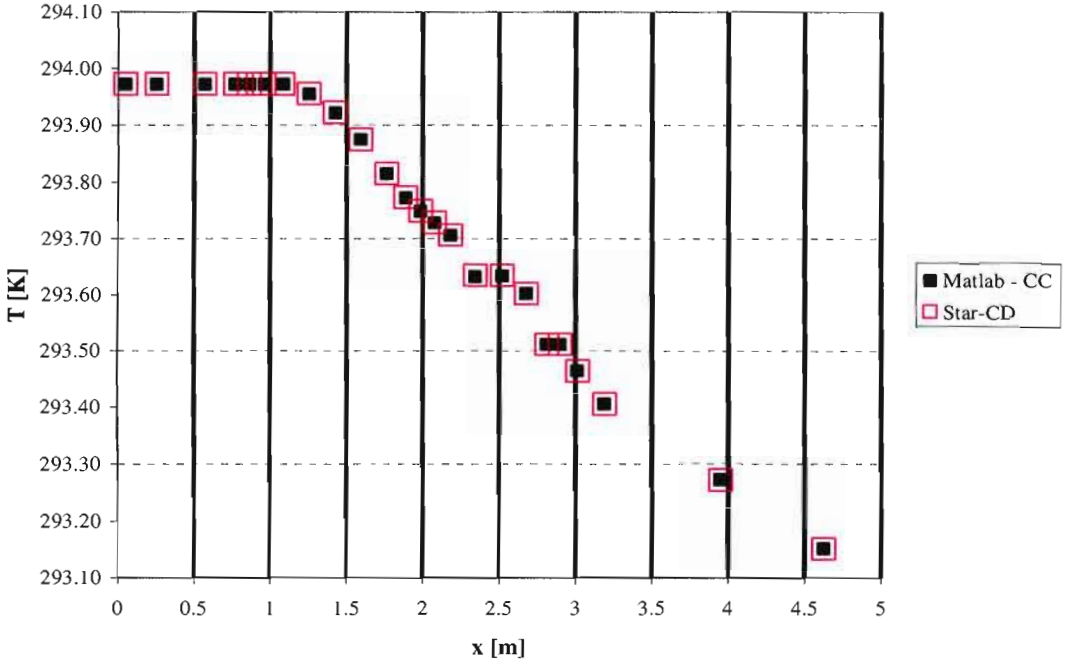

Figure 5-27: Cylindrical Test Case – MATLAB CC vs. Star-CD

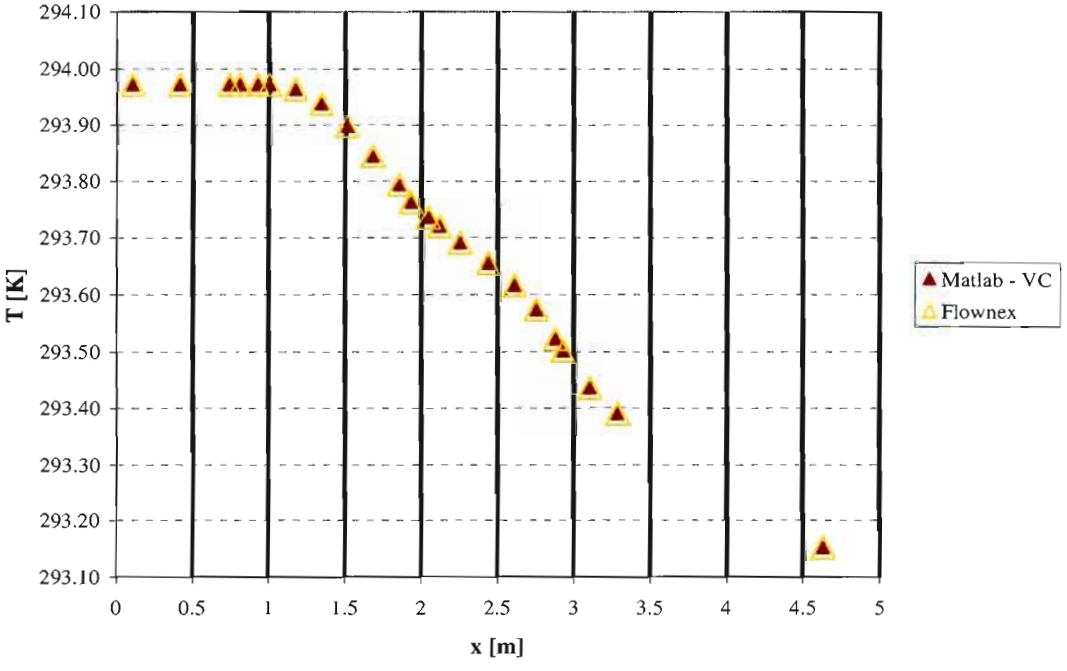

Figure 5-28: Cylindrical Test Case – MATLAB VC vs. Flownex

As expected the results match exactly. This is sufficient verification that the face areas and cell volumes are being correctly calculated for a cylindrical coordinate system.

At this stage, both the CC and VC implementations in MATLAB have been verified for the following:

- Cylindrical coordinate system
- Non-uniform grid
- Non-uniform effective thermal conductivity
- Non-uniform nuclear heat source
- Non-uniform convective sink

The next step is to model the OECD/NEA benchmark with the MATLAB implementations and compare this with the results of the 1D program written by Du Toit, (2008) to mimic THERMIX-KONVEK and DIREKT.

6 1D OECD/NEA PBMR THERMAL-HYDRAULIC BENCHMARK RESULTS

The 1D OECD/NEA benchmark as described in 3.3.1 was modelled using the CC and VC MATLAB implementations.

The results of the MATLAB CC implementation are compared with the results of the 1D program written by Du Toit, (2008) to mimic DIREKT, in Figure 6-1 .

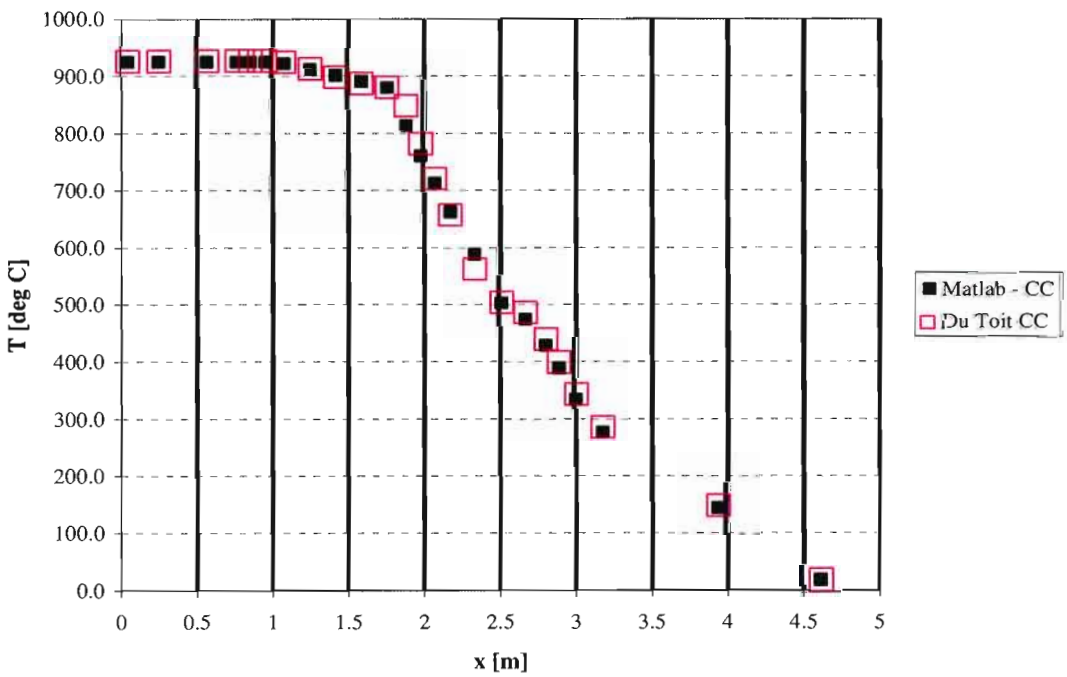

Figure 6-1: 1D OECD/NEA Benchmark Result – MATLAB CC vs. Du Toit, (2008) CC

The results of the MATLAB CC implementation compare quite well with the results of Du Toit, (2008) CC. The average error is 4.5°C. The largest errors occur at the outer reflector-core interfaces and the outer-reflector riser channel interfaces.

The results of the MATLAB VC implementation are compared with the results of the 1D program written by Du Toit, (2008) to mimic THERMIX-KONVEK, in Figure 6-2.

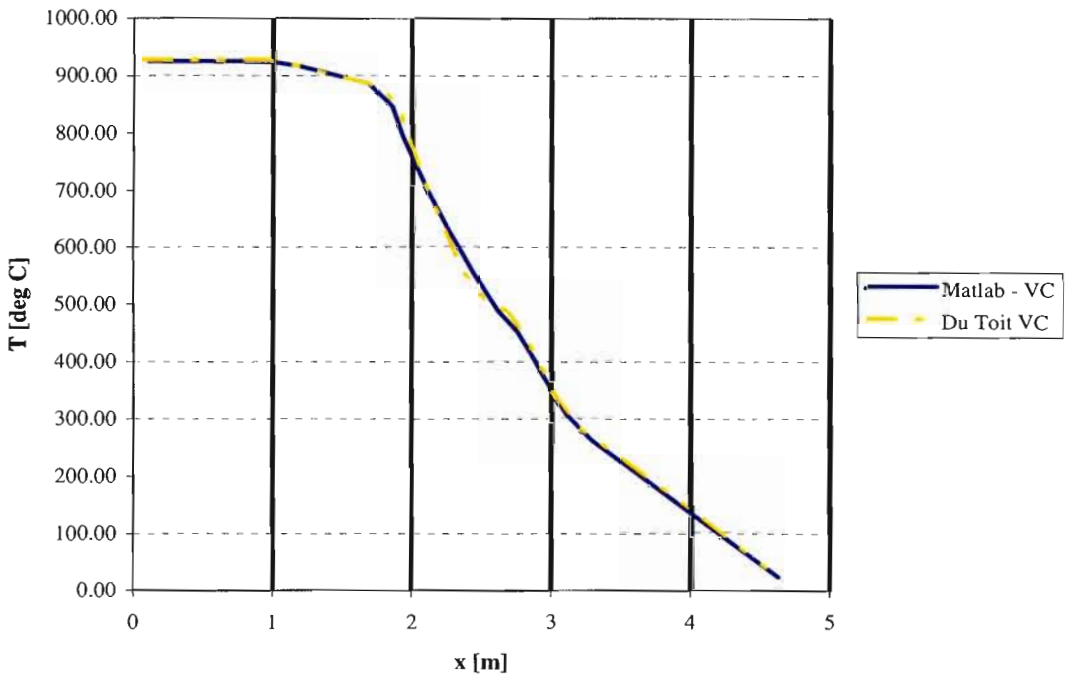

Figure 6-2: 1D OECD/NEA Benchmark Results – MATLAB VC vs. Du Toit, (2008) VC

The results of the 1D program written to mimic THERMIX-KONVEK are not reported by Du Toit, (2008) at the faces but rather at the cell centres. It is for this reason that the data in Figure 6-2 is shown as lines and not points.

As with the CC implementation, the results compare well overall. However, errors are again seen at the outer reflector-core interfaces and the outer reflector-riser channel interfaces.

7 DISCUSSION

Early on in the development of finite volume based codes, it was established that the simplest method of approximating properties between the nodal points, otherwise known as central differencing, led to erroneous results in the presence of discontinuities (Patankar, 1980). Finite volume based codes corrected the treatment of a discontinuity in the diffusion coefficient by calculating the interface diffusion coefficient as the harmonic mean of the nodal values rather than the arithmetic mean as was originally done.

Du Toit, (2008) showed that for the 2D OECD/NEA thermal-hydraulic benchmark, the results of THERMIX-KONVEK and DIREKT agreed reasonably well but there were large temperature differences originating at the material interfaces. Du Toit, (2008) wrote a 1D program that mimics THERMIX-KONVEK and DIREKT to investigate the reason for these discrepancies. Du Toit, (2008) identified the difference in the methodologies used by the CC and VC methods to treat a discontinuity in the source as the reason for these discrepancies.

In this study, a 1D CC and a 1D VC method were implemented in MATLAB. The implementations were verified against Star-CD (cell-centred based) and Flownex (vertex-centred based). Test 3, as described in 5.1.3, highlighted the difference in the way that the CC and VC methods report the temperature at the interface that sees the discontinuity in thermal conductivity. This is as a result of simple interpolation. Du Toit, (2008) showed that with sufficient grid refinement, the results of the CC method should approach that of the VC method. This behaviour was again highlighted in Test 4, on a non-uniform grid.

It is interesting to note that both the cell-centred codes of interest, TINTE and Star-CD, force the use of a small cell in the vicinity of a possible discontinuity and in this way improves their accuracy. TINTE specifies a 1mm cell at the interface while Star-CD uses a baffle, which is a zero thickness cell.

In Test 6, a discontinuity in the nuclear source was introduced. A difference in the temperatures reported by the CC and VC methods was seen. However, Test 6 also included a discontinuity in

the effective thermal conductivity. As a result no conclusion could be made regarding the discontinuous source. In Test 7, the effective thermal conductivity was kept uniform so as to eliminate any effects. A discontinuous convective sink was then added. There was a large discrepancy in the reported values at the cell neighbouring the discontinuity.

Du Toit, (2008) concluded from his findings that there are two linked factors that cause the discrepancies between the CC and VC methods at a discontinuous source/sink. Unlike the CC method, the face temperatures of the VC method are linked to the convection term. Also, for the VC method changes in the temperature gradient occur at the faces while for the CC method, changes occur at the cell centre. This means that for the VC method, the source/sink term is based on the neighbouring face temperature while for the CC method the source/sink term is based on the cell temperature.

In this study, the MATLAB CC and VC implementations were verified for a cylindrical coordinate system. The 1D OECD/NEA benchmark modified and modelled by Du Toit, (2008) was then evaluated. The 1D MATLAB implementations were shown to mimic Star-CD (CC) and Flownex (VC). The 1D program of Du Toit, (2008) was written to mimic THERMIX-KONVEK (VSOP) (VC) and DIREKT (TINTE) (CC). By comparing the 1D MATLAB implementations with the 1D program of Du Toit, (2008), an effective comparison was made between Star-CD, Flownex, VSOP and TINTE.

It was found that although the results compared well, there were large errors at the outer reflector-core interface as well as the outer reflector-riser channel interface for both the CC and VC methods. This implies that Star-CD treats the convective sink discontinuity differently from DIREKT and Flownex treats the convective sink discontinuity differently from THERMIX-KONVEK. This could be attributed to the way that the codes calculate the face areas and cell volumes. This needs to be investigated further.

8 CONCLUSIONS AND RECOMMENDATIONS

The differences between the VC and CC methods were studied using a benchmark problem. It has been shown that differences in these numerical methods result in different predicted temperatures. There are also differences in the prediction of the heat flux across the core-reflector boundary and the heat transfer to the gas through convection. In general, the different numerical methods will predict different temperatures, heat fluxes and (temperature-dependent) sink terms.

It was also shown that in addition to the differences resulting from numerical methods, differences were seen between Star-CD and DIREKT and Flownex and THERMIX-KONVEK in the region of the core-reflector boundary. It is believed that this could be attributed to the way that the codes calculate the face area and cell volume. This needs to be investigated further.

In conclusion, most commercial codes these days be it cell-centred or vertex-centred are used as "black boxes". Users are not fully aware of the numerical basis of the software packages and hence do not understand the possible reasons for errors in results. Although in very simple cases this may not pose a problem, in complicated simulations like the pebble bed, these differences need to be understood for the problem to be correctly modelled.

9 REFERENCES

Bauer, R. 1977, Effective Radial Thermal Conductivity of Gas Permeated Packed Beds Containing Particles of Different Shape and Size Distribution, VDI Forschungsh 582.

Bauer, R. & Schlünder, E.U. 1978, Effective Radical Thermal Conductivity of Packing in Gas Flow, Part I: Thermal Conductivity of the Packing Fraction without Gas Flow, International Chemical Engineering 18.

Chen, C.K. & Tien, C.-L. 1973, Conductance of a Packed Spheres in Vacuum, ASME Journal of Heat Transfer, 95.

Cheng, G.J., Yu, A.B., Zulli, P. 1999, Evaluation of Effective Thermal Conductivity from the Structure of a Packed Bed, Chemical Engineering Science 54.

Dixon, A.G. & Cresswell, D.L. 1979, Theoretical Predictions of Effective Heat Transport Parameters in Packed Beds, A.I.Ch.E. Journal 25(4).

Du Toit, C.G., Greyvenstein, G.P., Rousseau, P.G., 2003, A Comprehensive Reactor Model for the Integrated Network Simulation of the PBMR Power Plant, International Congress on Advances in Nuclear Power Plants (ICAPP'03). Cordoba, Spain, May 2003.

Du Toit, P.S. 2007, THERMIX/KONVEK Thermal –Hydraulics Calculation Theory Description, PBMR Internal Report.

Du Toit, P.S. 2008, Investigating Differences between THERMIX and DIREKT Results by Means of 1D Programs, PBMR Internal Report.

Greyvenstein, G.P. & Laurie, D.P. 1994, A Segregated CFD Approach to Pipe Network Analysis, International Journal for Numerical Methods in Engineering 37.

Hassan, Y.A. & Yesilyurt, G. 2002, Flow Distribution of Pebble Bed High Temperature Gas Cooled Reactors Using Large Eddy Simulation, 1st International Topical Meeting on High Temperature Reactor Technology.

Hennecke, F.W. & Schlünder, E.U. 1973, Heat Transfer in Heated or Cooled Tubes with Packings of Spheres, Cylinders and Raschig Rings, Chem. Ing. Technik 45(5).

Hoffmann, J.E. & van Rensburg, J.J. 2006, Verification and Validation of the CFD Model of the PBMR Reactor, 3rd International Topical Meeting on High Temperature Reactor Technology.

IAEA 2000, IAEA-TECDOC-1163: Heat Transport and Afterheat Removal for Gas Cooled Reactors under Accident Conditions, IAEA Vienna.

Ion, S., Nicholls, D., Matzie, R. & Matzner, D. 2003, Pebble Bed Modular Reactor: The First Generation IV Reactor to be Constructed, World Nuclear Association Annual Symposium.

KTA 1983, KTA 3102.2. Reactor Core Design of High-Temperature Gas-Cooled Reactors Part 2: Heat Transfer in Spherical Fuel Elements.

Lee, B., Gerwin, H., Niessen, H.F., Scherer, W. & Stöcker, B. 1995, On the Validation of the Reactor Dynamics Code-System TINTE: Post-Calculations of the SANA I Experiments with Radial Insulator, Interner Bericht KFA-ISR-IB-2/95, Forschungszentrum Jülich.

Lee, J.J., Kang, S.K., Yoon, S.J. & Park, G.C. 2005, Assessment of Turbulence Models in CFD Code and its Application to Pebble Bed Reactor, 4th International Conference on Heat Transfer, Fluid Mechanics and Thermodynamics, Cairo Egypt.

Lee, J.J., Park, G.C, Kim, K.Y. & Lee, W.J. 2007, Numerical Treatment of Pebble Contact in the Flow and Heat Transfer Analysis of a Pebble-Bed Reactor Core, Nuclear Engineering and Design 237.

Lerou, J.J. & Froment, G.F. 1978, Estimation of Heat Transfer Parameters in Packed Beds from Radial Temperature Profiles, Chem. Eng. Journal (Lausanne) 15(3).

Logtenberg, S.A. & Dixon, A.G. 1998, Computational Fluid Dynamic Studies of Fixed Bed Heat Transfer, Chemical Engineering and Processing 37.

Logtenberg, S.A., Nijemeisland, M. & Dixon, A.G. 1999, Computational Fluid Dynamics Simulations of Fluid Flow and Heat Transfer at the Wall-Particle Contact Points in a Fixed-Bed Reactor, Chemical Engineering Science 54.

Lübcke, H., Schmidt, St., & Rung, T. 2001, Comparison of LES and RANS in Bluff-Body Flows, Journal Wind Eng. Ind. Aerod. 89 1471.

Martin, H. & Nilles, M. 1993, Radiale Wärmeleitung in Durchströmten Schüttungsrohren, Chem. Ing. Techn. 65.

Niessen, H-F. & Stöcker, B. 1997, Data sets of SANA experiment: 1994-1996, Document JUEL-3409, Forschungszentrum, Jülich.

OECD/NEA 2009, OECD/NEA PBMR Coupled Neutronics/Thermal-hydraulics Transients Benchmark – The PBMR-400 Core Design, http://www.nea.fr/html/science/wprs/pbmr400 Date of access: November 2009.

Patankar, S.V. 1980, Numerical Heat Transfer and Fluid Flow, Hemisphere Publishing Corporation, 193.

Pebble Bed Modular Reactor Corporate Website 2008, Website: www.pbmr.co.za, accessed March 2008.

Peyret, R. & Taylor, T.D. 1983, Computational Methods for Fluid Flow, Springer-Verlag, New York.

Prasad, V., Kladias, N., Bandyopadhaya, A. & Tian, Q. 1989, Evaluation of Correlations for Stagnant Thermal Conductivity of Liquid-Saturated Porous Beds of Spheres, Int. J. Heat Mass Transfer 32.

Ritch, J. 2008. The Necessity of Nuclear Power: A Global and Environmental Imperative. http://www.world-nuclear.org/John_Ritch/The_Necessity_of_Nuclear_Power.html Date of access: March 2008.

Robold, K. 1982, Wärmetransport im Inneren und in der Randzone von Kugelschüttungen, Kernforschungsanlage Jülich, JÜL-1796.

Rodi, W. 1997, Comparison of LES and RANS Calculations of the Flow Around Bluff Bodies, Journal of Wind Eng. Ind. Aerod. 69-71 55.

Rousseau, P.G & van Staden, M. 2006, Introduction to the PBMR Heat Transfer Test Facility, 3rd International Topical Meeting on High Temperature Reactor Technology.

Slabber, J. 2006, Technical Description of the PBMR Demonstration Power Plant, PBMR Internal Report.

Strauss, J. 2006, Thermo-Hydraulic Benchmark Definition Report, PBMR Internal Report.

Strauss, J. 2007, Heat Transfer Benchmarking Report, PBMR Internal Report.

Taylor, J.B., Yavuzkurt, S. & Baratta, A. 2002, Modelling of the Fluid and Heat Transfer in a Pebble Bed Modular Core with a Computational Fluid Dynamics Code, 10th International Conference on Nuclear Engineering, Arlington VA.

Tomboulides, A., Orszag, S. & Karniadakis, G. 1993, Direct and Large Eddy Simulations of the Flow Past a Sphere, International Symposium on Engineering Turbulence Modelling and Measurements, Florence Italy.

Tsotsas, E. 1991, Wärmeleitfähigkeit von Schuttschichten, VDI-Wärmeatlas: Berechnungsblätter für den Wärmeübergang, Verein Deutscher Ingenieure, pp. Deb1-Deb9, Düsseldorf, 6th Edition.

Tsotsas, E. & Schlünder, E.U. 1991, Impact of Particle Size Dispersity on Thermal Conductivity of Packed Beds: Measurement, Numerical Simulation, Prediction, Chemical Engineering Technology 14.

Van Antwerpen, H.J 2007, Modelling a Pebble Bed High Temperature Gas-Cooled Reactor using a System CFD Approach, North-West University PhD Thesis.

Van der Merwe, J., van Antwerpen, H.J. & Mulder, E.J. 2006, Heat Transfer Correlation Limitations at the Pebble Bed-Reflector Interface, 3rd International Topical Meeting on High Temperature Reactor Technology.

Van Staden, M., van Rensburg, C.J. & Viljoen, C. 2002, CFD Simulation of Helium Gas Cooled Pebble Bed Reactor, 1st International Conference on Heat Transfer, Fluid Mechanics and Thermodynamics.

Versteeg, H.K. & Malalasekera, W. 1995, An Introduction to Computational Fluid Dynamics: The Finite Volume Method, Prentice Hall.

Viljoen, C. & Mtyobile, V. 2007, Star-CD Reactor Benchmarking Report, PBMR Internal Report.

Vortmeyer, D. & Le Mong, S. 1976, Ein Verfahren zur Messung von Wärmeübergangszahlen in durchströmten Schüttungen bei Reynolds-Zahlen Re < 200. Verfahrenstechnik 10 Nr.10, 650-654.

Westerterp, K.R., van Swaaij, W.P.M. & Beenackers, A.A.C.M. 1987, Chemical Reactor Design and Operation, Wiley, Chichester.

Wijngaarden, R.J. & Westerterp, K.R. 1992, A Heterogeneous Model for Heat Transfer in Packed Beds, Chem. Eng. Science 48(7).

Winterberg, M., Tsotsas, E., Krischke, A. & Vortmeyer, D. 2000, A Simple and Coherent Set of Coefficients for Modelling of Heat and Mass Transport With and Without Chemical Reaction in Tubes Filled with Spheres, Chem. Eng. Science 55.

World Nuclear Association, 2008, Global Warming: The Science, http://www.world-nuclear.org/info/inf59.html Date of access: October 2008.

World Nuclear Association, 2009, China's Nuclear Fuel Cycle, http://www.world-nuclear.org/info/default.aspx?id=26187 Date of access: March 2009.

Yesilyurt, G. & Hassan, Y.A. 2003, LES Simulation in Pebble Bed Modular Reactor Core through Randomly Distributed Fuel Elements, International Conference on Global Environment and Advanced Nuclear Powerplants, Kyoto Japan.

Zehner, P. 1973, Experimental and Theoretical Determination of the Effective Heat Conductivity of Solid Beds Consisting of Spheres with Through Flow at Moderate and High Temperatures, VDI Forschungsh. 45(5).

Zehner, P. & Schlünder, E.U. 1970, Thermal Conductivity of Granular Materials at Moderate Temperatures, Chem. Ing. Technik 42.

Zehner, P. & Schlünder, E.U. 1973, Effective Thermal Conductivity of Spherical Packings Perfused at Moderate and High Temperatures, Chem. Ing. Technik 45(5).

10 APPENDICES

RESULTS

Table A-1: Test 1 CC Result

Location [m]	MATLAB – CC Temperature [K]	Star-CD Temperature [K]	% Error
0.00	800.00	800.00	0.00
0.05	775.00	775.00	0.00
0.15	725.00	725.00	0.00
0.25	675.00	675.00	0.00
0.35	625.00	625.00	0.00
0.45	575.00	575.00	0.00
0.55	525.00	525.00	0.00
0.65	475.00	475.00	0.00
0.75	425.00	425.00	0.00
0.85	375.00	375.00	0.00

Table A-2: Test 1 VC Result

Location [m]	MATLAB – VC Temperature [K]	Flownex Temperature [K]	% Error
0.00	800.00	800.00	0.00
0.10	750.00	750.00	0.00
0.20	700.00	700.00	0.00
0.30	650.00	650.00	0.00
0.40	600.00	600.00	0.00
0.50	550.00	550.00	0.00
0.60	500.00	500.00	0.00
0.70	450.00	450.00	0.00
0.80	400.00	400.00	0.00
0.90	350.00	350.00	0.00
1.00	300.00	300.00	0.00

Table A-3: Test 2 CC Result

Location [m]	MATLAB – CC Temperature [K]	Star-CD Temperature [K]	% Error
0.00	800.00	800.00	0.00
0.04	779.50	779.50	0.00
0.13	737.50	737.50	0.00
0.21	693.50	693.50	0.00
0.31	647.50	647.50	0.00
0.40	599.50	599.50	0.00
0.50	549.50	549.50	0.00
0.61	497.50	497.50	0.00
0.71	443.50	443.50	0.00
0.83	387.50	387.50	0.00
0.94	329.50	329.50	0.00
1.00	300.00	300.00	0.00

Table A-4: Test 2 VC Result

Location [m]	MATLAB – VC Temperature [K]	Flownex Temperature [K]	% Error
0.00	800.00	800.00	0.00
0.08	759.00	759.00	0.00
0.17	716.00	716.00	0.00
0.26	671.00	671.00	0.00
0.35	624.00	624.00	0.00
0.45	575.00	575.00	0.00
0.55	524.00	524.00	0.00
0.66	471.00	471.00	0.00
0.77	416.00	416.00	0.00
0.88	359.00	359.00	0.00
1.00	300.00	300.00	0.00

Table A-5: Test 3 CC Result

Location [m]	MATLAB – CC Temperature [K]	Star-CD Temperature [K]	% Error
0.00	800.00	800.00	0.00
0.05	779.41	779.41	0.00
0.15	738.24	738.24	0.00
0.25	697.06	697.06	0.00
0.35	655.88	655.88	0.00
0.45	614.71	614.71	0.00
0.55	564.71	564.71	0.00
0.65	505.88	505.88	0.00
0.75	447.06	447.06	0.00
0.85	388.24	388.24	0.00
0.95	329.41	329.41	0.00
1.00	300.00	300.00	0.00

Table A-6: Test 3 VC Result

Location [m]	MATLAB – VC Temperature [K]	Flownex Temperature [K]	% Error
0.00	800.00	800.00	0.00
0.10	758.82	758.82	0.00
0.20	717.65	717.65	0.00
0.30	676.47	676.47	0.00
0.40	635.29	635.30	0.00
0.50	594.12	594.12	0.00
0.60	535.29	535.30	0.00
0.70	476.47	476.47	0.00
0.80	417.65	417.65	0.00
0.90	358.82	358.82	0.00
1.00	300.00	300.00	0.00

Table A-7: Test 4 CC Result

Location [m]	MATLAB – CC Temperature [K]	Star-CD Temperature [K]	% Error
0.00	800.00	800.00	0.00
0.04	783.40	783.41	0.00
0.13	749.40	749.40	0.00
0.21	713.79	713.79	0.00
0.31	676.55	676.55	0.00
0.40	637.69	637.69	0.00
0.50	588.54	588.54	0.00
0.61	528.40	528.40	0.00
0.71	465.95	465.95	0.00
0.83	401.19	401.19	0.00
0.94	334.12	334.12	0.00
1.00	300.00	300.00	0.00

Table A-8: Test 4 VC Result

Location [m]	MATLAB – VC Temperature [K]	Flownex Temperature [K]	% Error
0.00	800.00	800.00	0.00
0.08	766.82	766.82	0.00
0.17	732.02	732.02	0.00
0.26	695.61	695.61	0.00
0.35	657.57	657.57	0.00
0.45	617.92	617.92	0.00
0.55	558.96	558.96	0.00
0.66	497.69	497.69	0.00
0.77	434.10	434.10	0.00
0.88	368.21	368.21	0.00
1.00	300.00	300.00	0.00

Table A-9: Test 5 CC Result

Location [m]	MATLAB – CC Temperature [K]	Star-CD Temperature [K]	% Error
0.00	800.00	800.00	0.00
0.05	789.73	789.73	0.00
0.15	765.39	765.39	0.00
0.25	737.27	737.27	0.00
0.35	705.35	705.35	0.00
0.45	669.64	669.64	0.00
0.55	621.67	621.67	0.00
0.65	559.82	559.82	0.00
0.75	492.55	492.55	0.00
0.85	419.86	419.86	0.00
0.95	341.76	341.76	0.00
1.00	300.00	300.00	0.00

Table A-10: Test 5 VC Result

Location [m]	MATLAB – VC Temperature [K]	Flownex Temperature [K]	% Error
0.00	800.00	800.00	0.00
0.10	777.56	777.56	0.00
0.20	751.33	751.33	0.00
0.30	721.31	721.31	0.00
0.40	687.49	687.49	0.00
0.50	649.89	649.89	0.00
0.60	590.74	590.74	0.00
0.70	526.18	526.18	0.00
0.80	456.21	456.21	0.00
0.90	380.81	380.81	0.00
1.00	300.00	300.00	0.00

Table A-11: Test 6 CC Result

Location [m]	MATLAB – CC Temperature [K]	Star-CD Temperature [K]	% Error
0.00	800.00	800.00	0.00
0.05	786.94	786.94	0.00
0.15	757.03	757.03	0.00
0.25	723.33	723.33	0.00
0.35	685.83	685.83	0.00
0.45	644.54	644.54	0.00
0.55	589.80	589.80	0.00
0.65	525.40	525.40	0.00
0.75	461.00	461.00	0.00
0.85	396.60	396.60	0.00
0.95	332.20	332.20	0.00
1.00	300.00	300.00	0.00

Table A-12: Test 6 VC Result

Location [m]	MATLAB – VC Temperature [K]	Flownex Temperature [K]	% Error
0.00	800.00	800.00	0.00
0.10	771.98	771.98	0.00
0.20	740.18	740.18	0.00
0.30	704.58	704.58	0.00
0.40	665.19	665.19	0.00
0.50	622.00	622.00	0.00
0.60	557.60	557.60	0.00
0.70	493.20	493.20	0.00
0.80	428.80	428.80	0.00
0.90	364.40	364.40	0.00
1.00	300.00	300.00	0.00

Table A-13: Test 7 CC Result

Location [m]	MATLAB – CC Temperature [K]	Star-CD Temperature [K]	% Error
0.00	800.00	800.00	0.00
0.05	754.96	754.96	0.00
0.15	664.87	664.87	0.00
0.25	574.78	574.78	0.00
0.35	484.70	484.70	0.00
0.45	394.61	394.61	0.00
0.55	304.52	304.52	0.00
0.65	300.22	300.22	0.00
0.75	300.01	300.01	0.00
0.85	300.00	300.00	0.00
0.95	300.00	300.00	0.00
1.00	300.00	300.00	0.00

Table A-14: Test 7 VC Result

Location [m]	MATLAB – VC Temperature [K]	Flownex Temperature [K]	% Error
0.00	800.00	800.00	0.00
0.10	709.91	709.91	0.00
0.20	619.83	619.83	0.00
0.30	529.74	529.74	0.00
0.40	439.65	439.65	0.00
0.50	349.57	349.57	0.00
0.60	302.37	302.37	0.00
0.70	300.11	300.11	0.00
0.80	300.01	300.01	0.00
0.90	300.00	300.00	0.00
1.00	300.00	300.00	0.00

Table A-15: Cylindrical Test CC Result

Location [m]	MATLAB – CC Temperature [K]	Star-CD Temperature [K]	% Error
0.05	293.97	293.97	0.00
0.255	293.97	293.97	0.00
0.573	293.97	293.97	0.00
0.77075	293.97	293.97	0.00
0.863	293.97	293.97	0.00
0.96025	293.97	293.97	0.00
1.085	293.97	293.97	0.00
1.255	293.95	293.96	0.00
1.425	293.92	293.92	0.00
1.595	293.87	293.88	0.00
1.765	293.81	293.82	0.00
1.88975	293.77	293.77	0.00
1.987	293.75	293.75	0.00
2.07925	293.73	293.73	0.00
2.182	293.70	293.71	0.00
2.343	293.63	293.63	0.00
2.521	293.63	293.63	0.00
2.678	293.60	293.60	0.00
2.8125	293.51	293.51	0.00
2.9	293.51	293.51	0.00
3.0125	293.46	293.46	0.00
3.19	293.40	293.41	0.00
3.95	293.27	293.27	0.00
4.63	293.15	293.15	0.00

Table A-16: Cylindrical Test VC Result

Location [m]	MATLAB – VC Temperature [K]	Flownex Temperature [K]	% Error
0.1	294.18	294.18	0.00
0.41	294.18	294.18	0.00
0.736	294.18	294.18	0.00
0.8055	294.17	294.17	0.00
0.9205	294.17	294.17	0.00
1	294.17	294.1	0.00
1.17	294.16	294.16	0.00
1.34	294.13	294.13	0.00
1.51	294.09	294.09	0.00
1.68	294.03	294.03	0.00
1.85	293.97	293.97	0.00
1.9295	293.94	293.94	0.00
2.0445	293.92	293.92	0.00
2.114	293.89	293.89	0.00
2.25	293.86	293.86	0.00
2.436	293.82	293.82	0.00
2.606	293.78	293.78	0.00
2.75	293.75	293.75	0.00
2.875	293.67	293.67	0.00
2.925	293.64	293.64	0.00
3.1	293.54	293.54	0.00
3.28	293.49	293.49	0.00
4.62	293.15	293.15	0.00

MATLAB CODES

```
clc;
n = 10;
% number of cells

%_____________________________________________________________________________
% PROBLEM SPECIFICATION
%-----------------------------------------------------------------------------

% radii = xlsread('Test_Matrix.xls','Test 6 - Data','AT1:AT25');
% A_conv = (6*(1-epsilon)*V)/d;
% surface area of spheres in core
A_conv = 0.01;
h = [0,0,0,0,0,5,5,5,5,5];
% heat transfer coefficient
q_nuclear = [0,0,0,0,0,0,0,0,0,0];
% volumetric source
T_gas = [0,0,0,0,0,300,300,300,300,300];
% gas temperature
T_A = 800;
% boundary temperature
T_B = 300;
% boundary temperature

% epsilon = xlsread('Test_Matrix.xls','Test 6 - Data','AU1:AU25');
% cell porosity
% k =
[0.02637,0.02637,0.02637,0.02637,0.02637,0.018459,0.018459,0.018459,...
%    0.018459,0.018459];
% cell conductivity
k_eff = 0.02637*ones(1,n);

delta_x_we = 0.1*ones(1,n);
epsilon = 0*ones(1,n);



%_____________________________________________________________________________
% GRID PARAMETERS
%-----------------------------------------------------------------------------

for i = (1:n)

%     delta_x_we(i) = radii(i+1) - radii(i);
% grid spacing
% delta_x_we =
[0.082,0.086,0.090,0.094,0.098,0.102,0.106,0.110,0.114,0.118];
%     A(i) = 2*pi()*delta_x_we(i);
% radial face area

      A(i) = 0.1*delta_x_we(i);
      % cartesian face area

end

delta_x_A = delta_x_we(1,1)/2;
delta_x_B = delta_x_we(1,n)/2;

%_____________________________________________________________________________
% DISCRETISATION
%-----------------------------------------------------------------------------

for i = (1:n-1)

    delta_x_Pe(i) = delta_x_we(i)/2;
    delta_x_eE(i) = delta_x_we(i+1)/2;
    delta_x_PE(i) = delta_x_Pe(i) + delta_x_eE(i);

    delta_x_wP(i+1) = delta_x_we(i+1)/2;
    delta_x_Ww(i+1) = delta_x_we(i)/2;
    delta_x_WP(i+1) = delta_x_Ww(i+1) + delta_x_wP(i+1);

    f_wP(i+1) = (delta_x_wP(i+1)/delta_x_WP(i+1));
    f_Ww(i+1) = (delta_x_Ww(i+1)/delta_x_WP(i+1));
```

```
    f_eE(i) = (delta_x_eE(i)/delta_x_PE(i));
    f_Pe(i) = (delta_x_Pe(i)/delta_x_PE(i));

    k_w(i+1) = ((delta_x_we(i)*f_wP(i+1)+delta_x_we(i+1)*f_Ww(i+1))...
        *k_eff(i+1)*k_eff(i))/(delta_x_we(i)*f_wP(i+1)*k_eff(i)+ ...
        delta_x_we(i+1)*f_Ww(i+1)*k_eff(i+1));
    k_e(i) = k_w(i+1);

end

%-------------------------------------------------------------------------
% Boundary Nodes
%-------------------------------------------------------------------------
% Node 1

aW(1) = 0;
aE(1) = (k_e(1,1)*A(1,1))/delta_x_PE(1);
SP(1) = -h(1,1)*A_conv - (k_eff(1,1)*A(1,1))/delta_x_A;
aP(1) = aW(1) + aE(1) - SP(1);
Su(1) = q_nuclear(1,1)*(1-epsilon(1,1))*A(1,1)*delta_x_we(1,1) + h(1,1)*...
    A_conv*T_gas(1,1) + (k_eff(1,1)*A(1,1)*T_A)/delta_x_A;

%-------------------------------------------------------------------------
% Node n

aW(n) = (k_w(1,n)*A(1,n))/delta_x_WP(n);
aE(n) = 0;
SP(n) = -h(1,n)*A_conv - (k_eff(1,n)*A(1,n))/delta_x_B;
aP(n) = aW(n) + aE(n) - SP(n);
Su(n) = q_nuclear(1,n)*(1-epsilon(1,n))*A(1,n)*delta_x_we(1,n) + h(1,n)*...
    A_conv*T_gas(1,n) + (k_eff(1,n)*A(1,n)*T_B)/delta_x_B;

%-------------------------------------------------------------------------
% Interior Nodes
%-------------------------------------------------------------------------

for i = (2:n-1)

    aW(i) = (k_w(1,i)*A(1,i))/delta_x_WP(1,i);
    aE(i) = (k_e(1,i)*A(1,i))/delta_x_PE(1,i);
    SP(i) = -h(1,i)*A_conv;
    aP(i) = aW(i) + aE(i) - SP(i);
    Su(i) = q_nuclear(1,i)*(1-epsilon(1,i))*A(1,i)*delta_x_we(1,i) + ...
        h(1,i)*A_conv*T_gas(1,i);

end
%_____________________________________________________________________
% SOLUTION
%-------------------------------------------------------------------------

B = diag(aP) - diag(aE(1:n-1),1) - diag(aW(2:n),-1);
%[L,U] = lu(B);
% Gaussian Elimination
%T = U\(L\Su')
T = B\Su'
```

```
clc;


%_____________________________________________________________________
% PROBLEM SPECIFICATION
%---------------------------------------------------------------------

n = 23;
% number of cells
z = 0.5;
% cell height

radii = xlsread('Test_Matrix.xls','Test 6A - Data','AU1:AU26');
% outer radii
epsilon = xlsread('Test_Matrix.xls','Test 6A - Data','AV1:AV25');
% cell porosity
d = xlsread('Test_Matrix.xls','Test 6A - Data','AX1:AX25');
% sphere diameter
k_eff = xlsread('Test_Matrix.xls','Test 6A - Data','AW1:AW25');
% thermal conductivity

q_nuclear = xlsread('Test_Matrix.xls','Test 6A - Data','AY1:AY26');
% volumetric source
h = xlsread('Test_Matrix.xls','Test 6A - Data','AZ1:AZ26');
% heat transfer coefficient
T_gas = xlsread('Test_Matrix.xls','Test 6A - Data','BA1:BA26');
% gas temperature

T_B =293.15;
% boundary temperature


%_____________________________________________________________________
% GRID PARAMETERS
%---------------------------------------------------------------------

for i = (1:n)

    delta_x_we(i) = (radii(i+1) - radii(i));
    % grid spacing

    V(i) = z*pi()*(radii(i+1)^2 - radii(i)^2);

    A_w(i) = 2*pi()*radii(i)*z;
    A_e(i) = 2*pi()*radii(i+1)*z;

end

for i = (1:10)

    A_conv(i) = 0;

end

for i = (7:11)

    A_conv(i) = (6*(1-epsilon(i))*V(1,i))/d(i);
    % surface area of spheres in core

end

for i = (12:16)

    A_conv(i) = 0;

end

for i = 17

    A_conv(i) = (4*epsilon(i)*V(1,i))/d(i);

end
```

```
for i = (18:n)

    A_conv(i) = 0;

end


delta_x_B = (0.5*delta_x_we(1,n));

%_____________________________________________________________________
% DISCRETISATION
%---------------------------------------------------------------------

for i = (1:n-1)

    delta_x_Pe(i) = delta_x_we(i)/2;
    delta_x_eE(i) = delta_x_we(i+1)/2;
    delta_x_PE(i) = delta_x_Pe(i) + delta_x_eE(i);

    delta_x_wP(i+1) = delta_x_we(i+1)/2;
    delta_x_Ww(i+1) = delta_x_we(i)/2;
    delta_x_WP(i+1) = delta_x_Ww(i+1) + delta_x_wP(i+1);

    f_wP(i+1) = (delta_x_wP(i+1)/delta_x_WP(i+1));
    f_Ww(i+1) = (delta_x_Ww(i+1)/delta_x_WP(i+1));
    f_eE(i) = (delta_x_eE(i)/delta_x_PE(i));
    f_Pe(i) = (delta_x_Pe(i)/delta_x_PE(i));

    k_w(i+1) = ((delta_x_we(i)*f_wP(i+1)+delta_x_we(i+1)*f_Ww(i+1))...
        *k_eff(i+1)*k_eff(i))/(delta_x_we(i)*f_wP(i+1)*k_eff(i)+ ...
        delta_x_we(i+1)*f_Ww(i+1)*k_eff(i+1));
%     k_w = xlsread('Test_Matrix.xls','Test 6A - Data','BC3:BC26')';
    k_e(i) = k_w(i+1);

end

%---------------------------------------------------------------------
% Boundary Nodes
%---------------------------------------------------------------------
% Node 1

aW(1) = 0;
aE(1) = (k_e(1,1)*A_e(1,1))/delta_x_PE(1);
SP(1) = -h(1,1)*A_conv(1,1);
aP(1) = aW(1) + aE(1) - SP(1);
Su(1) = q_nuclear(1,1)*V(1,1) + h(1,1)...
    *A_conv(1,1)*T_gas(1,1);

%---------------------------------------------------------------------
% Node n

aW(n) = (k_w(1,n)*A_w(1,n))/delta_x_WP(n);
aE(n) = 0;
SP(n) = -h(n,1)*A_conv(1,n) - (k_eff(n,1)*A_e(1,n))/delta_x_B;
aP(n) = aW(n) + aE(n) - SP(n);
Su(n) = q_nuclear(n,1)*V(1,n) + h(n,1)*...
    A_conv(1,n)*T_gas(n,1) + (k_eff(n,1)*A_e(1,n)*T_B)/delta_x_B;

%---------------------------------------------------------------------
% Interior Nodes
%---------------------------------------------------------------------

for i = (2:n-1)

    aW(i) = (k_w(1,i)*A_w(1,i))/delta_x_WP(1,i);
    aE(i) = (k_e(1,i)*A_e(1,i))/delta_x_PE(1,i);
    SP(i) = -h(i,1)*A_conv(1,i);
    aP(i) = aW(i) + aE(i) - SP(i);
    Su(i) = q_nuclear(i,1)*V(1,i)+ h(i,1)*A_conv(1,i)...
        *T_gas(i,1);

end
%_____________________________________________________________________
```

```
% SOLUTION
%--------------------------------------------------------------------------

B = diag(aP) - diag(aE(1:n-1),1) - diag(aW(2:n),-1);
%[L,U] = lu(B);
% Gaussian Elimination
%T = U\(L\Su')
T = B\Su'
```

```
clc;
n = 10;
% number of cells
m = n + 1;

%_____________________________________________________________________________
% PROBLEM SPECIFICATION
%-----------------------------------------------------------------------------

A = 0.01;
% face area
A_conv = 0.01;
% surface area of spheres in core
h = [0,0,0,0,0,5,5,5,5,5];
% heat transfer coefficient
q_nuclear = [0,0,0,0,0,0,0,0,0,0];
% volumetric source
T_gas = [0,0,0,0,0,300,300,300,300,300];
% gas temperature
T_A = 800;
% boundary temperature
T_B = 300;
% boundary temperature

epsilon = [0,0,0,0,0,0,0,0,0,0];
% cell porosity
% k =
[0.02637,0.02637,0.02637,0.02637,0.02637,0.018459,0.018459,0.018459,...
%   0.018459,0.018459];
% cell conductivity
k = 0.02637*ones(1,n);

for i=1:n
    k_eff(1,i) = (1-epsilon(1,i))*k(1,i);
end

%_____________________________________________________________________________
% GRID PARAMETERS
%-----------------------------------------------------------------------------

delta_x_we = [0.1,0.1,0.1,0.1,0.1,0.1,0.1,0.1,0.1,0.1];
% grid spacing
% delta_x_we =
[0.082,0.086,0.090,0.094,0.098,0.102,0.106,0.110,0.114,0.118];

% delta_x_A = delta_x_we(1,1)/2;
% delta_x_B = delta_x_we(1,n)/2;

%_____________________________________________________________________________
% DISCRETISATION
%-----------------------------------------------------------------------------

for i = (1:n-1)

    delta_x_Pe(i) = delta_x_we(i)/2;
    delta_x_eE(i) = delta_x_we(i+1)/2;
    delta_x_PE(i) = delta_x_Pe(i) + delta_x_eE(i);

    delta_x_wP(i+1) = delta_x_we(i+1)/2;
    delta_x_Ww(i+1) = delta_x_we(i)/2;
    delta_x_WP(i+1) = delta_x_Ww(i+1) + delta_x_wP(i+1);

    delta_x_we_inter(i) = (delta_x_we(i+1)+ delta_x_we(i))/4;

end

for i = (1:n-2)

     delta_x_we_new(i) = delta_x_we_inter(i+1) + delta_x_we_inter(i);

end

%-----------------------------------------------------------------------------
```

```
% Boundary Nodes
%-------------------------------------------------------------------------
% Node 2

aW(2) = 0;
aE(2) = (k_eff(1,2)*A)/delta_x_we_new(1,1);
SP(2) = -h(1,2)*A_conv - (k_eff(1,1)*A)/delta_x_we(1,1);
aP(2) = aW(2) + aE(2) - SP(2);

Su(2) = q_nuclear(1,2)*(1-epsilon(1,1))*A*(0.5*delta_x_we(1,1)...
    + 0.5*delta_x_we(1,2)) + h(1,2)*A_conv*T_gas(1,2) + (k_eff(1,1)*A*...
    T_A)/(delta_x_we(1,1));

%-------------------------------------------------------------------------
% Node m-1

aW(n) = (k_eff(1,n-1)*A)/delta_x_we(1,n-1);
aW(n) = (k_eff(1,n-1)*A)/delta_x_we_new(1,n-2);
aE(n) = 0;
SP(n) = -h(1,n)*A_conv - (k_eff(1,n)*A)/((delta_x_we(1,n)));
aP(n) = aW(n) + aE(n) - SP(n);
Su(n) = q_nuclear(1,n)*(1-epsilon(1,n))*A*(0.5*delta_x_we(1,n-1)...
    + 0.5*delta_x_we(1,n)) + h(1,n)*A_conv*T_gas(1,n)  + (k_eff(1,n)*A*...
    T_B)/((delta_x_we(1,n)));
%-------------------------------------------------------------------------
% Interior Nodes
%-------------------------------------------------------------------------

for i = (3:n-1)

    aW(i) = (k_eff(1,i-1)*A)/delta_x_we(1,i-1);
    aE(i) = (k_eff(1,i)*A)/delta_x_we(1,i);
    SP(i) = -h(1,i)*A_conv;
    aP(i) = aW(i) + aE(i) - SP(i);

    Su(i) = q_nuclear(1,i)*(1-epsilon(1,i-1))*A*(0.5*delta_x_we(1,i-1)...
        + 0.5*delta_x_we(1,i)) + h(1,i)*A_conv*T_gas(1,i);

end
%_____________________________________________________________________
% SOLUTION
%-------------------------------------------------------------------------

B = diag(aP(2:n)) - diag(aE(2:n-1),1) - diag(aW(3:n),-1);
%[L,U] = lu(B);
% Gaussian Elimination
%T = U\(L\Su')
T = B\Su(2:n)'
```

```
clc;


%_____________________________________________________________________________
% PROBLEM SPECIFICATION
%-----------------------------------------------------------------------------

n = 23;
% number of cells
m = n + 1;
z = 0.5;
% cell height

radii = xlsread('Test_Matrix.xls','Test 6 - Data','AU1:AU26');
% outer radii
epsilon = xlsread('Test_Matrix.xls','Test 6 - Data','AV1:AV25');
% cell porosity
d = xlsread('Test_Matrix.xls','Test 6 - Data','AX1:AX25');
% sphere diameter
k_eff = xlsread('Test_Matrix.xls','Test 6 - Data','AW1:AW25');
% thermal conductivity

q_nuclear = xlsread('Test_Matrix.xls','Test 6 - Data','AY1:AY26');
% volumetric source
h = xlsread('Test_Matrix.xls','Test 6 - Data','AZ1:AZ26');
% heat transfer coefficient
T_gas = xlsread('Test_Matrix.xls','Test 6 - Data','BA1:BA26');
% gas temperature

T_B = 293.15;
% boundary temperature

%_____________________________________________________________________________
% GRID PARAMETERS
%-----------------------------------------------------------------------------

for i = (1:n)

    delta_x_we(i) = (radii(i+1) - radii(i));
    A(i) = 2*pi()*(0.5*radii(i+1) + 0.5*radii(i))*z;
    % radial face area
    V_w(i) = z*pi()*((0.5*radii(i+1)+0.5*radii(i))^2 - radii(i)^2);
    V_e(i) = z*pi()*(radii(i+1)^2 - (0.5*radii(i+1)+0.5*radii(i))^2);
    A_conv(i) = 0;

end

%_____________________________________________________________________________
% DISCRETISATION
%-----------------------------------------------------------------------------

for i = (1:n-1)

%     delta_x_Pe(i) = delta_x_we(i)/2;
%     delta_x_eE(i) = delta_x_we(i+1)/2;
%     delta_x_PE(i) = delta_x_Pe(i) + delta_x_eE(i);
%
%     delta_x_wP(i+1) = delta_x_we(i+1)/2;
%     delta_x_Ww(i+1) = delta_x_we(i)/2;
%     delta_x_WP(i+1) = delta_x_Ww(i+1) + delta_x_wP(i+1);

    delta_x_we_inter(i) = (delta_x_we(i+1)+ delta_x_we(i))/4;

end

for i = (2:n)

    V(i) = V_e(i-1) + V_w(i);

end

for i = (1:n-2)
```

```
    delta_x_we_new(i) = delta_x_we_inter(i+1) + delta_x_we_inter(i);

end

% for i = (1:10)
%
%     A_conv(i) = 0;
% surface area of spheres in core
%
% end
%
% for i = (7:11)
%
%     A_conv(i) = (6*(1-epsilon(i))*V(1,i))/d(i);
% surface area of spheres in core
%
% end
%
% for i = (12:16)
%
%     A_conv(i) = 0;
%
% end
%
% for i = 17
%
%     A_conv(i) = (4*epsilon(i)*V(1,i))/d(i);
%
% end
%
% for i = (18:n)
%
%     A_conv(i) = 0;
%
% end

%-------------------------------------------------------------------------
% Boundary Nodes
%-------------------------------------------------------------------------
% Node 2

aW(2) = 0;
aE(2) = (k_eff(2,1)*A(1,2))/delta_x_we_new(1,1);
SP(2) = -(0.5*h(2,1)+0.5*h(1,1))*A_conv(1,2);
aP(2) = aW(2) + aE(2) - SP(2);
Su(2) = (q_nuclear(1,1)*V_e(1,1) + q_nuclear(2,1)*V_w(1,2)...
    + (0.5*h(2,1)+0.5*h(1,1)*A_conv(1,2)*T_gas(2,1));

%-------------------------------------------------------------------------
% Node m-1

aW(n) = (k_eff(n-1,1)*A(1,n-1))/delta_x_we_new(1,n-2);
aE(n) = 0;
SP(n) = -h(n,1)*A_conv(1,n) - (k_eff(n,1)*A(1,n))/((delta_x_we(1,n)));
aP(n) = aW(n) + aE(n) - SP(n);
Su(n) = (q_nuclear(n-1,1)*V_e(1,n-1) + q_nuclear(n,1)*V_w(1,n)...
    + h(n,1)*A_conv(1,n)*T_gas(n,1)  + (k_eff(n,1)...
    *A(1,n)*T_B)/((delta_x_we(1,n))));

%-------------------------------------------------------------------------
% Interior Nodes
%-------------------------------------------------------------------------

for i = (3:n-1)

    aW(i) = (k_eff(i-1,1)*A(1,i-1))/delta_x_we_new(1,i-2);
    aE(i) = (k_eff(i,1)*A(1,i))/delta_x_we_new(1,i-1);
    SP(i) = -h(i,1)*A_conv(1,i);
    aP(i) = aW(i) + aE(i) - SP(i);
    Su(i) = (q_nuclear(i-1,1)*V_e(1,i-1) + q_nuclear(i,1)*V_w(1,i)...
        + 0.5*V(1,i)) + h(i,1)*A_conv(1,i)*T_gas(i,1);

end
```

```
%_____________________________________________________________________________
% SOLUTION
%-----------------------------------------------------------------------------

B = diag(aP(2:n)) - diag(aE(2:n-1),1) - diag(aW(3:n),-1);
%[L,U] = lu(B);
% Gaussian Elimination
%T = U\(L\Su')
T = B\Su(2:n)'
```